Summer 5-16-2020

Statistical Models and Analysis of Univariate and Multivariate Degradation Data

Lochana Palayangoda
lpalayangoda@smu.edu

STATISTICAL MODELS AND ANALYSIS OF

UNIVARIATE AND MULTIVARIATE DEGRADATION DATA

Approved by:

Dr. Hon Keung Tony Ng
Professor in Department of Statistical Science, Southern Methodist University

---

Dr. Ronald W. Butler
Professor in Department of Statistical Science, Southern Methodist University

---

Dr. Lynne S. Stokes
Professor in Department of Statistical Science, Southern Methodist University

---

Dr. Narayanaswamy Balakrishnan (External)
Professor in Department of Mathematics and Statistics, McMaster University

STATISTICAL MODELS AND ANALYSIS OF UNIVARIATE AND MULTIVARIATE DEGRADATION DATA

A Dissertation Presented to the Graduate Faculty of the

Dedman College

Southern Methodist University

in

Partial Fulfillment of the Requirements

for the degree of

Doctor of Philosophy

with a

Major in Statistical Science

by

Palayangoda Lochana Kanishka

B.S., University of Moratuwa
M.S., Sam Houston State University

May 16, 2020

ACKNOWLEDGMENTS

First, I would like to thank my adviser, Professor Hon Keung Tony Ng for his consistent support and encouragement to complete my thesis. He was available to help every time when I needed and guided me with his knowledge and experience to complete this thesis with success. In addition, I would like express my sincere gratitude to Professor Ronald Butler for his valuable suggestions and critical inputs to improve the findings of this thesis. I would like to thank Professor Lynne Stokes for her valuable guidance and feedback. Her Statistical Analysis course during my first year greatly helped me to improve my conceptual thinking for this study. I also want to thank Professor Narayanaswamy Balakrishnan for his valuable suggestions and comments to enhance the quality of findings of this thesis.

I would like to thank all the other faculty members for their outstanding teaching and mentoring. Furthermore, I especially want to thank our department secretary, Mrs. Sheila Crain, for all her help throughout my time at SMU. I am also greatly thankful to Professor Wayne Woodward (Professor Emeritus of Statistical Science, SMU) and Professor Cecil Hallum (Professor Emeritus of Statistics, Sam Houston State University) for giving me the opportunity to pursue a PhD degree at SMU.

Finally, I would like to thank my parents (Sarath Palayangoda and Anula Palayangoda), brothers (Loshan Palayangoda and Nelushan Palayangoda), my wife (Hansani Wijewardana) and my son (Vidu Palayangoda) for their support, encouragement and understanding.

Lochana Kanishka, Palayangoda

B.S., University of Moratuwa
M.S., Sam Houston State University

Statistical Models and Analysis of
Univariate and Multivariate Degradation Data

Advisor: Dr. Hon Keung Tony Ng
Doctor of Philosophy degree conferred May 16, 2020
Dissertation completed February 07, 2020

For degradation data in reliability analysis, estimation of the first-passage time (FPT) distribution to a threshold provides valuable information on reliability characteristics. Recently, Balakrishnan and Qin (2019; Applied Stochastic Models in Business and Industry, 35:571-590) studied a nonparametric method to approximate the FPT distribution of such degradation processes if the underlying process type is unknown. In this study, we propose improved techniques based on saddlepoint approximation, which enhance upon their suggested methods. Numerical examples and Monte Carlo simulation studies are used to illustrate the advantages of the proposed techniques. Limitations of the improved techniques are discussed and some possible solutions to such are proposed.

Then, we study the parametric, semiparametric and nonparametric statistical analysis of bivariate degradation data. In system engineering, the reliability of a system depends on the reliability of each subsystem (or component) and those subsystems have their own performance characteristics which can be dependent. The degradation measurements of those dependent performance characteristics of the subsystems are used to access the reliability of the system. Parametric frameworks have been developed to model bivariate and multivariate degradation processes in the literature; however, in practical situations, the underlying degradation process of a subsystem is usually unknown. Therefore, it is desired to develop semiparametric and nonparametric approaches to model bivariate and multivariate degradation processes. In this study, we proposed different semiparametric

and nonparametric methods to estimate the first passage time distribution of dependence bivariate degradation data. The saddlepoint approximation and bootstrap methods are used to estimate the marginal FPT distributions empirically and the empirical copula is used to estimate the joint distribution of two dependence degradation processes nonparametrically. A Monte Carlo simulation study is used to demonstrate the effectiveness and robustness of the proposed semiparametric and nonparametric approaches. Furthermore, for both univariate and bivariate cases, numerical examples are presented to illustrate the methodologies developed.

To apply the Lévy process models, the degradation measurements shall linearly relate to time throughout the lifetime of the product. However, the degradation data may not be linearly related to time in practice. For this reason, in our study, trend-renewal-process (TRP)-type models are considered for degradation modeling. In TRP-type models, a proper trend function is used to transform the degradation data so that the Lévy process approach can be applied. We proposed several parametric and semiparametric models and approaches to estimate the FPT distribution and mean-time-to-failure for the degradation data that may not be linearly related with time. A Monte Carlo simulation study is used to demonstrate the performance of the proposed methods. In addition, a model selection procedure is proposed to select among the Lévy process and TRP-type models. Two numerical examples on lithium-ion battery degradation data are applied to illustrate the proposed methodologies.

TABLE OF CONTENTS

LIST OF FIGURES

LIST OF TABLES

This thesis is dedicated to Professor Wayne Woodward and Professor Cecil Hallum.

Chapter 1
Introduction

Often system failures result from a gradual and irreversible accumulation of damage that occurs during a system's life cycle. This is known as a degradation process (Bogdanoff and Kozin, 1985). Degradation data analysis involves the measurements of the degradation of a product, where the degradation measurements can be directly related to the expected failure of the product. The information obtained from the degradation measurements is then used to estimate the failure time for the product. Many statistical models have been proposed for degradation data analysis (see, for example, Nikulin et al., 2010; Gorjian et al., 2010; Chen et al., 2017). For example, nonlinear regression models with random effect regression coefficients for degradation data are studied by Lu and Meeker (1993) and Meeker and Escobar (1998). Furthermore, Gebraeel et al. (2005) improved upon these regression models in the Bayesian framework.

This chapter covers preliminary information relates to the types of stochastic processes in degradation data analysis and their first-passage time distributions. In particular, for this study, we assume that the degradation data follows a Lévy process, and thereby, Section 1.1 is used to explain the types of Lévy processes and their first-passage time distributions. Furthermore, in Section 1.2, saddlepoint approximation techniques will be discussed since with this study, saddlepoint techniques are introduced to evaluate the first-passage time distribution. Furthermore, in this study, we developed models to estimate the first-passage time distribution for bivariate degradation data using copula functions. Thus, copula functions and their properties are discussed in Section 1.3. Moreover, in the same section, reliability analysis for series and parallel systems are discussed.

1.1. Degradation Processes and their First-passage Time Distributions

Stochastic processes such as Wiener, gamma and inverse Gaussian (IG) processes are commonly used in degradation modeling. These stochastic processes satisfy the conditions associated with a Lévy process. When stochastic processes are used for degradation modeling, the lifetime of the system can be defined as the first-passage time (FPT) for achieving a given threshold/failure level for the degradation measure. Determining the FPT distribution from the degradation data is important in reliability analysis because the FPT distribution provides valuable information on the reliability characteristics such its as $100p$-th percentile, mean-time-to-failure (MTTF), and remaining-useful-life (RUL). For a comprehensive review on RUL estimation methods related to data driven approaches, see Si et al. (2011).

1.1.1. First-passage time distribution

Let $\{X_t, t \geq 0\}$ be a degradation process (increasing with probability 1) with a threshold $c > 0$. The FPT of the stochastic process X_t can be defined as

$$T_c = \inf\{t : X_t > c\}.$$

Since the stochastic process is increasing, the survival function of the FPT, T_c, is given by

$$\Pr(T_c > t) = \Pr(X_t < c), \tag{1.1}$$

which means that the CDF of X_t at the threshold c is the survival function of T_c at the time t.

1.1.2. Lévy process

For the degradation process considered in this study, we assume that the degradation process $\{X_t, t \geq 0\}$ is a right-continuous stochastic process, which satisfies the properties of the Lévy process:

1. X_t consists of stationary increments, where $X_{t+v} - X_t$ has the same distribution $\forall t \geq 0, v \geq 0$;
2. X_t consists of independent increments, where $X_{t_i} - X_{t_{i-1}}$ are independent $\forall t_i \geq 0$ where $t_0 < t_1 < \ldots$.

With the above assumptions, there are mainly three types of degradation processes: Wiener process, gamma process and inverse-Gaussian (IG) process. Among them, only the Wiener process allows non-monotonic increments and has a closed-form expression for the FPT distribution, which is the IG distribution. On the other hand, the gamma process and the IG process are suitable for monotonic increments and the corresponding FPT distributions; however, do not have a closed-form yet they can be easily computed.

1.1.3. Birnbaum-Saunders distribution

The two-parameter Birnbaum-Saunders (BS) distribution (Birnbaum and Saunders, 1969) can be used to approximate the FPT distribution of a monotone degradation process (Park and Padgett, 2005; Balakrishnan and Qin, 2019; Qin, 2017). This distribution was proposed as a fatigue failure life distribution based on the physical considerations of a fatigue process in which the crack extension at each cycle is assumed to be a random variable with mean μ_0 and standard deviation σ_0 with failure defined as a crack length in excess of c (Birnbaum and Saunders, 1969; Owen and Ng, 2015; Balakrishnan and Kundu, 2019). The BS distribution has numerous applications in different fields such as

stochastic inventory modeling (Leiva et al., 2016b; Wanke and Leiva, 2015), environmental science (Leiva et al., 2016a) and quality control (Leiva et al., 2015; Lio and Park, 2008). Based on the central limit theorem, the sum of the crack lengths with a large number of cycles is approximately normally distributed and the probability of the FPT (i.e., the time at which the sum of crack lengths exceeds c) can be approximated as (Park and Padgett, 2005; Balakrishnan and Qin, 2019; Balakrishnan and Kundu, 2019)

$$\widehat{\Pr}(T_c \leq t) = \Phi\left[\frac{1}{\gamma}\left(\sqrt{\frac{t}{\kappa}} - \sqrt{\frac{\kappa}{t}}\right)\right], \quad t > 0, \gamma > 0, \kappa > 0 \tag{1.2}$$

where $\gamma = \sigma_0/\sqrt{c\mu_0}$ and $\kappa = c/\mu_0$.

Following the same idea, Kundu et al. (2010) introduced bivariate BS distribution for a bivariate random vector (T_1, T_2) with parameters $\gamma_1, \kappa_1, \gamma_2, \kappa_2$ and correlation coefficient ρ.

$$\Pr(T_1 < t_1, T_1 < t_2) = \Phi_2[U(t_1), V(t_2); \rho], \quad t_1 > 0, t_2 > 0 \tag{1.3}$$

where Φ_2 is the CDF of standard bivariate normal. Furthermore,

$$U(t_1) = \frac{1}{\gamma_1}\left(\sqrt{\frac{t_1}{\kappa_1}} - \sqrt{\frac{\kappa_1}{t_1}}\right); \quad V(t_2) = \frac{1}{\gamma_2}\left(\sqrt{\frac{t_2}{\kappa_2}} - \sqrt{\frac{\kappa_2}{t_2}}\right),$$

where $\gamma_1 > 0, \kappa_1 > 0, \gamma_2 > 0$, and $\kappa_2 > 0$.

1.1.4. Wiener process

In the study of FPT distributions for different degradation processes, it is well known that the FPT distribution can be obtained analytically as the IG distribution when the underlying degradation process is a Wiener process (Cox and Miller, 1965; Chhikara and Folks, 1989) (denote as Wiener(ν, σ)). Specifically, consider the Wiener process $W(t) = \nu t + \sigma B(t)$, where $\nu > 0$ is the drift parameter, $\sigma > 0$ is the volatility/variance pa-

rameter and $B(t)$ is the standard Brownian motion (Wiener, 1923). The FPT distribution of the process $W(t)$ with threshold value $c > 0$ is the IG distribution with probability density function (PDF) and cumulative distribution function (CDF),

$$\phi_{IG}(x) = \sqrt{\frac{\lambda}{2\pi x^3}} \exp\left[-\frac{\lambda(x-\mu)^2}{2\mu^2 x}\right], \quad x > 0, \tag{1.4}$$

and

$$\Phi_{IG}(x) = \Phi\left[\sqrt{\frac{\lambda}{x}}\left(\frac{x}{\mu} - 1\right)\right] + \exp\left(\frac{2\lambda}{\mu}\right)\Phi\left[-\sqrt{\frac{\lambda}{x}}\left(\frac{x}{\mu} + 1\right)\right], \quad x > 0, \tag{1.5}$$

respectively, where $\Phi(\cdot)$ is the CDF of the standard normal distribution, $\mu > 0$ and $\lambda > 0$ are both shape-type parameters with relations to the Wiener process by

$$\mu = \frac{c}{\nu} \text{ and } \lambda = \frac{c^2}{\sigma^2}. \tag{1.6}$$

1.1.5. Gamma process

Let $\{X_t, t \geq 0\}$ be a gamma degradation process with a threshold level c. Suppose $\Delta X_i = X_{t_i} - X_{t_{i-1}}$ and $\Delta t_i = t_i - t_{i-1}$ is the associated time difference between the degradation measurements X_{t_i} and $X_{t_{i-1}}$. Then, ΔX_i follows a gamma distribution with shape parameter $\alpha\Delta t_i > 0$ and scale parameter $\beta > 0$ (denoted as $\Delta X_i \sim gamma(\alpha\Delta t_i, \beta)$), which has the PDF

$$g_{\Delta X_i}(\Delta x_i; \alpha, \beta) = \frac{1}{\beta^{\alpha\Delta t_i}\Gamma(\alpha\Delta t_i)}(\Delta x_i)^{\alpha\Delta t_i - 1}\exp[-(\Delta x_i)/\beta], \quad \Delta x_i > 0.$$

We denote this gamma degradation process as a Gamma(α, β) process. Suppose $t_0 = 0$, $X_{t_0} = 0$ and the m-th degradation measurement is taken at time $t = t_m$, then $X_t = \sum_{i=1}^{m} \Delta X_i$, and thus, the distribution of X_t is $X_t \sim gamma(\alpha t, \beta)$, where $t = \sum_{i=1}^{m} \Delta t_i$. The

cumulant generating function (CGF) of X_t is given by

$$\mathscr{K}_{X_t}(s) = \ln[\mathscr{M}_{X_t}(s)] = -\alpha t \ln(1-\beta s) \text{ for } s < 1/\beta. \tag{1.7}$$

Using Eq. (1.1), the true FPT distribution can be directly obtained by $\Pr(T_c > t) = G_{X_t}(c; \alpha t, \beta)$, the CDF of a $gamma(\alpha t, \beta)$ at c. Park and Padgett (2005) proposed an approximation of the FPT distribution of the gamma degradation process based on the BS distribution. Specifically, the CDF of the FPT, T_c, can be approximated by Eq. (1.2) with $\gamma = \sqrt{\beta/c}$ and $\kappa = c/(\alpha\beta)$. Using the BS approximation in Eq. (1.2), the MTTF for the gamma degradation process can be approximated as $c/(\alpha\beta) + 1/(2\alpha)$.

Pan and Balakrishnan (2011a) extended the results to approximate the FPT distribution of a bivariate gamma degradation process using the bivariate BS distribution. The effect on approximating the FPT distribution under misspecification of the degradation model between the Wiener and gamma processes is studied by Tsai et al. (2011).

1.1.6. Inverse-Gaussian process

Let $\{X_t, t \geq 0\}$ be an IG degradation process (Wang and Xu, 2010; Ye and Chen, 2014) with a threshold level c. If $\Delta X_i = X_{t_i} - X_{t_{i-1}}$ and $\Delta t_i = t_i - t_{i-1}$ is the associated time difference between X_{t_i} and $X_{t_{i-1}}$, then ΔX_i follows an IG distribution with mean parameter $\mu\Delta t_i$ and shape parameter $\lambda(\Delta t_i)^2$ (denoted as $\Delta X_i \sim IG(\mu\Delta t_i, \lambda(\Delta t_i)^2)$, which has the PDF (Wang and Xu, 2010; Chhikara and Folks, 1989)

$$g(\Delta x_i) = \left[\frac{\lambda(\Delta t_i)^2}{2\pi\Delta x_i^3}\right]^{1/2} \exp\left[-\frac{\lambda(\Delta x_i - \mu\Delta t_i)^2}{2\Delta x_i \mu^2}\right], \ \Delta x_i > 0, \mu > 0, \lambda > 0.$$

If $t_0 = 0$, $X_{t_0} = 0$ and the m-th degradation measurement is taken at time $t = t_m$, then $X_t = \sum_{i=1}^{m} \Delta X_i$, and thus, the distribution of X_t is $X_t \sim IG(\mu t, \lambda t^2)$, where $t = \sum_{i=1}^{m} \Delta t_i$. The

CGF of X_t is given by

$$\mathscr{K}_{X_t}(s) = \ln[\mathscr{M}_{X_t}(s)] = (\lambda t/\mu)\left(1 - \sqrt{1 - (2\mu^2 s/\lambda)}\right) \text{ for } s \leq \lambda/(2\mu^2). \tag{1.8}$$

We denote this degradation process as IG(μ, λ) process.

Using Eq. (1.1) the true FPT distribution can be directly obtained by $\Pr(T_c > t) = IG_{X_t}(c; \mu t, \lambda t^2)$, the CDF of an $IG(\mu t, \lambda t^2)$ at c. Furthermore, Peng (2015) showed that the FPT distribution of the IG process can also be approximated by the BS distribution. Based on the BS distribution in Eq. (1.2), the CDF of the FPT with threshold c (i.e., T_c) can be approximated by Eq. (1.2) with $\gamma = \mu(\lambda c)^{-\frac{1}{2}}$ and $\kappa = c/\mu$. The MTTF for the IG degradation process can be approximated using the BS approximation as $c/\mu + \mu/(2\lambda)$.

1.2. Saddlepoint Approximation Methods

The saddlepoint approximation method, originally proposed by Daniels (1954), provides an approximation formula for the probability distribution of a random variable based on the moment generating function (MGF), $\mathscr{M}(s)$, or the CGF, $\mathscr{K}(s) = \ln \mathscr{M}(s)$. Saddlepoint approximation methods can be used to approximate the PDF or the CDF of a continuous random variable. We will briefly review the formulations of the saddlepoint approximation methods for PDF and CDF in following subsections.

1.2.1. Saddlepoint approximation for PDF

Suppose a continuous random variable X has a PDF $f(x)$ and the associated CGF is $\mathscr{K}(s)$, then the saddlepoint approximation of the PDF is given as (Daniels, 1954; Butler, 2007)

$$\hat{f}(x) = \frac{1}{\sqrt{2\pi \mathscr{K}''(\hat{s})}} \exp[\mathscr{K}(\hat{s}) - \hat{s}x], \tag{1.9}$$

where $\hat{s}$ is the *saddlepoint*, which is the unique solution to the *saddlepoint equation* $\mathscr{K}'(\hat{s}) = x$, and $\mathscr{K}'(s)$ and $\mathscr{K}''(s)$ are the first and second derivatives of $\mathscr{K}(s)$ with respect to s, respectively. Here, $\hat{f}(x)$ is the *saddlepoint density*; however, it may not be a proper density because $\int_{-\infty}^{\infty} \hat{f}(x)\, dx$ may not equal to 1. Therefore, a proper approximate density based on the saddlepoint approximation, denoted as $\bar{f}(x)$, can be obtained by (see, for example, Butler, 2007, Chapter 1)

$$\bar{f}(x) = c^{-1}\hat{f}(x),$$

where $c = \int_{\chi} \hat{f}(x)\, dx$ and $\chi = \{x : f(x) > 0\}$.

1.2.2. Saddlepoint approximation for CDF

To approximate the CDF of a continuous random variable X, Lugannani and Rice (1980) introduced a saddlepoint approximation as

$$\hat{F}(x) = \begin{cases} \Phi(\hat{w}) + \phi(\hat{w})\left(\frac{1}{\hat{w}} - \frac{1}{\hat{u}}\right) & \text{if } x \neq \mu_X, \\ \frac{1}{2} + \frac{\mathscr{K}'''(0)}{6\sqrt{2\pi}\mathscr{K}''(0)^{3/2}} & \text{if } x = \mu_X, \end{cases} \tag{1.10}$$

where $\mathscr{K}'''(s)$ is the third derivative of $\mathscr{K}(s)$ with respect to s, $\Phi(\cdot)$ and $\phi(\cdot)$ are respectively the CDF and PDF of the standard normal distribution, μ_X is the mean of X,

$$\hat{w} = sgn(\hat{s})\sqrt{2\{\hat{s}x - \mathscr{K}(\hat{s})\}}, \hat{u} = \hat{s}\sqrt{\mathscr{K}''(\hat{s})},$$

and sgn is the sign function. Similar to Eq. (1.9), $\hat{s}$ is the saddlepoint, which is the unique solution to the saddlepoint equation $\mathscr{K}'(\hat{s}) = x$.

1.2.3. Empirical saddlepoint approximation

The empirical saddlepoint approximation (ESA) is a nonparametric approach to evaluate the distribution of a random variable when the MGF is not available. In this approach, an empirical MGF is used as a surrogate for the true unknown MGF. This is analogous to the use of an empirical CDF as a surrogate for the true unknown for the nonparametric bootstrap distribution (Efron, 1979; Butler, 2007, Chapter 14). Suppose $x_1, x_2, \ldots, x_m$ are independent and identically distributed observations from a distribution with CDF F, then the empirical MGF and empirical CGF can be obtained as (Butler, 2007)

$$\hat{\mathscr{M}}_{X_i^*}(s) = \int \exp(sx)\, d\hat{F}(x) = \frac{1}{m}\sum_{i=1}^{m} \exp(sx_i) \tag{1.11}$$

and

$$\hat{\mathscr{K}}_{X_i^*}(s) = -\ln m + \ln\left\{\sum_{i=1}^{m} \exp(sx_i)\right\},$$

respectively.

When a random sample is available, the ESA for PDF and CDF can be obtained by finding and applying the empirical CGF in Eq. (1.9) and Eq. (1.10).

1.2.4. Inverse-Gaussian-based saddlepoint approximation

Up to now, we have discussed only saddlepoint equations under the normal-based where saddlepoint equations consist of univariate normal density and CDF. In some situations, a better accuracy can be reached by using the saddlepoint approximation in different distributional base other than the standard normal base (Butler, 2007; Wood et al., 1993). Wood et al. (1993) provided the generalized Lugannani and Rice (1980) formula along with standard formulas for saddlepoint approximations with different distributional base. In addition, detailed explanations have been provided about the saddlepoint ap-

proximation based on generalized Lugannani and Rice (1980) and different bases such as the chi-squared-base and the IG-base in Butler (2007, Chapter 16).

In addition, Wood et al. (1993) extend the Lugannani-Rice tail probability approximation formula to the non-Gaussian base distribution. Furthermore, Booth and Wood (1995) illustrate with an example in which the performance of the Lugannani-Rice formula can be rather poor. Their modified approximation formula, in which the normal-base is replaced by an IG-base, gives a better accuracy.

For the IG distribution with PDF and CDF in Eqs. (1.4) and (1.5), respectively, and $\lambda = 1$, the CGF of the IG distribution can be expressed as

$$\mathscr{L}(\mathfrak{s}) = \mu^{-1} - (\mu^{-2} - 2\mathfrak{s}) \quad \mathfrak{s} \leq 1/(2\mu^2).$$

The IG-based saddlepoint approximation of the CDF the random variable X is given by (Wood et al., 1993; Butler, 2007, Chapter 16).

$$\widehat{\Pr}(X < x) = \begin{cases} \Phi_{IG}(\hat{z}) + \phi_{IG}(\hat{z}) \left(\frac{1}{\hat{\mathfrak{s}}} - \frac{\sqrt{\mathscr{L}''(\hat{\mathfrak{s}})}}{\hat{u}} \right) & \text{if } x \neq \mu_X, \\ \Phi_{IG}\{\mathscr{L}'(0)\} + \frac{1}{6}\sqrt{\mathscr{L}''(0)}\phi_{IG}\{\mathscr{L}'(0)\} \left\{ \frac{\mathscr{K}'''(0)}{[\mathscr{K}''(0)]^{3/2}} - \frac{\mathscr{L}'''(0)}{[\mathscr{L}''(0)]^{3/2}} \right\} & \text{if } x = \mu_X, \end{cases} \tag{1.12}$$

where the saddlepoint $\hat{s}$ is obtained by solving $\mathscr{K}'(\hat{s}) = c$, μ_{T_c} is the mean of the FPT distribution,

$$
\begin{aligned}
\hat{w} &= sgn(\hat{s})\sqrt{2\{\hat{s}c - \mathscr{K}(\hat{s})\}}, \\
\hat{u} &= \hat{s}\sqrt{\mathscr{K}''(\hat{s})}, \\
\hat{z} &= \hat{\mu} + \frac{1}{2}\hat{\mu}^2(\hat{w}^2 + \hat{w}\sqrt{\hat{w}^2 + 4/\hat{\mu}}), \\
\hat{\mathfrak{s}} &= \frac{1}{2}(\hat{\mu}^{-2} - \hat{z}^{-2}), \\
\text{and } \hat{\mu} &= \frac{[\mathscr{K}'''(\hat{s})]^2}{[\mathscr{K}''(\hat{s})]^3}\left(3 + \hat{w}\sqrt{\frac{[\mathscr{K}'''(\hat{s})]^2}{[\mathscr{K}''(\hat{s})]^3}}\right)^{-1} \quad \text{if} \quad \mathscr{K}'''(\hat{s}) > 0.
\end{aligned}
$$

1.3. Copula Functions and their Properties

1.3.1. Definition

A copula is a function that links the multivariate distribution to the corresponding one-dimensional marginal distributions, where the marginals are uniform on [0, 1] (see, for example, Nelsen, 1999; Balakrishnan and Lai, 2009). In this study, we mainly focus on two-dimensional copulas where we can obtain the bivariate joint distribution of two random variables. If $u, v \in [0,\ 1]$, then the two-dimensional copula is denoted as $C(u,v) \in [0,\ 1]^2$ and it has following properties:

1. For every $u, v \in [0,\ 1]$

$$
C(u,0) = 0 = C(0,v) \text{ and } C(u,1) = u \text{ and } C(1,v) = v; \tag{1.13}
$$

2. If $0 \leq u_1 \leq u_2 \leq 1$ and $0 \leq v_1 \leq v_2 \leq 1$ then

$$C(u_2, v_2) - C(u_2, v_1) - C(u_1, v_2) + C(u_1, v_1) \geq 0. \tag{1.14}$$

Theorem 1 (Sklar's Theorem) *Let H be a joint distribution function with marginal distribution functions F and G. Then, there exists a copula $C(\cdot,\cdot)$ such that for all $x, y \in (-\infty, \infty)$ (Sklar, 1959; Nelsen, 1999)*

$$H(x,y) = \Pr(X \leq x, Y \leq y) = C(F(x), G(y)). \tag{1.15}$$

$C(\cdot,\cdot)$ is unique if F and G are continuous; otherwise, $C(\cdot,\cdot)$ is uniquely determined on the (Range of F $\times$ Range of G). If C is a copula and F and G are marginal distribution functions, then the function H defined in Eq. (1.15) is a joint distribution function with margins F and G.

Using the joint distribution H, the joint PDF of X and Y can be derived as

$$h(x,y) = c(F(x), G(y)) f(x) g(y), \tag{1.16}$$

where $f(x)$ and $g(y)$ are marginal PDFs of the random variables X and Y, respectively, and $c(u,v) = \partial^2 C(u,v)/\partial u \partial v$ is the bivariate copula density function.

1.3.2. Generate bivariate random samples from copula

For Monte Carlo simulations, the data shall be generated from a known joint distribution. When a copula function is used as a joint distribution, Sklar's theorem is applied to generate a pair (u,v), which are uniform $(0,1)$ random variables (U,V). Thus, the joint distribution of (U,V) is C, where C is the copula of X and Y. According to Nelsen (1999), let the conditional distribution of V given $U = u$ denoted by $c_u(v)$ and bivariate random

samples of (X,Y) can be generated using following procedure:

$$c_u(v) = \Pr(V \leq v | U = u) = \partial C(u,v)/\partial u. \tag{1.17}$$

1. Generate two independent uniform [0, 1] variables, denoted as u and w;
2. Set $v = c_u^{-1}(w)$, where $c_u^{-1}(w)$ denotes the inverse of c_u with respect to the w;
3. Using the pair (u,v), determine the bivariate random sample (x,y) as $x = F^{-1}(u)$ and $y = G^{-1}(v)$.

1.3.3. Survival copula

The survival copula of two random variables X and Y is the joint survival (reliability) function given by $\tilde{H}(x,y) = \Pr(X > x, Y > y)$. Suppose the marginal survival functions of the random variables X and Y are $R(x)$ and $R(y)$, then the joint survival function is

$$\tilde{H}(x,y) = R(x) + R(y) - 1 + H(x,y), \tag{1.18}$$

then the survival copula can be expressed using a copula function C as

$$\tilde{C}(u,v) = 1 - u - v + C(u,v). \tag{1.19}$$

1.3.4. Archimedean copulas

Depending on the copula construction methods such as inversion method, geometric method and algebraic method, there are several classes of copulas; for example, Gaussian copula, Archimedean copula and extreme value copula. The Archimedean copulas

can be found in many applications due to convenience in construction, flexibility to model with different families of distributions, and ability to model multivariate joint distributions with one or few parameters.

The following lemma provides a way to generate the Archimedean copulas.

Lemma 2 *Let ψ be a continuous, strictly decreasing function, where $\psi : [0,1] \to [0,\infty]$, then $\psi(H(x,y)) = \psi(F(x)) + \psi(G(y))$. This is also equivalent to $\psi(C(u,v)) = \psi(C(u)) + \psi(C(v))$. The copula function C is therefore given as*

$$C(u,v) = \psi^{-1}(\psi(u) + \psi(v)), \tag{1.20}$$

where ψ is the Archimedean copula generator function and $\psi^{-1}(t)$ is the pseudo-inverse of ψ, which is defined as (Nelsen, 1999, Definition 4.1.1)

$$\psi^{-1}(t) = \begin{cases} \psi(t)^{-1}, & 0 \le t \le \psi(0), \\ 0, & \psi(0) \le t \le \infty. \end{cases} \tag{1.21}$$

Depending on the choice of the generator function ψ, different Archimedean copulas can be developed. In this study, we focus on three Archimedean copulas families: Frank, Clayton, and Gumbel copulas.

1.3.4.1. Frank copula

The Frank copula (Frank, 1979) is obtained with Archimedean copula generator $\psi_\xi(t) = -\ln\left(\frac{e^{\xi t}-1}{e^{\xi}-1}\right)$. Furthermore, the Frank copula is a symmetric copula with $C(u,v) = \tilde{C}(u,v)$.

The Frank copula function can be expressed as

$$C(u,v) = -\frac{1}{\xi_F}\ln\left(1+\frac{(e^{-\xi_F u}-1)(e^{-\xi_F v}-1)}{e^{-\xi_F}-1}\right), \tag{1.22}$$

where $\xi_F \in \mathbb{R}\setminus\{0\}$. The parameter ξ_F has relationship to the Kendall's tau correlation coefficient as

$$\tau = 1+4(D_1(\xi_F)-1)/\xi_F,$$

where $D_1(\xi_F) = 1/\xi_F \int_0^{\xi_F} t/(e^t-1)dt$ is the Debye function of first kind.

1.3.4.2. Clayton copula

The Clayton copula (Clayton, 1978) is an asymmetric copula of which the generator is $\psi_{\xi_C}(t) = 1/\xi_C(t^{-\xi_C}-1)$. The Clayton copula is given by

$$C(u,v) = \max\left(\left[u^{-\xi_C}+v^{-\xi_C}-1\right]^{-1/\xi_C}, 0\right), \tag{1.23}$$

where $\xi_C \in [-1,\infty)\setminus\{0\}$. The parameter ξ_C has relationship to the Kendall's tau correlation coefficient as $\tau = \xi_C/(\xi_C+2)$.

1.3.4.3. Gumbel copula

The Gumbel copula (Gumbel, 1960) is an asymmetric copula of which the generator is $\psi_{\xi_G}(t) = (-\ln t)^{\xi_G}$. The Gumbel copula is given by

$$C(u,v) = \exp\left(-\left[(-\ln u)^{\xi_G}+(-\ln v)^{\xi_G}\right]^{1/\xi_G}\right), \tag{1.24}$$

where $\xi_G \in [1,\infty)$. The parameter ξ_G has relationship to the Kendall's tau correlation coefficient as $\tau = (\xi_G-1)/\xi_G$.

1.3.5. Empirical copula

In this study, we focus on nonparametric and semiparametric approaches to model the bivariate degradation data. The empirical copula enable us to obtain the joint distribution of dependent random variables after a transformation to ranks. Suppose x_j and z_j, $j = 1,2,\ldots,m$ are random samples from continuous CDFs F_X and F_Z, respectively. Let $x^{(j)}$ be the rank of x_j in the sample $\{x_1,x_2,\ldots,x_m\}$ and $z^{(j)}$ be the rank of z_j in the sample $\{z_1,z_2,\ldots,z_m\}$. The empirical copula $\hat{C}_m$ is defined as (Joe, 2015, Section 5.10.1)

$$\hat{C}_m(u,v) = \frac{1}{m}\sum_{j=1}^{m} \mathbf{1}\left(\frac{\left[x^{(j)}-\frac{1}{2}\right]}{m} \leq u, \frac{\left[z^{(j)}-\frac{1}{2}\right]}{m} \leq v\right), \tag{1.25}$$

where $u \in [0,1]$ and $v \in [0,1]$ are the evaluation points of the empirical copula function and $\mathbf{1}(A)$ is an indicator function defined as $\mathbf{1}(A) = 1$ if A is true and 0 otherwise.

1.3.6. Kendall's tau

The copula function provide a joint distribution between two random variables. The copula parameter has a one-to-one relationship for the population version of the Kendall's tau. Let (X,Y) are two continuous random variables which have a joint distribution $H(x,y)$. For all $i \neq j$, assume (X_i,Y_i) and (X_j,Y_j) are independently and identically distributed random variables of which the joint distribution of each is H. Then the population version of the Kendall's tau is defined as (Nelsen, 1999, Section 5.1.1)

$$\tau_{X,Y} = P[(X_1-X_2)(Y_1-Y_2) > 0] - P[(X_1-X_2)(Y_1-Y_2) < 0] \tag{1.26}$$

The relationship between the population version of Kendall's tau and copula function

for the random variables (X,Y) is given by (Nelsen, 1999, Theorem 5.1.3)

$$\tau_{X,Y} = 4\int\int_{I^2} C(u,v)dC(u,v) - 1, \tag{1.27}$$

where $I^2 \in [0,\ 1]^2$.

1.4. System Reliability Analysis

A complex system consists of dependent individual subsystems with components connected in series or/and in parallel. Therefore, to evaluate the failure time distribution of a complex system, we consider developing models and techniques to obtain the failure time distribution of series and parallel systems. The bivariate distribution of two components connected either in series or in parallel can be used as a minimum structure to construct the failure time distribution of a complex system.

1.4.1. Series system

A series system is one of the basic structures of a complex system. The failure time of a series system is minimum failure time of all the components. In other words, the first component failure leads to the failure of the entire system. Let $T_1,\ldots,T_n$ be the failure times of individual components of an n-component system and the components are connected in series. Therefore, the survival function of the lifetime of a series system is the joint survival function of the individual components:

$$R_s(t) = \Pr(T_{min} > t) = \Pr(\min(T_1,\ldots,T_n) > t) = \Pr(T_1 > t, T_2 > t, \ldots, T_n > t).$$

Consider a bivariate degradation process (X_t, Z_t) with thresholds c_x and c_z, respec-

tively; and assume that the components are connected in series, if the FPTs are T_{c_x} and T_{c_z}, then the system survival function of a series system, $R_s(t)$, can be obtained through the copula function as

$$\begin{aligned} R_s(t) = \Pr(T_{min} > t) &= \Pr(T_{c_x} > t, T_{c_z} > t) \\ &= \Pr(X_t \leq c_x, Z_t \leq c_z) \\ &= C(R_X(t), R_Z(t)), \end{aligned} \tag{1.28}$$

where $R_X(t) = \Pr(X_t \leq c_x) = \Pr(T_{c_x} > t)$ and $R_Z(t) = \Pr(Z_t \leq c_z) = \Pr(T_{c_z} > t)$.

1.4.2. Parallel system

The parallel system is another fundamental structure of a complex system where components are connected in parallel. The failure time of a parallel system is the maximum failure time of the components. Let $T_1, \ldots, T_n$ be the failure times of individual components of a n-component system and the components are connected in parallel. Therefore, the survival function of the lifetime of a parallel system is given by

$$R_p(t) = \Pr(T_{max} > t) = \Pr(\max(T_1, \ldots, T_n) > t) = 1 - \Pr(T_1 \leq t, T_2 \leq t, \ldots, T_n \leq t).$$

Consider a bivariate degradation process (X_t, Z_t) with thresholds c_x and c_z, respectively; and assume that the components are connected in parallel. If the FPTs are T_{c_x} and T_{c_z}, then the system survival function, $R_p(t)$, can be obtained through the copula survival functions as

$$
\begin{aligned}
R_p(t) = \Pr(T_{max} > t) &= 1 - \Pr(T_{c_x} \leq t, T_{c_z} \leq t) \\
&= 1 - \Pr(X_t > c_x, Z_t > c_z) \\
&= 1 - \tilde{C}(R_X(t), R_Z(t))
\end{aligned} \tag{1.29}
$$

where $R_X(t) = \Pr(X_t \leq c_x) = \Pr(T_{c_x} > t)$ and $R_Z(t) = \Pr(Z_t \leq c_z) = \Pr(T_{c_z} > t)$. The survival copula $\tilde{C}(\cdot,\cdot)$ can be obtained using Eq. (1.19).

1.5. Organization of the Thesis

In this thesis, we investigate and propose different novel parametric, semiparametric and nonparametric approaches to model the FPT distribution based on degradation data. Those approaches are applicable to univariate and bivariate degradation data.

This thesis is organized as follows. In Chapter 2, we introduce the improved saddlepoint approximation methods for FPT distribution and illustrate the two major issues of the methods proposed in Balakrishnan and Qin (2019) in order to justify the needs for the proposed methods. We propose to use the Lugannani and Rice (1980) saddlepoint method described in Section 1.2.2 to improve the accuracy of the estimate. Furthermore, methods to obtain the FPT distribution using the ESA are presented in Section 1.2.3 and introduced for the case that the data are measured at unequal time intervals. Monte Carlo simulations are carried out to evaluate and compare the proposed models and methods. In Chapter 3, we propose semiparametric and nonparametric approaches to estimate the FPT distribution of degradation data when two degradation processes are correlated. Those methods are introduced for both series and parallel systems, which enable us to evaluate the FPT distribution for complex systems. To obtain the joint distribution of two

degradation processes, copula functions are applied. Moreover, a Monte Carlo simulation study is used to validate the propose techniques in different parameter settings. Degradation data models and MTTF estimates for nonlinear data are introduced and discussed in Chapter 4. Chapter 5 consists of the summary and future research directions based on the findings of studies related to Chapters 2, 3 and 4.

Chapter 2

Improved Techniques for Parametric and Nonparametric Evaluations of the First-Passage Time for Degradation Processes

2.1. Introduction

Recently, Balakrishnan and Qin (2019) proposed an approximation method for the FPT distributions of gamma and IG processes using a saddlepoint approximation. They demonstrated that the BS approximation to the FPT distribution deviates from the true FPT distribution, and thus, recommended using a saddlepoint approximation. When the underlying degradation model is specified, Balakrishnan and Qin (2019) concluded that the saddlepoint approximation performs better than the BS approximation in both gamma and IG degradation processes in terms of accuracy in estimating various percentiles of the FPT distribution. In addition, Balakrishnan and Qin (2019) also used the empirical (nonparametric) saddlepoint method to estimate the FPT distribution based on degradation data when the underlying degradation model is not specified. They showed that the empirical saddlepoint estimate performs better in capturing the heterogeneity in the practical data sets.

Although the results presented in Balakrishnan and Qin (2019) are promising, the saddlepoint approximations suggested by Balakrishnan and Qin (2019) have two main shortcomings: (i) the parametric saddlepoint approximation and empirical (nonparametric) saddlepoint estimate proposed in Balakrishnan and Qin (2019) give significant bias in approximating the left-tail of the FPT distribution and may result in approximated FPT distributions which are improper; and (ii) the empirical saddlepoint estimate works prop-

erly only if the degradation measurements are taken at equal time distance. In this study, we aim to address these two issues by proposing alternative saddlepoint approximations and suitable modifications for unequally spaced data. We also investigate the limitations of the various saddlepoint approximations.

This chapter is organized as follows. In Section 2.2, we introduce the improved saddlepoint approximation methods for FPT distribution and illustrate the two major issues of the methods proposed in Balakrishnan and Qin (2019) in order to justify the needs for the proposed methods. In Section 2.3.1, we focus on the empirical saddlepoint estimate for the FPT distribution, which does not require specification of the underlying degradation model. The advantage of the empirical saddlepoint estimate under model uncertainty is illustrated by a Monte Carlo simulation study. The implicit equal time interval assumption of the empirical saddlepoint estimate is discussed and different modifications are proposed to deal with the situation at which the degradation measurements are measured at unequal time intervals. The performance of the proposed modifications of the empirical saddlepoint estimate is studied via a Monte Carlo simulation study. In Section 2.4, a numerical example with the laser device degradation data is used to illustrate the methodologies proposed in Sections 2.2 and 2.3.1. Section 2.5 discusses the limitations related the improved saddlepoint approximation methods and some possible solutions to these limitations. Finally, some concluding remarks are provided in Section 2.6.

2.2. Improved Saddlepoint Approximation of the First-Passage Time Distribution

Balakrishnan and Qin (2019) suggested approximating the CDF of X_t in Eq. (1.1) using a saddlepoint first introduced by Helstrom and Ritcey (1984) and discussed by Daniels (1987, Eq. 3.3). Let $\mathscr{M}_{X_t}(s) = \mathbb{E}(e^{sX_t})$ be the moment generating function (MGF) of X_t

convergent on $(-\infty, b) \ni 0$. The CDF is the inversion integral

$$\Pr(X_t \leq c) = \frac{1}{2\pi i} \int_{\varepsilon - i\infty}^{\varepsilon + i\infty} \frac{\mathscr{M}_{X_t}(s)}{-s} e^{-sc} ds \qquad \varepsilon < 0 \tag{2.1}$$

on the vertical contour $\mathrm{Re}(s) = \varepsilon < 0$ to the left of the integrand pole at $s = 0$ with $\varepsilon \in (-\infty, 0)$; see Widder (1941, p. 242, Thm. 5b) for the result expressed in terms of Laplace transforms. The above authors used the standard method of steepest descents approximation as described in Copson (1965, Chapter 7), which leads to the approximation

$$\Pr_{BQ}(T_c > t) = \Pr(X_t \leq c) = \frac{1}{\sqrt{2\pi \mathscr{K}_{X_t}^{-\prime\prime}(\hat{s})}} \exp\{\mathscr{K}_{X_t}^{-}(\hat{s}) - \hat{s}c\}. \tag{2.2}$$

Here, $\mathscr{K}_{X_t}^{-}(s) = \ln\{\mathscr{M}_{X_t}(s)/(-s)\}$ and $\hat{s} \in (-\infty, 0)$ is the saddlepoint defined as the unique solution to the saddlepoint equation

$$c = \mathscr{K}_{X_t}^{-\prime}(\hat{s}) = \mathscr{K}_{X_t}^{\prime}(\hat{s}) - 1/\hat{s} \qquad \hat{s} \in (-\infty, 0), \tag{2.3}$$

where $\mathscr{K}_{X_t}(\hat{s}) = \ln\{\mathscr{M}_{X_t}(s)\}$ is the cumulant generating function (CGF) of X_t. Note that $\hat{s}$ achieves a local minimum of the log integrand $\mathscr{K}_{X_t}^{-}(s) - sc$ along the negative real line $s \in (-\infty, 0)$, a line segment along which $\mathscr{K}_{X_t}^{-}$ is a strictly convex function since

$$0 < \mathscr{K}_{X_t}^{-\prime\prime}(s) = \mathscr{K}_{X_t}^{\prime\prime}(s) + 1/s^2 \qquad s \in (-\infty, 0).$$

The approximation applies for any c, which is in the interior of the range of the support for the distribution of X_t. Implicit differentiation of Eq. (2.3) gives $d\hat{s}/dc = \{\mathscr{K}_{X_t}^{-\prime\prime}(\hat{s})\}^{-1} > 0$ so that large (small) c results in large (small) $\hat{s}$, which cannot exceed 0 due to the term $-1/\hat{s}$ in Eq. (2.3).

This saddlepoint approximation is well-defined for all thresholds $c > 0$ and maintains its accuracy when $\hat{s}$ is well below 0 (i.e. $\hat{s} << 0$). Daniels (1987, just below Eq. (3.3)) pointed out that this approximation becomes inaccurate as $\hat{s} \uparrow 0$ and for $\hat{s}$ in a left-hand

neighborhood of 0. The steepest descents method was not designed to deal with the close or even moderately close presence of the saddlepoint $\hat{s}$ to the pole at $s = 0$ when approximating the inversion integral of Eq. (2.1). As a consequence, the survival function of T_c is inaccurately approximated in Eq. (2.2) for small t in a right-hand neighborhood of 0.

2.2.1. Addressing the left tail

The inaccuracy in the left tail may be addressed using an alternative approximation to Eq. (2.2) but with a positive saddlepoint $\hat{s} > 0$. If $\mathscr{I}_\varepsilon$ for $\varepsilon < 0$ denotes the inversion integral in Eq. (2.1), then it can be deformed so the integration is along $\mathrm{Re}(s) = \varepsilon_1 \in (0, b)$ rather than $\mathrm{Re}(s) = \varepsilon \in (-\infty, 0)$. The relation of $\mathscr{I}_\varepsilon$ to $\mathscr{I}_{\varepsilon_1}$ is given by Cauchy's theorem applied to counterclockwise integration around the rectangle with corners $\varepsilon \pm Ni$ and $\varepsilon_1 \pm Ni$. As $N \to \infty$, the integrals along the top and bottom horizontal edges converge to 0. This leaves the vertical integrals and the residue at $s = 0$ related by Cauchy's theorem as

$$\mathscr{I}_{\varepsilon_1} - \mathscr{I}_\varepsilon = \mathrm{Res}\{-s^{-1}\mathscr{M}_{X_t}(s)e^{-sc}; s = 0\} = -1.$$

Thus,

$$\frac{1}{2\pi i}\int_{\varepsilon_1 - i\infty}^{\varepsilon_1 + i\infty} \frac{\mathscr{M}_{X_t}(s)}{s} e^{-sc} ds = -\mathscr{I}_{\varepsilon_1} = 1 - \mathscr{I}_\varepsilon = 1 - \Pr(X_t \le c) = \Pr(X_t > c) \tag{2.4}$$

as specified in Widder (1941, p. 242, Thm. 5b) in terms of Laplace transforms. The method of steepest descents applied to the integral in Eq. (2.4) gives

$$\Pr{}_L(T_c > t) = \Pr(X_t \le c) = 1 - \frac{1}{\sqrt{2\pi \mathscr{K}^{+\prime\prime}_{X_t}(\hat{s})}} \exp\{\mathscr{K}^{+}_{X_t}(\hat{s}) - \hat{s}c\}, \tag{2.5}$$

where $\hat{s} \in (0, b)$ solves $\mathscr{K}^{+\prime}_{X_t}(\hat{s}) = c$ for $\mathscr{K}^{+}_{X_t}(s) = \ln\{\mathscr{M}_{X_t}(s)/s\}$. The saddlepoint achieves a local minimum of the log-integrand $\mathscr{K}^{+}_{X_t}(\hat{s}) - \hat{s}c$ since $\mathscr{K}^{+\prime\prime}_{X_t}(s) = \mathscr{K}''_{X_t}(s) + 1/s^2$ for $s \in (0, b)$.

Each value of $t > 0$ leads to an approximation $\Pr_L(T_c > t)$ as in Eq. (2.5) with positive saddlepoint $\hat{s} > 0$ and also an approximation $\Pr_{BQ}(T_c > t)$ with negative saddlepoint $\hat{s} < 0$. We can expect the accuracy of $\Pr_L(T_c > t)$ to complement that of $\Pr_{BQ}(T_c > t)$ by being the most accurate in the left tail (for small t where $\hat{s}$ is closer to b than 0) and inaccurate in the middle and right tail (where $\hat{s}$ is closer to 0) where accuracy is affected by the presence of the pole at $s = 0$.

The two approximations can be applied in the respective tails in which they show accuracy, but neither of these two approximations is capable of providing accuracy in the middle of the distribution where the saddlepoint is near 0. The next approximation will be seen to provide accuracy throughout the whole range of $t > 0$.

2.2.2. Addressing both tails

We suggest a much more accurate saddlepoint approximation devised for the specific purpose of dealing with the presence of a simple pole in the inversion integrand as in Eq. (2.1). The Lugannani and Rice (1980) approximation used a method due to Bleistein (1966) to accommodate the simple pole at $s = 0$ and leads to accurate survival function approximation for all values of $t > 0$ including small values. Define the quantities

$$\hat{w} = \operatorname{sgn}(\hat{s}) \sqrt{2\{\hat{s}c - \mathscr{K}_{X_t}(\hat{s})\}} \qquad \text{and} \qquad \hat{u} = \hat{s}\sqrt{\mathscr{K}''_{X_t}(\hat{s})}, \tag{2.6}$$

where the saddlepoint $\hat{s} \in (a, b)$ solves saddlepoint equation $\mathscr{K}'_{X_t}(\hat{s}) = c$ with $t > 0$ (assuming the support of X_t is $(0, \infty)$). The Lugannani and Rice (1980) approximation to the

survival function $\Pr(T_c > t)$ is

$$\Pr_{LR}(T_c > t) = \Phi(\hat{w}) + \phi(\hat{w})\left(\frac{1}{\hat{w}} - \frac{1}{\hat{u}}\right), \tag{2.7}$$

where Φ is the standard normal cumulative distribution function (CDF), ϕ is the standard normal density, and $\hat{w}$ and $\hat{u}$ are as given in Eq. (2.6). A simple introduction to this approximation is given in Butler (2007, Sections 1.2.1 and 2.3.2). The expression on the right of Eq. (2.7) has a removable singularity at $\hat{s} = 0$, which occurs for the value t_s, where t_s is the solution to $c = \mathbb{E}(X_{t_s})$. As $t \to t_s$ the approximation in Eq. (2.7) approaches $1/2 + \mathscr{K}'''_{X_{t_s}}(0)/\{6\sqrt{2\pi}[\mathscr{K}''_{X_{t_s}}(0)]^{3/2}\}$, which is $1/2$ with an additive standardized skewness term.

Note that if $\{X_t, t \geq 0\}$ follows a Lévy process, the MGF of X_t can be expressed as

$$\mathscr{M}_{X_t}(s) = [\mathscr{M}_Y(s)]^t,$$

where the random variable Y is the degradation in a unit time interval and hence, the CGF of X_t can be expressed as $\mathscr{K}_{X_t}(s) = t\mathscr{K}_Y(s)$, which is a function of time t.

In the following subsections, we illustrate the inaccuracy in the left-tail of the FPT distribution when approximating the survival function of T_c using the Balakrishnan and Qin (2019) approximation in Eq. (2.2) and compare different methods to approximate the FPT distribution. Three different methods to approximate the CDF/survival function of the FPT T_c are considered:

(i) The Balakrishnan and Qin (2019) saddlepoint approximation in Eq. (2.2) (BQ);

(ii) The Lugannani and Rice (1980) saddlepoint approximation in Eq. (2.7) (LR);

(iii) The Birnbaum and Saunders (1969) approximation in Eq. (1.2) (BS).

The gamma process and the IG process are reviewed and different methods for approxi-

mating the FPT distribution are compared under some specific parameter settings following the settings studied in Balakrishnan and Qin (2019). We shall see that the Lugannani and Rice (1980) approximation is consistently most accurate.

2.2.3. Gamma degradation process

The FPT distribution can be approximated for the Gamma(α,β) degradation process from the LR method by substituting the gamma CGF in Eq. (2.6) and then applying Eq. (2.7). The singularity point is, therefore, $t_s = c/(\alpha\beta)$.

2.2.3.1. Gamma(1, 1) process

We consider a gamma degradation process with associated parameters $\alpha = 1$, $\beta = 1$ and the threshold level $c = 10$. The FPT distribution of the degradation process is approximated by the three aforementioned methods: LR, BQ and BS methods. The resulting approximated survival functions for the FPT are shown in Figure 2.1. We also present the approximated $100p$-th percentile of the FPT distribution based on the four different methods with $p = 0.05(0.05)0.90$ in Table 2.1. From Figure 2.1 and Table 2.1, we observe that the LR method provides an approximate distribution close to the true distribution, while the BQ and BS methods deviate from the true.

It is noteworthy that the approximation based on the BQ method results in a substantial deviation from about 12 (above the approximated mean of 10.5) to 0 and the approximated survival curve contains values above one creating an approximate distribution which is improper. The BQ saddlepoint procedure only attains the same accuracy as LR at the 90-th percentile when the saddlepoint $\hat{s}$ is sufficiently far from the pole at $s = 0$. For percentiles 5-th to 85-th, the saddlepoint $\hat{s}$ is close enough to 0 to render the accuracy of the BQ method less than that of the LR method.

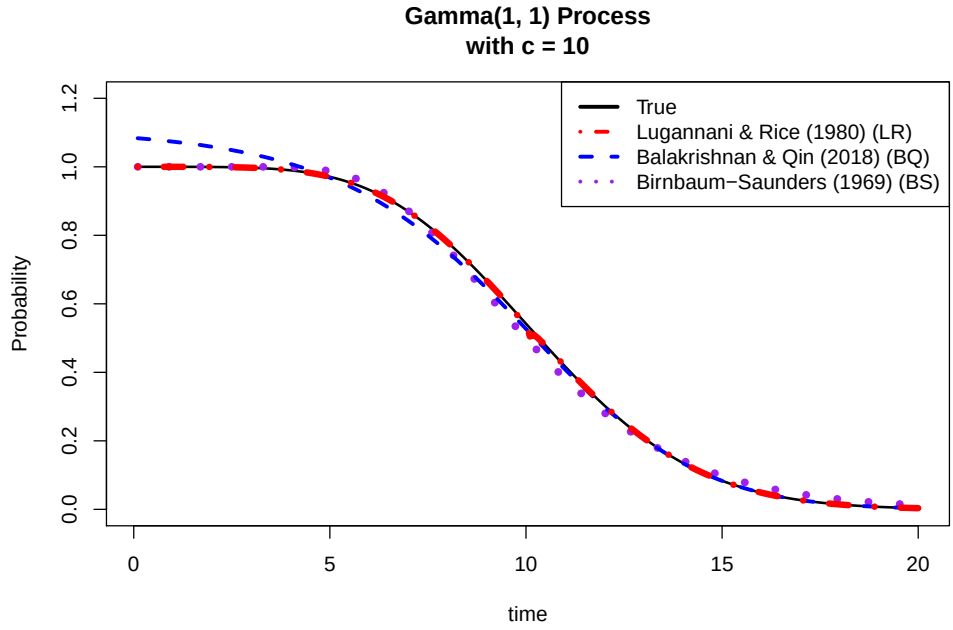

Figure 2.1: Approximate survival functions for FPT of the Gamma(1, 1) degradation process with $c = 10$ based on three different methods.

To further compare the three approximation methods, we consider different threshold levels for the Gamma (1, 1) process with $c = 1(1)10$ and plot the corresponding approximated 5-th, 10-th and 90-th percentiles of the FPT distributions in Figure 2.2. From Figures 2.2(a) and 2.2(b), we observe that the approximated 5-th percentiles and 10-th percentiles of the BQ method deviate quite far from the true values as compared with the LR method. From Figure 2.2(c), except for the BS method, both the LR and BQ methods provide approximate 90-th percentiles, which are close to the values obtained by the true distribution. As in Table 2.1, the 90-th percentiles have saddlepoints $\hat{s}$, which are sufficiently far from the pole at $s = 0$ so accuracy is not impaired.

Figure 2.3 illustrates the FPT distribution of the Gamma (1,1) process approximated using the steepest descents approximation methods explained in Eq. (2.5) and Eq. (2.2). As can be seen, these approximation methods are only capable of approximating the FPT distribution on one tail side, whereas the LR method provides accurate approximation in both tails.

Table 2.1: Approximate $100p$-th percentiles of the FPT distribution of the Gamma(1, 1) degradation process with threshold level $c = 10$.

p	True	LR	BQ	BS	p	True	LR	BQ	BS
0.05	5.62	5.62	5.38	5.98	0.50	10.34	10.31	10.23	10.00
0.10	6.58	6.58	6.22	6.69	0.55	10.74	10.74	10.65	10.41
0.15	7.25	7.25	6.91	7.22	0.60	11.15	11.14	11.08	10.83
0.20	7.80	7.80	7.50	7.67	0.65	11.58	11.58	11.52	11.29
0.25	8.29	8.29	8.03	8.08	0.70	12.04	12.04	11.99	11.80
0.30	8.73	8.73	8.51	8.47	0.75	12.54	12.54	12.51	12.37
0.35	9.15	9.15	8.96	8.85	0.80	13.11	13.11	13.08	13.04
0.40	9.55	9.54	9.39	9.23	0.85	13.78	13.78	13.77	13.86
0.45	9.94	9.87	9.81	9.61	0.90	14.64	14.64	14.64	14.96

2.2.3.2. Gamma(10, 1) process

We consider a gamma degradation process with associated parameters $\alpha = 10$, $\beta = 1$ and threshold level $c = 10$. Once again, the FPT distribution of the degradation process is approximated by the three aforementioned methods, LR, BQ and BS. The approximate quantile functions of the FPT of the Gamma(10, 1) process based on the three different methods are presented in Figure 2.4.

From Figure 2.4, the quantile function using the LR method is accurate for all p, while the BQ method is less accurate for $p < 0.8$. Plots of the approximate 5-th, 10-th and 90-th percentiles of the FPT distributions for the Gamma (10, 1) process with thresholds $c = 1(1)10$ are shown in Figure 2.5. Only at the 90-th percentile does the BQ method provides similar accuracy to the LR method.

2.2.4. Inverse-Gaussian degradation process

The FPT distribution of a IG(μ,λ) degradation process using the LR saddlepoint ap-

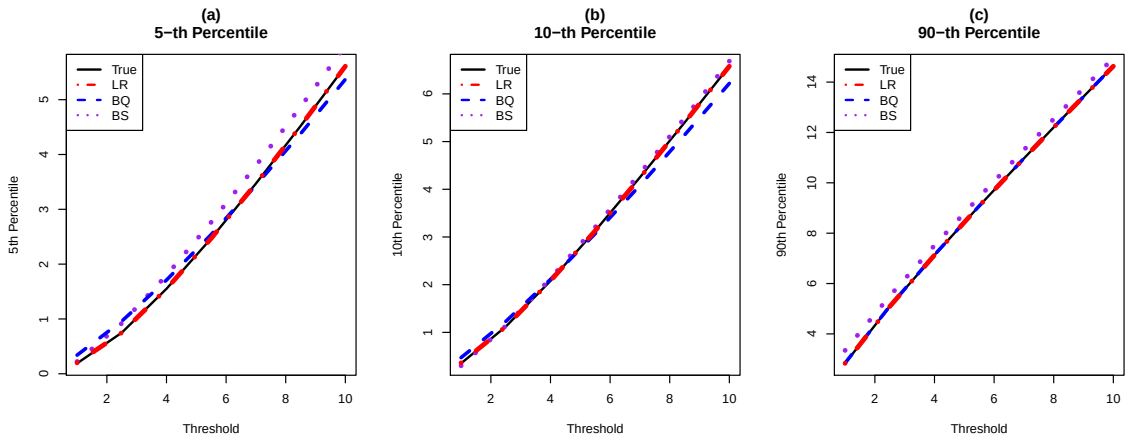

Figure 2.2: Approximate 5-th, 10-th, and 90-th percentiles of the FPT distribution of the Gamma(1, 1) degradation process with $c = 1(1)10$.

proximation method can be approximated by substituting the IG CGF in Eq. (2.6) and then applying Eq. (2.7). The singularity point is, therefore, $t_s = c/\mu$.

2.2.4.1. IG(1, 10) process

We consider an IG degradation process with parameters $\mu = 1$, $\lambda = 10$. Figure 2.6 shows the approximated FTP distributions for the IG(1, 10) process with a threshold level $c = 10$ based on the LR, BQ and BS methods. As with the gamma degradation processes, left-tail inaccuracy of the BQ method remains, while the LR and BS approximations closely follow the true distribution. In addition to the IG(1, 10) process, we also studied the performance of these approximation methods with different parameter settings. We found that for some parameter settings with small threshold levels, the LR method may perform poorly for the IG process. This issue will be addressed in Section 2.5.

From the numerical illustrations in this section, we can conclude that the LR approximation outperforms both BQ and BS approximations of gamma and IG processes. The BQ method is deficient below the 90-th percentile and the BS method can be deficient throughout.

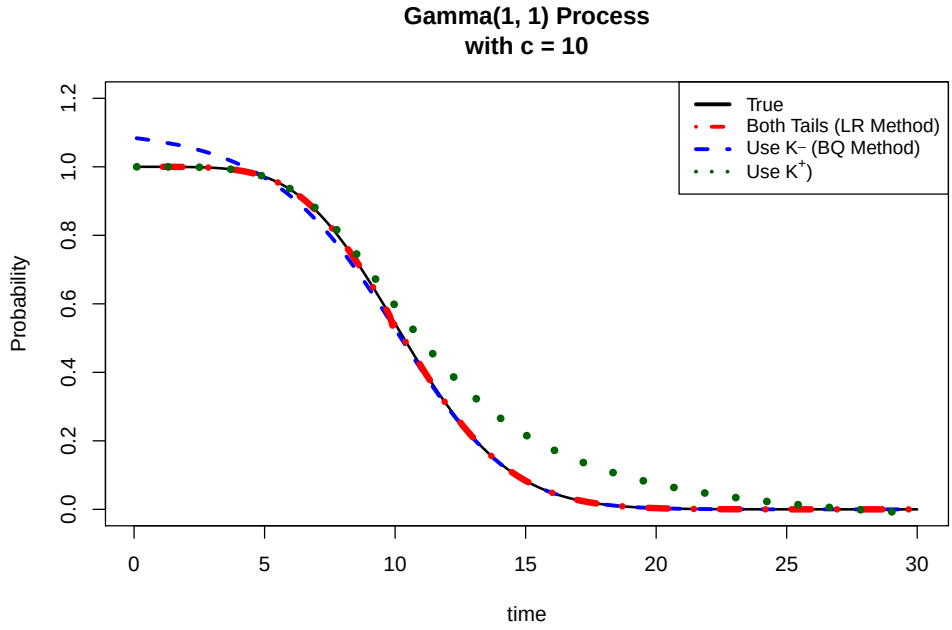

Figure 2.3: Steepest descents approximation methods

2.3. Empirical Saddlepoint Approximation

Balakrishnan and Qin (2019) applied the ESA to approximate the FPT distribution of a degradation process under the implicit assumption that the degradation measurements are taken with equal time intervals. In this subsection, we abandon the equal time interval assumption and propose several methods along with the ESA to deal with the situation that the degradation measurements are taken with unequal time intervals. The proposed methods will broaden the range of possible applications for the ESA since degradation measurements are not necessary taken with equal time intervals in practice.

2.3.1. ESA with equal time intervals

If $\{X_t, t \geq 0\}$ follows a Lévy process, then the MGF of X_t can be expressed as $\mathscr{M}_{X_t}(s) = [\mathscr{M}_Y(s)]^t$, where the random variable Y is independent of variable t (i.e., Y is degradation

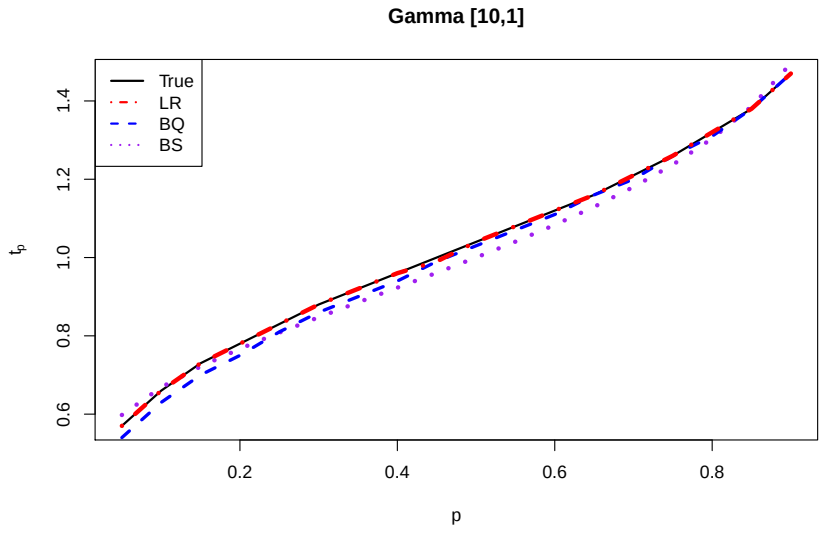

Figure 2.4: Approximate quantile functions of the FPT for the Gamma(10, 1) degradation process with $c = 10$.

for 1 unit of time) even when the degradation measurements are taken at unequal time intervals. For example, if X_t follows a Gamma(α, β) process described in Section 2.2.3, then the MGF of X_t can be expressed as

$$\mathscr{M}_{X_t}(s) = (1-\beta s)^{\alpha t} = [\mathscr{M}_Y(s)]^t, \tag{2.8}$$

where Y is a random variable named degradation per unit time interval, which follows a $gamma(\alpha, \beta)$ distribution and is independent of variable t.

We denote the difference between two consecutive measurements as $\Delta X_i = X_{t_i} - X_{t_{i-1}}$ and the time interval between these measurements is $\Delta t_i = t_i - t_{i-1},\ i = 1, 2, \ldots, m$. Let $\Delta x_1, \Delta x_2, \ldots, \Delta x_m$ be the observed values of the random variables $\Delta X_1, \Delta X_2, \ldots, \Delta X_m$, respectively. If these measurements are taken at equal time intervals, those time intervals can be rescaled as increments of 1. Therefore, without loss of generality, we assume these measurements are taken with unit time intervals (i.e., $\Delta t_i = \Delta t_0 = 1$ for $i = 1, 2, \ldots, m$). Then, the empirical MGF and CGF of the Lévy process at time t are given by

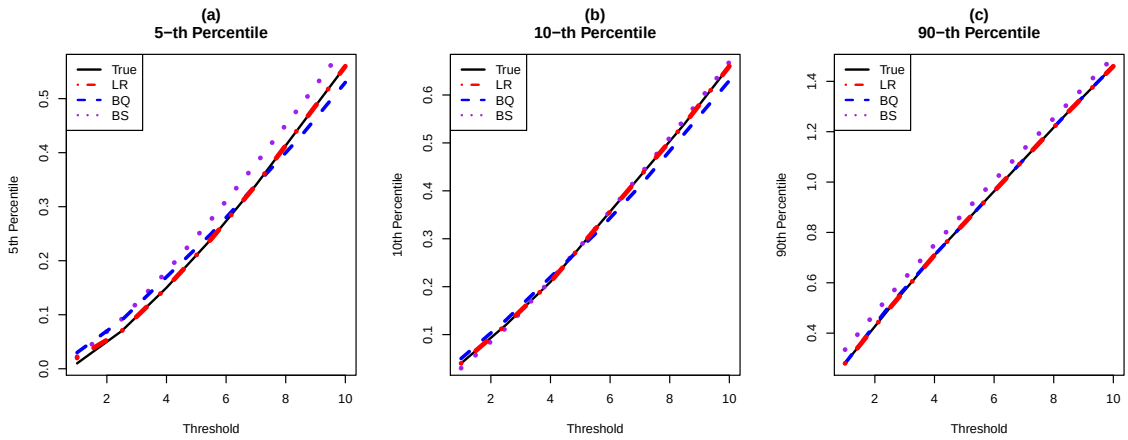

Figure 2.5: Approximate 5-th, 10-th and 90-th percentiles of the FPT distribution of the Gamma(10, 1) degradation process with $c = 1(1)10$.

$$\hat{\mathscr{M}}_{X_t}(s) = \left\{ \frac{1}{m} \sum_{i=1}^{m} \exp(s\Delta x_i) \right\}^t, \tag{2.9}$$

$$\hat{\mathscr{K}}_{X_t}(s) = t \ln \left\{ \frac{1}{m} \sum_{i=1}^{m} \exp(s\Delta x_i) \right\}. \tag{2.10}$$

The empirical saddlepoint method consists of using $\hat{\mathscr{M}}_{X_t}(s) = [\hat{\mathscr{M}}_Y(s)]^t$ as a surrogate for the true unknown $\mathscr{M}_{X_t}(s) = [\mathscr{M}_Y(s)]^t$ in the saddlepoint expressions in Eq. (2.7), for the LR approximation, and in Eq. (2.2) for the approximation of BQ. This is analogous to the bootstrap approach in which the empirical CDF $\hat{F}$ is used as a surrogate for the true unknown F when estimating functionals of F. This is why the empirical saddlepoint method can be referred to as "bootstrapping in the transform domain" as discussed in Butler (2007, Chapter 14).

There are limitations to such plug-in methods. For example, $\hat{\mathscr{M}}_{X_t}(s)$ is analytic for all values of s, while the true $\mathscr{M}_{X_t}(s)$ is analytic for $\mathrm{Re}(s) \in (-\infty, 1)$ or $(-\infty, 5]$ for the gamma and IG process examples. The singularities of $\mathscr{M}_{X_t}(s)$ at 1 and 5 convey information about the right tail of the distribution for X_t, which cannot be captured by $\hat{\mathscr{M}}_{X_t}(s)$, which has no

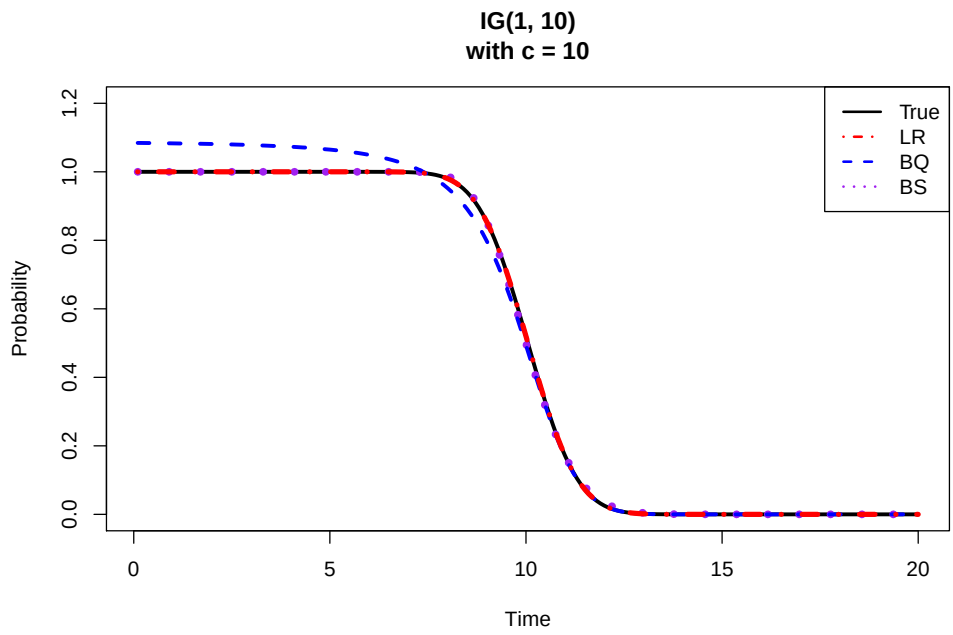

Figure 2.6: FPT distribution of IG(1,10) degradation process with $c = 10$

such singularity.

Another issue is the existence of the ESA. If the data used to compute $\hat{\mathscr{M}}_Y$ range from $\Delta x_{\min}$ to $\Delta x_{\max}$, then the span of the support of this distribution is the open interval $(\Delta x_{\min}, \Delta x_{\max})$. This means that $\hat{\mathscr{M}}_Y$ reflects a distribution with no tails unlike $\mathscr{M}_Y$.

2.3.1.1. Requirement for equal time intervals

In the parametric approach, we assume a parametric form for the distribution of Y. The unknown parameters in the model can be estimated based on the observed degradation data using different methods (e.g., maximum likelihood estimation method), and hence, the distribution of X_t can be determined for each time t no matter if the degradation measurements are taken at equal or unequal time intervals. In this case, the distribution of

ΔX_i is $gamma(\alpha\Delta t_i, \beta)$ and the MGF of ΔX_i is

$$\mathscr{M}_{\Delta X_{t_i}}(s) = (1-\beta s)^{\alpha\Delta t_i} = [\mathscr{M}_Y(s)]^{\Delta t_i}. \tag{2.11}$$

However, for the ESA, the MGF and the CGF are statistics that depends on the observed degradation data. If $X_t = \sum_{i=1}^{m} \Delta X_i$, the empirical MGF of X_t can be written as

$$\hat{\mathscr{M}}_{X_t}(s) = \left[\frac{1}{m}\sum_{i=1}^{m} \exp(s\Delta x_i)\right]^t = [\hat{\mathscr{M}}_Y(s)]^t.$$

The presumption made here is that $\Delta X_1, \ldots, \Delta X_m$ have the common distribution of Y. This only holds when $\Delta t_i = \Delta t_0$ for all i. If measurements are taken with unequal time intervals, we suggest modified CGF methods and data imputation techniques in Section 2.3.5 to approximate the FPT distribution using the ESA.

2.3.1.2. Validity of $\hat{\mathscr{M}}_{X_t}(s)$

While $\hat{\mathscr{M}}_Y(s) = m^{-1}\sum_{i=1}^{m} \exp(s\Delta x_i)$ is an MGF which places mass $1/m$ at each datum, $[\hat{\mathscr{M}}_Y(s)]^t$ is not an MGF when t is not a positive integer. Since we are allowing t to vary continuously with time, this raises questions about the validity of using the empirical saddlepoint method both here and in Balakrishnan and Qin (2019).

In the equally-spaced setting with common increment Δt_0, $\hat{\mathscr{M}}_Y(s)$ is an unbiased estimate of $\mathscr{M}_Y(s)$, the MGF for the amount of degradation in time Δt_0. Therefore, at grid points $\mathscr{G}_{\Delta t_0} = \{k\Delta t_0 : k \in \mathbb{I}^+\}$ the saddlepoint approximation is formally valid since at $t = k\Delta t_0$ the degradation is $[\hat{\mathscr{M}}_Y(s)]^k$ and this is an MGF. For values of $t \notin \mathscr{G}_{\Delta t_0}$, the saddlepoint approximation is not formally valid; however, it still provides a smooth interpolation in between the grid points.

Once the FPT distribution is obtained through the ESA method, the essential step is to estimate the moments of the FPT distribution. In following section, we discuss the moment estimates for the FPT distribution from the ESA method.

2.3.2. Properties of ESA

The following theorem provides an approximation for the first and second moments of the FPT of a degradation process which follows a Lévy process with a threshold level c.

THEOREM 1. *The residue approximation given into the MTTF (i.e., the first moment of T_c) and the second moment of T_c are, respectively,*

$$\mathbb{E}(T_c) \simeq \frac{c}{\mathscr{K}_Y'(0)} + \frac{\mathscr{K}_Y''(0)}{2\{\mathscr{K}_Y'(0)\}^2} \tag{2.12}$$

$$\text{and } \mathbb{E}(T_c^2) \simeq \frac{1}{\{\mathscr{K}_Y'(0)\}^2}\left[c\left\{2\frac{\mathscr{K}_Y''(0)}{\mathscr{K}_Y'(0)} + c\right\} + \frac{3}{2}\left\{\frac{\mathscr{K}_Y''(0)}{\mathscr{K}_Y'(0)}\right\}^2 - \frac{2}{3}\frac{\mathscr{K}_Y'''(0)}{\mathscr{K}_Y'(0)}\right]. \tag{2.13}$$

The proof of Theorem 1 is presented in A.1. The error integral is shown to be at most $O(e^{-(b-\varepsilon)c})$ as $c \to \infty$ in the following theorem.

THEOREM 2. *Subject to condition AC below on $\mathscr{K}_Y$, an upper bound for $|E|$ is $O(e^{-(b-\varepsilon)c})$ as $c \to \infty$ for some small $\varepsilon > 0$ where b is the upper boundary for convergence of $\mathscr{K}_Y$.*

(AC) For some $\varepsilon > 0$ and $\alpha \in (0, \pi/2)$, $\mathscr{K}_Y$ can be analytically continued into the sector $S_{\varepsilon,\alpha} = \{s_{r\phi} = b - \varepsilon + r\varepsilon^{i\phi} \in \mathbb{C} : r > 0, \phi \in [\alpha, \pi/2]\}$. Furthermore, within this sector, suppose

$$\min_{\alpha \le \phi \le \pi/2} \left|\mathscr{K}_Y(b - \varepsilon + r\varepsilon^{i\phi})\right| \to \infty \qquad r \to \infty.$$

The proof of Theorem 2 is presented in Appendix A.2. Condition AC holds for all pre-

viously considered Lévy processes such as gamma, inverse-Gaussian, and Wiener processes.

Since $\mathscr{K}_Y'(0)$ and $\mathscr{K}_Y''(0)$ are the mean and variance of Y, respectively, the first moment of T_c in Eq. (2.12) is analogy to the first moment of the FPT distribution obtain from the BS approximation (Park and Padgett, 2005). The major advantage of Eqs. (2.12) and (2.13) is that using statistics based on Y, we can estimate the first and second moments of the FPT distribution nonparametrically.

2.3.3. Estimation of MTTF based on the ESA

From Theorem 1, the MTTF estimate obtained from the ESA method for a degradation process, X_t, with threshold level c, is given by

$$\widehat{T_{ESA}} = \widehat{\mathbb{E}}(T_c) = \frac{c}{\bar{y}} + \frac{s_y^2}{2\bar{y}^2}, \tag{2.14}$$

where $\bar{y} = \sum_{j=1}^{m} \Delta x_j$ and $s_y = \sqrt{\sum_{j=1}^{m} \{\Delta x_j - \bar{y}\}^2/(m-1)}$ are the sample mean and the sample standard deviation of the sample degradation measurements per unit interval (i.e., Y), respectively. The confidence interval for the estimate in Eq. (2.14) can be obtained by using Taylor series expansion with normal approximation. Suppose the $\Delta x_1, \Delta x_2, \ldots, \Delta x_m$ are the observed differences at unit time intervals from a Lévy process with a threshold level c.

The estimate for MTTF in Eq. (2.14) is approximated for larger threshold values (i.e. $c >>$) as $\widehat{\mathbb{E}}(T_c) \approx c/\bar{y}$. By taking Taylor series expansion, we can obtain the variance of $\widehat{\mathbb{E}}(T_c)$ as $\mathbb{V}(\widehat{\mathbb{E}}(T_c)) \approx (c^2/\mu_Y^4)\sigma_Y^2$, where μ_y and σ_Y^2 are the population mean and variance of the degradation measurements per unit interval (i.e., Y), respectively. Therefore, the

variance of the estimate in Eq. (2.14) can be approximated as

$$\widehat{\mathbb{V}}\left(\widehat{T_{ESA}}\right) \approx \left(\frac{c^2}{\bar{y}^4}\right) s_y^2. \tag{2.15}$$

Note that approximation in Eq. (2.15) of the variance of the FPT distribution can also be applied to all the parametric Lévy processes such as Wiener, gamma and IG processes.

2.3.4. Advantage of the ESA under model uncertainty

In majority of settings where degradation data are collected, we do not have information about the underlying distribution of the degradation process. If the degradation process is known to be monotonic, the FPT distribution of that process can be evaluated based on either the gamma process or the IG process. In addition, a monotonic degradation process can be analyzed with the Wiener process. Nevertheless, the ESA facilitates the estimation of the FPT distribution without any distributional assumptions if the degradation process is monotonic. Here, a Monte Carlo simulation study is used to investigate the effect of mis-specifying the underlying degradation process and to demonstrate the advantages of the ESA based on the LR method using Eq. (2.7).

In the simulation study, we generate the degradation data from a known degradation process and then obtain the approximated FPT distributions based on assuming different degradation processes with LR saddlepoint approximation using maximum likelihood estimates (MLEs) and the ESA. We consider generating the degradation data from the Gamma(1, 2), Gamma(0.5, 4), IG(2, 5), and IG(2, 10) processes with 10 items ($n = 10$), time points for the last measurement as 30 ($t_m = 30$) and different threshold values ($c =$ 60 and 100). The performance of the approximated FPT distributions are evaluated using mean squared errors (MSEs) for the estimated 5-th, 10-th and 90-th percentiles of the FPT distributions. The results based on 1000 simulations for each setting are presented in Tables 2.2 and 2.3.

Table 2.2: Simulated MSEs of the estimates of 5-th, 10-th and 90-th percentiles based on assuming different degradation models using the LR saddlepoint approximation and ESA when the data are generated from the Gamma(1, 2) and Gamma(0.5, 4) processes.

			True Process: Gamma(1, 2)				True Process: Gamma(0.5, 4)			
5-th percentile			Assumed Process				Assumed Process			
n	t_m	c	Gamma	IG	Wiener	ESA	Gamma	IG	Wiener	ESA
10	30	60	2.3	87.7	2.5	2.5	4.1	278.1	4.7	4.6
10	30	100	7.0	211.4	7.4	7.6	13.2	893.6	13.3	14.3
			True Process: Gamma(1, 2)				True Process: Gamma(0.5, 4)			
10-th percentile			Assumed Process				Assumed Process			
n	t_m	c	Gamma	IG	Wiener	ESA	Gamma	IG	Wiener	ESA
10	30	60	2.5	48.6	2.5	2.5	4.5	210.3	4.7	4.8
10	30	100	7.3	118.9	7.4	7.8	14.3	656.9	13.7	15.0
			True Process: Gamma(1, 2)				True Process: Gamma(0.5, 4)			
90-th percentile			Assumed Process				Assumed Process			
n	t_m	c	Gamma	IG	Wiener	ESA	Gamma	IG	Wiener	ESA
10	30	60	3.8	186.0	4.0	3.9	9.0	378.8	9.6	9.3
10	30	100	10.6	387.7	10.5	10.7	23.1	1229.7	22.7	22.4

From Table 2.2, we observe that when the degradation data are generated from the gamma process and mis-specified as IG process, the MSEs for the estimated percentiles are significantly larger than the case where the model is correctly specified. From Table 2.3, when the data are generated from the IG process, it appears that there is no substantial difference in the MSEs if the process is mis-specified as the gamma or Wiener processes. In Tables 2.2 and 2.3, the ESA provides estimates of the percentiles with MSEs closest to the estimates when the model is correctly specified in most cases. Complete simulation results for $n = 20$ and $t_m = 30$ cases are presented in Section A.3 of Appendix A.

These results demonstrate the advantages of the ESA under model mis-specification and we would suggest using the ESA in practice. Moreover, it may not be a good idea to assume an IG process when the underlying degradation process is unknown.

Table 2.3: Simulated MSEs of the estimates of 5-th, 10-th and 90-th percentiles based on assuming different degradation models using the LR saddlepoint approximation and ESA when the data are generated from the IG(2, 5) and IG(2, 10) processes.

			True Process: IG(2, 5)				True Process: IG(2, 10)			
5-th percentile			Assumed Process				Assumed Process			
n	t_m	c	IG	Gamma	Wiener	ESA	IG	Gamma	Wiener	ESA
10	30	60	1.3	1.7	1.4	1.4	0.6	0.7	0.7	0.7
10	30	100	3.7	4.5	3.9	3.9	1.8	1.9	1.9	1.9
			True Process: IG(2, 5)				True Process: IG(2, 10)			
10-th percentile			Assumed Process				Assumed Process			
n	t_m	c	IG	Gamma	Wiener	ESA	IG	Gamma	Wiener	ESA
10	30	60	1.3	1.5	1.3	1.3	0.6	0.7	0.6	0.6
10	30	100	3.7	4.2	3.8	3.8	1.8	1.9	1.8	1.8
			True Process: IG(2, 5)				True Process: IG(2, 10)			
90-th percentile			Assumed Process				Assumed Process			
n	t_m	c	IG	Gamma	Wiener	ESA	IG	Gamma	Wiener	ESA
10	30	60	1.3	1.5	1.3	1.3	0.6	0.7	0.7	0.6
10	30	100	3.6	3.9	3.7	3.7	1.8	1.8	1.8	1.8

2.3.5. ESA for data with unequal time intervals

Using the ESA in Eq. (2.10), we make the implicit assumption that the degradation measurements are taken at equal time intervals as mentioned in Section 2.3.1. In this section, we propose several modifications that can be used with the ESA to approximate the FPT distribution when degradation data are obtained with unequal time intervals. Based on our preliminary studies, the ESA using the LR method is most appropriate; therefore, we only consider the LR method for data with unequal time intervals.

2.3.5.1. Modified empirical CGF

To incorporate the unequal time intervals into the ESA, we first propose a simple mod-

ification of the empirical CGF as

$$\hat{\mathscr{K}}_{X_t^*}(s) \approx t \log \left\{ \frac{1}{m} \sum_{i=1}^{m} \exp\left(s \frac{\Delta x_i}{\Delta t_i} \right) \right\}. \tag{2.16}$$

The empirical MGF in curly brackets represents an estimate of the degradation per unit of time. In addition, we propose three different data imputation techniques to account for unequal spacing.

2.3.5.2. Data Imputation Techniques

These proposed data imputation methods only require the general assumption that the degradation process follows a Lévy process. The techniques are built upon setting the unit time interval as the highest common factor (HCF) of the different time intervals and then imputing the missing values. The analysis is then based on the pseudo-completed degradation data with equal time intervals.

Suppose $\{X_t : t \geq 0\}$ is a Lévy process and the degradation measurements, $x_t = \{x_{t_0}, x_{t_1}, \ldots, x_{t_m}\}$, are taken at time points $t = \{t_i; i = 1, 2, \ldots, m\}$. Let the i-th time interval be $\Delta t_i = t_i - t_{i-1}$ with $t_0 = 0$. We define the pseudo-unit-time-interval, $\Delta t_0 = HCF\{\Delta t_i : i = 1, \ldots, m\}$. The Highest Common Factor (HCF) is the largest real number, which when used to divide the time increments leads to all the ratios as positive integers. In this setting, the saddlepoint approximation is formally valid on grid $\mathscr{G}_{\Delta t_0}$ and interpolates for values of t in between. For example, suppose the degradation measurements are measured at time $t = \{4, 6, 10, 14, 18, 24, 32\}$, then we have $\Delta t_0 = HCF(2, 4, 6, 8) = 2$.

We define the number of pseudo-unit-time intervals inside the i-th interval $(t_{i-1}, t_i]$ as

$$\ell_i = \frac{t_i - t_{i-1}}{\Delta t_0} = \frac{\Delta t_i}{\Delta t_0},$$

and the total number of pseudo-unit-time-intervals up to time t_i (i.e., in $(0,t_i]$] as

$$k_i = \sum_{j=1}^{i} \ell_j,$$

for $i = 1,2,\ldots,m$, with $k_0 = 0$. Therefore, the imputed pseudo-complete degradation data with unit-time-interval Δt_0 contains $k_m = \sum_{j=1}^{m} \ell_j$ degradation measurements including those m observed degradation measurements $x_{t_1}, x_{t_2}, \ldots, x_{t_m}$. We denote the imputed pseudo-complete degradation data as $(y_1, y_2, \ldots, y_m)$, where

$$\begin{aligned} y_i &= (y_{k_{i-1}+1}, y_{k_{i-1}+2}, \ldots, y_{k_{i-1}+\ell_i-2}, y_{k_{i-1}+\ell_i-1}, y_{k_{i-1}+\ell_i}) \\ &= (y_{k_i-\ell_i+1}, y_{k_i-\ell_i+2}, \ldots, y_{k_i-2}, y_{k_i-1}, y_{k_i}), \end{aligned}$$

with $y_{k_i} = x_{t_i}$ for $i = 1,2,\ldots,m$. Hence, in the i-th interval $(t_{i-1}, t_i]$, there are $\ell_i - 1$ measurements, $(y_{k_i-\ell_i+1}, y_{k_i-\ell_i+2}, \ldots, y_{k_i-2}, y_{k_i-1})$ which need to be imputed. Figure 2.7 illustrates the data imputation scheme in the i-th interval.

To impute the degradation data with pseudo-unit-time-interval Δt_0 when $\ell_i \neq 1$, we define the unit-drift in the i-th time interval $(t_{i-1}, t_i]$ as

$$\delta_i = \left(\frac{x_{t_i} - x_{t_{i-1}}}{t_i - t_{i-1}} \right) \Delta t_0, \tag{2.17}$$

and obtain the set of m unit-drifts as $\delta = \{\delta_1, \delta_2, \ldots, \delta_m\}$ for m time intervals. We propose the following three data imputation methods to obtain the pseudo-complete degradation data with unit-time-interval Δt_0.

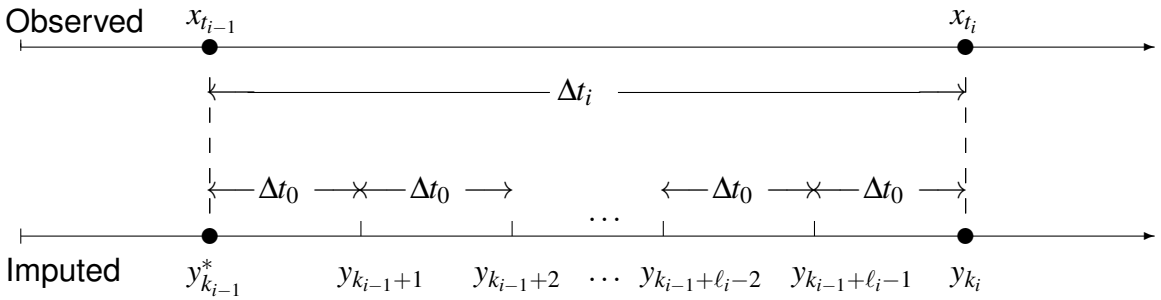

Figure 2.7: A schematic diagram for the data imputation method in the i-th interval $(t_{i-1}, t_i]$.

Linear Imputation Method (LImp): For the LImp method, we assume the change in the degradation measurements at time t_{i-1} to time t_i follows a linear relationship. We impute all the missing increments in the time interval $(t_{i-1}, t_i]$ with δ_i (i.e., the corresponding drift of the particular time interval). Specifically, in the i-th interval $(t_{i-1}, t_i]$, after setting $y_{k_i} = x_{t_i}$, we impute the other values in y_i as

$$y_{k_i - j} = y_{k_i} - j\delta_i = x_{t_i} - j\delta_i,$$

for $j = 1, 2, \ldots, \ell_i - 1$ and $i = 1, 2, \ldots, m$.

Random Imputation Method (RImp): For the RImp method, we assume that all the n items under the degradation test are measured at the same time points and the increments of the degradation measurements follows the same distribution. Hence, we can create the unit-drift sampling frame for the n items as $(\delta_1, \delta_2, \ldots, \delta_n)$ where $\delta_l = \{\delta_{l1}, \delta_{l2}, \ldots, \delta_{lm}\}$ is the set of unit-drifts for the l-th item ($l = 1, 2, \ldots, n$). In the i-th interval $(t_{i-1}, t_i]$, after setting $y_{k_i} = x_{t_i}$, the other values in y_i can be imputed by the following algorithm:

1. Set $L = y_{k_{i-1}}$ and COUNT = 0;

2. Draw a random sample of n values with replacement from the unit-drifts $\{\delta_{1i}, \delta_{2i}, \ldots, \delta_{ni}\}$

and denote each as δ_i^*;

3. For each item set $y_{k_{i-1}+1} = L + \delta_i^*$, then set $L = y_{k_{i-1}+1}$ and COUNT = COUNT + 1;

4. If COUNT $< \ell_i - 1$, repeat Steps 2 and 3.

Conditional Random Imputation Method (CRImp): Note that the RImp method described above may result in negative increment at the last imputation in the i-th interval, i.e., it is possible that $x_{t_i} - y_{k_i-1} < 0$. Although the ESA does not require all the increments to be positive, it may not be appropriate if a monotone degradation process is under consideration. Therefore, we propose here the CRImp method, which ensures that all the increments are positive by using a constrained sampling frame. In the i-th interval $(t_{i-1}, t_i]$, after setting $y_{k_i} = x_{t_i}$, the other values in y_i can be imputed by the following algorithm:

1. Set $L = y_{k_{i-1}}$ and COUNT = 0;

2. Draw a random sample of n values with replacement from the constrained sampling frame $\{\delta_{1i}, \delta_{2i}, \ldots, \delta_{ni} : \delta_{li} < x_{t_i} - L, l = 1, 2, \ldots, n\}$, denote each as δ_i^*;

3. Set $y_{k_{i-1}+1} = L + \delta_i^*$, then set $L = y_{k_{i-1}+1}$ and COUNT = COUNT + 1;

4. If COUNT $< \ell_i - 1$, repeat Steps 2 and 3.

Numerical example to illustrate the proposed modified empirical CGF method and the three imputation methods: Based on a degradation data generated from the Gamma(1, 2) process with threshold value $c = 100$, sample size $n = 10$, $m = 12$ and **t** = {1, 6,13, 14, 19, 26, 27, 32, 39, 40, 45, 52}; we have $\Delta t_1 = \Delta t_4 = \Delta t_7 = \Delta t_{10} = 1$, $\Delta t_2 = \Delta t_5 = \Delta t_8 = \Delta t_{11} = 5$ and $\Delta t_3 = \Delta t_6 = \Delta t_9 = \Delta t_{12} = 7$ with the pseudo-unit-time-interval $\Delta t_0 = HCF(1, 5, 7) = 1$. In Figure 2.8, the approximated FPT distributions obtained by the modified ESA in Eq. (2.16) and the three proposed data imputation methods are presented. The approximated FPT distribution based on the ESA without modification is also

presented. The FPT distribution obtained based on the MLEs of parameters in the gamma degradation model is used as the reference distribution (i.e., $\Pr(T_c > t) = G_{X_t}(c; \hat{\alpha}t, \hat{\beta})$, the $gamma(\hat{\alpha}t, \hat{\beta})$ CDF at c). The ESA without adjustment is very inaccurate. The random imputation and conditional imputation methods provide approximated FPT distributions, which are close to the reference distribution. To further evaluate the performance of the proposed methodologies in adjusting for the unequal time intervals, a Monte Carlo simulation study is used in the following subsection.

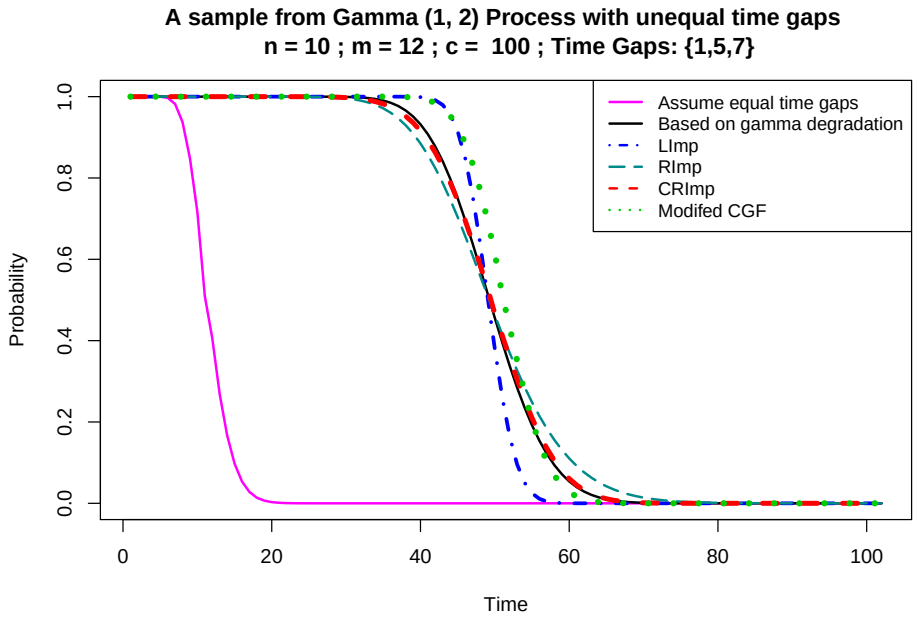

Figure 2.8: Approximated FPT distributions based on the ESA with and without modifications.

2.3.6. Monte Carlo simulation study for unequal time intervals situations

A Monte Carlo simulation study is carried out to evaluate the performance of the data imputation methods and the modified CGF method. The degradation data are generated from gamma, IG and Wiener degradation processes with time gaps $\{1,3,5\}$ (i.e., degradation data are measured at time $t_1 = 1$, $t_2 = 4$, $t_3 = 9$, $t_4 = 10$, $t_5 = 13$, $t_6 = 18$, $\ldots$). We

consider generating the degradation data from the Gamma(1, 2), Gamma(0.5, 4), IG(2, 5), and IG(2, 10) processes with 10 items ($n = 10$), 11 time points ($m = 11$ with $t_m = 31$) and different threshold values ($c = 60$ and 100). The performance of the approximated FPT distributions are evaluated using the MSEs of the estimated 5-th, 10-th and 90-th percentiles of the true FPT distributions. The results used on 10000 simulations for each setting and are presented in Tables 2.4 and 2.5 for the gamma and IG, respectively.

From the results in Tables 2.4 and 2.5, we observe that in most cases the conditional random imputation method (CRImp) gives MSEs closest to the LR parametric saddlepoint approximation based on the correct degradation process. However, the LR parametric saddlepoint approximation required specification of the underlying degradation model, while the other methods using the ESA did not. Overall, based on the simulation results presented here, we would recommend the use of the ESA in Eq. (2.7) with the conditional random imputation method to adjust for unequal time intervals. Complete simulation results for $n = 20$ and $t_m = 54$ cases are presented in Section A.4 of Appendix A.

Table 2.4: Simulated MSEs of the estimates of 5-th, 10-th and 90-th percentiles based on LR parametric saddlepoint approximation, modified CGF and different data imputation methods when the data are generated from the Gamma(1, 2) and Gamma(0.5, 4) processes.

5-th percentile			Simulated from Gamma(1, 2)					Simulated from Gamma(0.5, 4)				
n	t_m	c	LR	MCGF	LImp	RImp	CRImp	LR	MCGF	LImp	RImp	CRImp
10	31	60	2.29	11.21	15.53	3.93	2.39	3.90	21.38	27.79	5.73	4.18
10	31	100	6.14	20.59	24.70	12.63	7.26	10.39	39.42	45.48	19.66	11.84
10-th percentile			Simulated from Gamma(1, 2)					Simulated from Gamma(0.5, 4)				
n	t_m	c	LR	MCGF	LImp	RImp	CRImp	LR	MCGF	LImp	RImp	CRImp
10	31	60	2.22	7.98	9.98	3.85	2.31	3.82	13.89	16.09	7.15	4.22
10	31	100	6.37	18.86	20.46	9.56	6.55	11.03	34.07	35.46	17.01	11.57
90-th percentile			Simulated from Gamma(1, 2)					Simulated from Gamma(0.5, 4)				
n	t_m	c	LR	MCGF	LImp	RImp	CRImp	LR	MCGF	LImp	RImp	CRImp
10	31	60	3.50	9.17	13.62	13.01	4.06	7.56	23.40	34.99	28.07	8.14
10	31	100	9.23	18.62	24.10	24.18	10.17	18.52	44.97	60.40	48.40	19.54

Table 2.5: Simulated MSEs of the estimates of 5-th, 10-th and 90-th percentiles based on LR parametric saddlepoint approximation, modified CGF and different data imputation methods when the data are generated from the IG(2, 10) and IG(2, 5) processes.

5-th percentile			Simulated from IG(2, 10)					Simulated from IG(2, 5)				
n	t_m	c	LR	MCGF	LImp	RImp	CRImp	LR	MCGF	LImp	RImp	CRImp
10	31	60	0.78	1.55	345.35	2.50	1.87	1.16	4.70	426.68	2.64	1.67
10	31	100	1.74	6.21	938.47	2.45	1.90	3.20	11.44	1072.52	4.98	3.47
10-th percentile			Simulated from IG(2, 10)					Simulated from IG(2, 5)				
n	t_m	c	LR	MCGF	LImp	RImp	CRImp	LR	MCGF	LImp	RImp	CRImp
10	31	60	0.86	2.80	345.35	0.74	0.64	1.21	4.19	386.53	1.71	1.20
10	31	100	1.69	2.99	820.25	3.77	2.90	2.94	7.64	946.12	5.02	3.51
90-th percentile			Simulated from IG(2, 10)					Simulated from IG(2, 5)				
n	t_m	c	LR	MCGF	LImp	RImp	CRImp	LR	MCGF	LImp	RImp	CRImp
10	31	60	0.70	2.33	134.86	1.34	0.83	1.17	3.12	115.25	4.28	1.93
10	31	100	1.68	4.63	427.38	2.54	1.86	3.13	5.90	393.90	8.78	4.86

2.4. Numerical Example: Laser Device Degradation Data

In general, laser devices are designed to maintain a constant light intensity by increasing the operating current over time. Thus, the failure time of laser devices can be evaluated when the operating current passes a specific threshold level. Meeker and Escobar (1998) provided a data set from an experiment conducted with 15 GaAs laser devices at temperature $80°$C. In the experiment, the percent increase in operating current of 15 GaAs lasers are recorded for every 250 hours up to 4000 hours. The degradation paths of the 15 laser devices are presented in Figure 2.9.

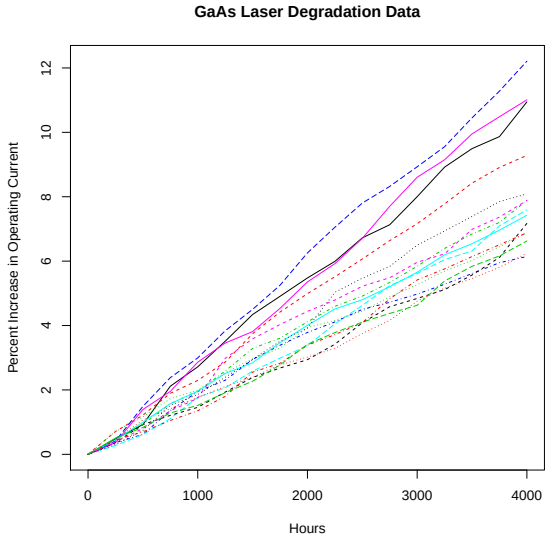

Figure 2.9: Degradation paths of the 15 GaAs Laser degradation in an experiment described in Meeker and Escobar (1998).

2.4.1. Equal time intervals

In the original data set, the degradation measurements are taken at equal time intervals with $\Delta t_0 = 250$ hours; therefore, the ESA using Eq. (2.7) can be evaluated without any modification. The FPT distribution (or failure time distribution) of the laser devices is approximated by both parametric and nonparametric saddlepoint approximation

methods in Figure 2.10. For the parametric approaches, we assume that the underlying degradation model is a gamma degradation process. The approximated FPT distributions using parametric methods include Gamma process MLE (i.e. the reference distribution: $\Pr(T_c > t) = G_{X_t}(c; \hat{\alpha}t, \hat{\beta})$, the $gamma(\hat{\alpha}t, \hat{\beta})$ CDF at c), LR-Gamma in Eq. (2.7), BQ-Gamma in Eq. (2.2), and BS in Eq. (1.2) described in Section 2.2. Applying empirical CGF for Eq. (2.7) and Eq. (2.2), ESA methods LR-Emp and BQ-Emp are obtained, respectively.

Apart from the parametric and ESA methods suggested by Balakrishnan and Qin (2019) (i.e., BQ-Gamma and BQ-Emp), all other methods provide similar approximation of the survival curve. For the right-tail, probabilities for all the methods appear to be very similar. Table 2.6 presents estimates of the 5-th, 10-th and 90-th percentiles for the FPT of the Laser degradation data for different threshold levels based on different approximation methods. We also provide the 2.5-th and 97.5-th bootstrap percentiles (i.e., the upper and lower limits of the 95% bootstrap confidence intervals) of the 5-th, 10-th and 90-th percentiles for the FPT for comparison.

For the 5-th and 10-th percentiles, the saddlepoint approximation methods suggested by Balakrishnan and Qin (2019) are not within the 95% bootstrap confidence interval, while the estimates obtained based on the saddlepoint approximations using the LR method suggested in this study are inside the 95% bootstrap confidence interval. Once again, we observe the inaccuracy of the estimates based on the BQ method for lower percentiles in this example. Complete results of the analysis for $c = 1(1)10$ cases are presented in Section A.5 of Appendix A.

2.4.2. Unequal time intervals

To illustrate the proposed ESA for unequal time intervals, we alter the laser degradation data set by removing some of the degradation measurements and we only considered the measurements at time points {250, 500, 1000, 1750, 2000, 2500, 3250,

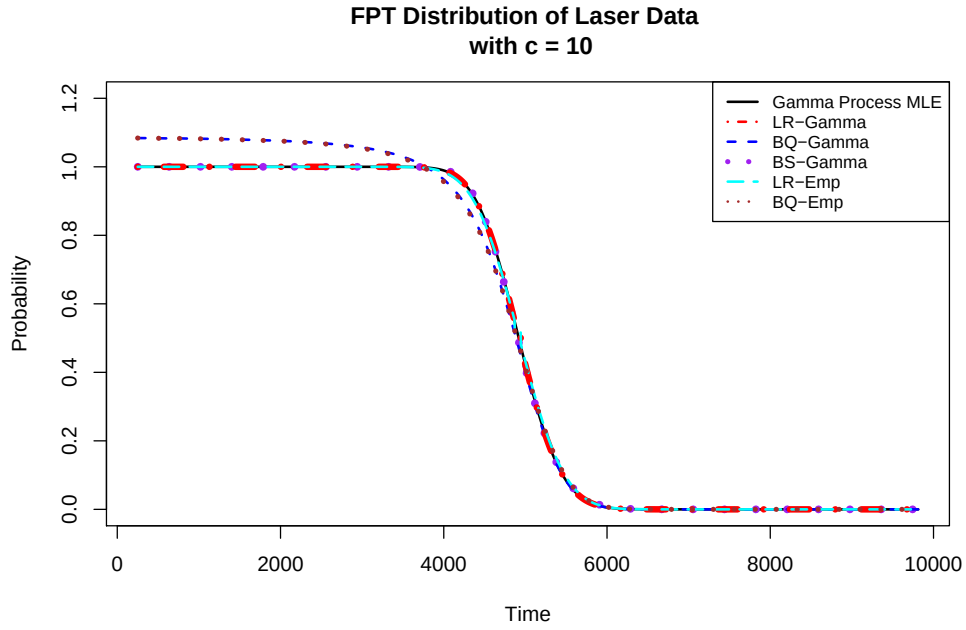

Figure 2.10: FPT distribution of GaAs Laser degradation data with threshold$= 10$

3500, 4000} with $\Delta t_1 = \Delta t_4 = \Delta t_7 = 250$, $\Delta t_2 = \Delta t_5 = \Delta t_8 = 500$, $\Delta t_3 = \Delta t_6 = 750$ and $\Delta t_0 = HCF(250, 500, 750) = 250$. Based on the altered degradation data set, we approximate the FPT distribution using the MLEs of the gamma process and also using the ESA with modifications.

From Figure 2.11, we observe that the modified ESA methods proposed in Section 2.3.1, especially the modified CGF method and the CRImp, provide approximation close to the result obtained from the gamma degradation process FPT with MLEs. The ESA without adjustment for the unequal time intervals is clearly inappropriate for the case that the degradation measures are taken with different time intervals. Complete results of the analysis for $c = 1(1)10$ cases are presented in Section A.6 of Appendix A.

2.5. Limitations of the Proposed Saddlepoint Approximation Methods

The numerical work suggests that both the parametric and ESAs based on the LR

Table 2.6: Estimates and the 2.5-th and 97.5-th bootstrap percentiles of the 5-th, 10-th and 90-th percentiles of FPT distribution for the GaAs Laser degradation data (original data with equal time intervals) with different threshold levels $c = \{2, 6, 10\}$

.

5-th Percentile	Bootstrap Percentile		Empirical		Parametric (Gamma)			
c	2.5%	97.5%	LR	BQ	LR	BQ	MLE	BS
2	673.2	713.7	682.5	652.5	705.0	655.0	705.0	720.0
6	2379.4	2459.6	2410.0	2292.5	2445.0	2310.0	2445.0	2462.5
10	4161.3	4269.4	4212.5	4027.5	4255.0	4057.5	4255.0	4272.5
10-th Percentile	Bootstrap Percentile		Empirical		Parametric (Gamma)			
c	2.5%	97.5%	LR	BQ	LR	BQ	MLE	BS
2	734.0	773.8	747.5	720.0	765.0	717.5	765.0	770.0
6	2496.9	2568.5	2530.0	2427.5	2555.0	2440.0	2555.0	2560.0
10	4329.2	4417.3	4367.5	4212.5	4397.5	4232.5	4397.5	4405.0
90-th Percentile	Bootstrap Percentile		Empirical		Parametric (Gamma)			
c	2.5%	97.5%	LR	BQ	LR	BQ	MLE	BS
2	1225.0	1265.6	1247.5	1247.5	1237.5	1235.0	1237.5	1247.5
6	3357.3	3430.9	3395.0	3392.5	3372.5	3370.0	3372.5	3382.5
10	5435.0	5530.4	5482.5	5480.0	5455.0	5452.5	5455.0	5465.0

method perform better than the BQ method, especially in the left-tail of the FPT distribution. Nevertheless, we show below that there are situations for which the LR method gives an approximate FPT distribution which is improper. It is fortunate that such an ill-behaved situation can be easily identified simply by plotting the approximated FPT distributions.

We have identified two situations for which the proposed LR saddlepoint approximation methods may be ill-behaved:

(i). the mean increment per unit time (drift) of the degradation process is larger than the threshold leading to a FPT distribution with small mean (i.e. threshold/mean of drift ratio is less than one (threshold/mean ratio));

(ii). the distribution of the increment per unit length is a heavy-tailed distribution.

If $\{X_t, t \geq 0\}$ is a Lévy process, then the MGF of X_t can be expressed as $\mathscr{M}_{X_t}(s) =$

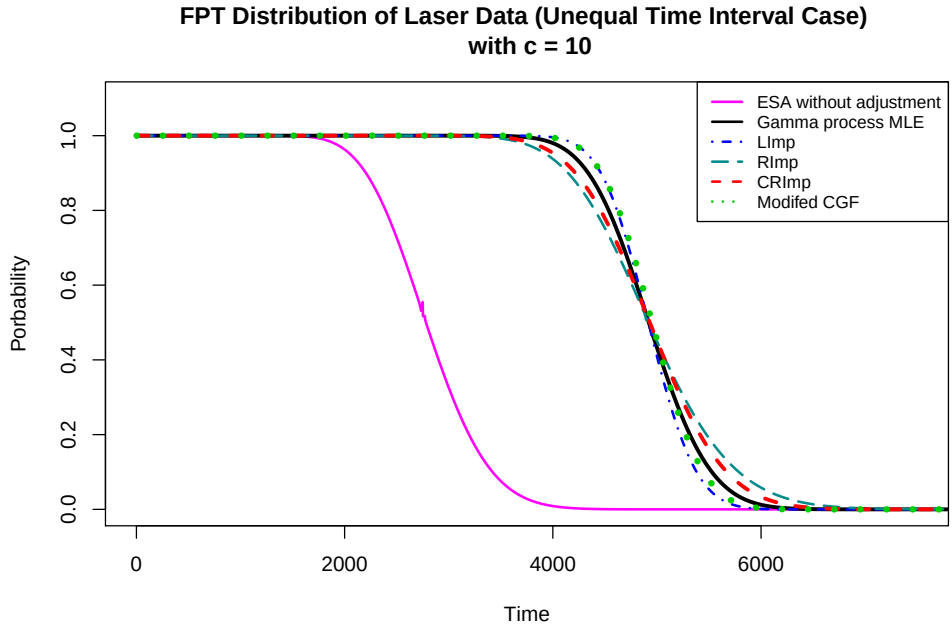

Figure 2.11: FPT distribution of GaAs Laser degradation data with threshold $c = 10$ for unequal time intervals.

$[\mathscr{M}_Y(s)]^t$, where the random variable Y is the degradation measure at unit-time-interval, and thus, independent of time t. Without loss of generality, we set the width of the unit-time interval equal to 1 in this discussion. We observe that when the threshold level c is lower than the mean of Y and/or when the distribution of Y has a heavy tail, the approximated FPT distribution obtained from the LR method can deviates quite far from the true distribution, especially in the left-tail of the distribution.

To illustrate the problem in case (i), consider the IG(5, 10) process with threshold values $c = 1$ and $c = 10$. The threshold/mean of $IG(5, 10)$ distribution ratios are $c/\mu = 0.2$ and 2 for $c = 1$ and 10, respectively. Figures 2.12(a) and 2.12(b) compare FPT distributions of the IG(5, 10) process using two different threshold values with the true FPT distribution, the LR method, the BQ method, and the BS method. We can see that both the LR method and the BQ method deviate from the true FPT distribution and give approximated probabilities > 1 when threshold/mean of drift ratio is 0.2 (< 1). For the LR method, this issue does not appear in the case when $c = 10$.

Table 2.7: Estimates of the 5-th, 10-th and 90-th percentiles of the FPT distribution for the GaAs Laser degradation data (altered data with unequal time intervals) with different threshold levels $c = \{2, 6, 10\}$.

5-th Percentile	Parametric	Empirical			
c	MLE	MCGF	LImp	RImp	CRImp
2	677.5	722.5	732.5	607.5	600.0
6	2390.0	2495.0	2502.5	2242.5	2277.5
10	4180.5	4330.0	4332.5	3937.5	4017.5
10-th Percentile	Parametric	Empirical			
c	MLE	MCGF	LImp	RImp	CRImp
2	745.0	782.5	787.5	690.0	685.0
6	2512.5	2600.0	2600.0	2402.5	2425.0
10	4340.0	4465.0	4460.0	4145.0	4215.0
90-th Percentile	Parametric	Empirical			
c	MLE	MCGF	LImp	RImp	CRImp
2	1275.0	1220.0	1200.0	1355.0	1337.5
6	3432.5	3357.5	3312.5	3552.5	3527.5
10	5527.5	5445.0	5380.0	5785.0	5670.0

To illustrate case (ii), we consider the IG(5, 1) process with threshold values $c = 10$. The kurtosis of the $IG(5, 1)$ distribution is 78. The inaccuracy of the LR method in Figure 2.12(c) contrasts with its accuracy in 2.12(a).

The limitations of the LR saddlepoint approximation in case (ii) can be dealt with by considering the IG-based generalized LR saddlepoint approximation proposed by Wood et al. (1993). The details of this approximation are given in Section 1.2.4 and have been implemented following the guidelines given in Butler (2007, Section 16.2.2), which also provides a simple explanation of the approximation.

Figure 2.13 shows the IG-based LR saddlepoint approximation, for the degradation processes of Figures 2.12. The IG-based LR saddlepoint approximated distributions are quite close to the true FPT distribution, and do not show the left-tail deficiencies associated with the normal-based LR method. This suggests that IG-based saddlepoint

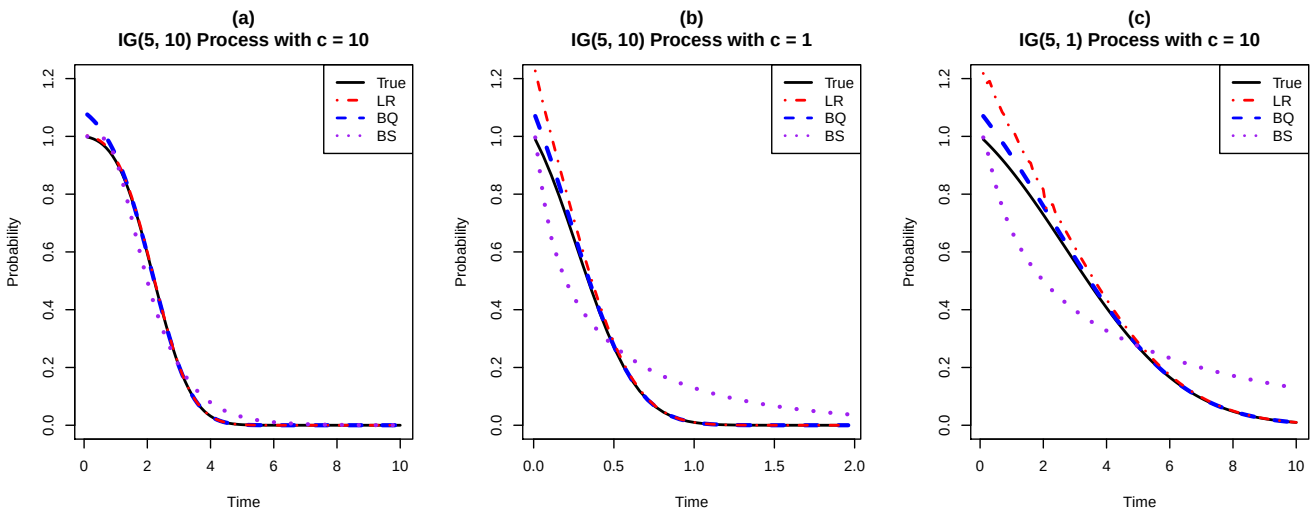

Figure 2.12: FPT distribution IG(5, 1) process and IG(5, 10) process with threshold level $c = 10$.

approximation can correct the ill-behaved issues observed in Figures 2.12.

2.6. Concluding Remarks

In this study, we have improved upon the parametric and nonparametric techniques for approximating the FPT distribution of a degradation process proposed by Balakrishnan and Qin (2019) based on the LR saddlepoint approximation. We have demonstrated that the proposed methodologies can provide more accurate approximation of the FPT distribution as compared to those existing approximation methods, especially on the left-tail of the FPT distribution. Moreover, we have proposed different modifications to the ESA to handle the situations where the equal time intervals assumption is violated. The performance of the proposed approximation methods and those modifications have been studied using different numerical examples and Monte Carlo simulation studies. The numerical results show that the proposed methods can approximate the FPT distribution well in a wide range of situations.

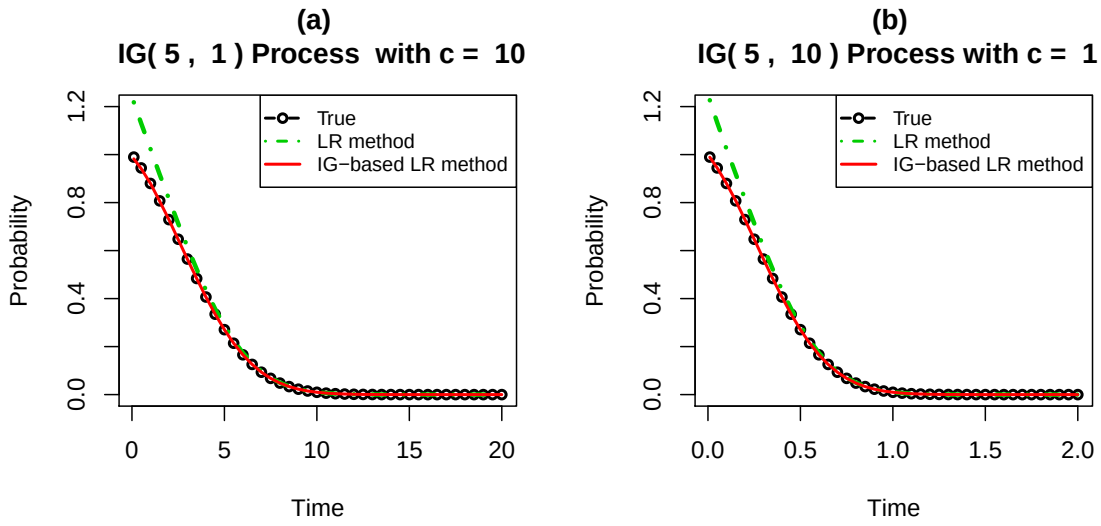

Figure 2.13: FPT distribution of two IG processes from the inverse-Gaussian-based LR saddlepoint approximation of Wood et al. (1993).

Although the proposed methodologies work well in most cases, situations can be found in which methods based on the LR saddlepoint approximation can be inaccurate. We have illustrated these situations and have provided satisfactory solutions for these issues when we observe that the LR methods do not provide reasonable approximations. In practice, especially when the degradation measurements are taken with unequal time intervals, we suggest that practitioners apply several different methods proposed in this study and examine the plots of the resulting approximated FPT distributions using both parametric and nonparametric methods. In general, when the underlying degradation process is unknown, we recommend the use of the ESA with the CRImp method for the unequal time intervals situations. Since the IG-based saddlepoint approximation can effectively improve the performance of the approximation of the FPT distribution, future work will develop the IG-based ESA and study its performance in different settings.

Chapter 3

Semiparametric and Nonparametric Approaches to Estimate the First-Passage Time Distribution for Bivariate Degradation Processes

3.1. Introduction

In system engineering, the reliability of a system depends on the reliability of each subsystem (or component) and those subsystems have their own performance characteristics (PCs). For highly reliable subsystems or components in a system, information on the lifetime distribution of the subsystems may not be easy to obtain and hence, it is common to access the reliability of the system based on the degradation of those PCs of the subsystems which may not be independent. Therefore, the dependence between those PCs of the subsystems can be an important factor in the evaluation of the reliability of a system.

When using the degradation measurements to evaluate the reliability characteristics, a soft failure of a subsystem is defined as the first-passage time (FPT) at which the degradation measurement of the corresponding PC reaches a pre-defined threshold, and the lifetime distribution of the subsystem is the FPT distribution. In this study, we aim to provide some effective approaches to model the marginal FPT distribution of each PC as well as the joint distribution of all the PCs when the degradation processes of those PCs of subsystems are dependent. Those approaches will allow us to appropriately evaluate the reliability characteristics of the system.

In this context, we generally assume the degradation measurements of each PC follows a Lévy process, which includes some commonly used stochastic processes for

degradation modeling such as Wiener, the gamma and the inverse Gaussian (IG) processes. Furthermore, we consider using copula functions to model the joint distribution of the correlated degradation processes of the PCs of subsystems. Thereby, using a particular Lévy process and a particular copula function, many research works have been carried out to model bivariate or multivariate degradation measurements and to provide estimation of reliability characteristics such as the mean-time-to-failure (MTTF) and remaining-useful-time (RUL) of a system. For example, Sari et al. (2009) and Sari (2007) applied generalized linear models (GLM) to predict the reliability of light-emitting diode (LED) tube lights with two sets of LED lamps as two PCs and used a copula function to model the dependence. Zhou et al. (2010) proposed using a bivariate gamma degradation process with copula functions for degradation data analysis. Furthermore, Zhou et al. (2010) suggested to apply a Bayesian approach with Monte Carlo Markov Chain (MCMC) for parameter estimation of the two marginal gamma distributions and the copula parameter. Moreover, Zhou et al. (2010) also used the fatigue crack data set presented in Meeker and Escobar (1998) to illustrate their proposed model and estimation method. The FPT distribution of a bivariate gamma degradation model is approximated by a bivariate Birnbaum-Saunders (BS) (Birnbaum and Saunders, 1969) distribution in Pan and Balakrishnan (2011b) and Pan et al. (2016) and the model parameters are estimated with the Bayesian MCMC approach.

In addition to the bivariate gamma degradation process, an adaptive method of residual life estimation with two degradation measurements follows a bivariate Wiener process is studied by Wang et al. (2013). Furthermore, Wang et al. (2013) characterized the dependency by a copula function. A similar study is done by Pan et al. (2013), where bivariate Wiener process with time scale transformation has been modeled with a copula function. Likewise, Hao and Su (2014) proposed a nonlinear bivariate Wiener process with random effects modeled with copula. Peng et al. (2016) investigated a bivariate IG degradation process and modeled the joint distribution with copula functions.

Although there are existing research works on modeling bivariate and multivariate degradation processes, to the best of our knowledge, these bivariate or multivariate degradation models are studied only in a parametric framework in which a parametric form of the degradation process and a parametric form of the dependence structure need to be specified. Nevertheless, in practical situations, the underlying degradation process of a subsystem is usually unknown and the dependence structure between subsystems are not specified. Thus, it is decided to develop efficient semiparameteric and nonparametric approaches to obtain the FPT distribution of a system. In this chapter, we aim to address this important research problem.

Following the methods proposed by Balakrishnan and Qin (2019), an improved ESA method is proposed in Section 2.3.1 to enhance the accuracy of estimation of FPT distribution. Furthermore, in Section 2.4.2, we proposed different imputation techniques to obtain the FPT distribution using ESA when the degradation measurements are not taken at equal time points. In this study, we consider a systems with two subsystems (components) subject to a bivariate degradation process and propose different efficient semiparametric and nonparametric approaches to estimate the FPT distribution of a two-component series or parallel system. The results presented here can be generalized to system with $k > 2$ components with some straightforward extensions.

This chapter is organized as follows. Parametric, semiparametric, and nonparametric methods for estimating the FPT distribution of bivariate degradation process are introduced and elaborated in Section 3.2. In Section 4.4, the performance of the proposed methods are studies via a Monte Carlo simulation. A numerical example on LED system is used to illustrate the methodologies in Section 3.4. Finally, some concluding remarks are provided in Section 3.5.

3.2. First-Passage Time Distribution of Bivariate Degradation Processes

Suppose a system with two dependent PCs, which are subjected to degradation. Let the corresponding degradation measurements of two PCs follow a monotone degradation processes $\{X_t; t \geq 0\}$ and $\{Z_t; t \geq 0\}$, respectively. In addition, suppose each PC follow a Lévy process with a parameter vector θ_x and θ_z, respectively. Assume that all degradation measurements of X_t and Z_t are measured at the same predetermined time intervals and let the degradation processes of X_t and Z_t have threshold levels c_x and c_z, respectively.

Let $X_t = \sum_{j:t_j<t} \Delta X_j \sim F_{X_t}(x;\theta_x)$ and $Z_t = \sum_{j:t_j<t} \Delta Z_j \sim F_{Z_t}(z;\theta_z)$, then $\Delta X_t \sim F_{\Delta X_t}(\Delta x;\theta_x)$ and $\Delta Z_t \sim F_{\Delta Z_t}(\Delta z;\theta_z)$. In addition, suppose there are I samples (degradation paths) and each sample has m_i measurements for the two degradation processes X_t and Z_t, where $i = 1,2,\ldots,I$.

Here, we first describe a fully parametric approach available in the literature and then propose two novel semiparametric and two novel nonparametric approaches in order to approximate the FPT distribution, when the degradation processes of the components are dependent and the components are connected either in series or in parallel. The proposed semi-parametric and nonparametric approaches are summarized as follows:

1. Semi-Parametric Method (Semi1): Empirical marginals with parametric copula functions
2. Semi-Parametric Method (Semi2): Parametric marginals with empirical copula function
3. Nonparametric Saddlepoint Method (NP1): Empirical marginals with empirical copula
4. Nonparametric Bootstrap Method (NP2)

Assume two components are connected in series; thus, the survival function of the

system can be obtained from Eq. (1.28). The joint distribution of (X_t, Z_t), which is also the system survival function for a series system, can be obtained using a copula function by,

$$R_s(t) = H(X_t, Z_t) = C(F_{X_t}(c_x; \theta_x), F_{Z_t}(c_z; \theta_z); \xi), \tag{3.1}$$

where ξ is the copula parameter (i.e., θ_F, θ_C, or θ_G in Eq. (1.22), Eq. (1.23), and Eq. (1.24), respectively) and $\Pr(T_{c_x} > t) = F_{X_t}(c_x; \theta_x)$ and $\Pr(T_{c_z} > t) = F_{Z_t}(c_z; \theta_z)$ are the marginal FPT distributions of X_t and Z_t.

Since the dependency between X_t and Z_t is the same as the dependency between ΔX_t and ΔZ_t, following Pan et al. (2011), we assume that the joint distribution of (X_t, Z_t) and $(\Delta X_t, \Delta Z_t)$ have the same copula structure, i.e.,

$$R_s(t) = H(X_t, Z_t) \approx H(\Delta X_t, \Delta Z_t). \tag{3.2}$$

In Section 4.4, we will show that this assumption is reasonable using a simulation study.

Suppose the density of the copula function is $c(u, v) = \partial C / \partial u \partial v$, then the joint density of $(\Delta X_t, \Delta Z_t)$ is given by

$$h(\Delta X_t, \Delta Z_t; \theta_x, \theta_z, \xi) = c(F_{\Delta X_t}(\Delta x; \theta_x), F_{\Delta Z_t}(\Delta z; \theta_z), \xi) f_{\Delta X_t}(\Delta x; \theta_x) f_{\Delta Z_t}(\Delta z; \theta_z). \tag{3.3}$$

3.2.1. Fully parametric approach

For comparative purposes, we consider here a fully parametric modeling approach in which the underlying distributions of the degradation processes (i.e. $F_{\Delta X}$ and $F_{\Delta Z}$) and the parametric form of the copula function (i.e. $C(\cdot, \cdot)$) are known. Maximum likelihood estimation method is used to estimate the model parameters and the marginal FPT distributions are approximated based on the definition of the FPT with the maximum likelihood

estimates (MLEs).

Based on the bivariate degradation measurements, $(\Delta x_{ij}, \Delta z_{ij}), i = 1, \ldots, I, j = 1, \ldots, m_i$, the log-likelihood function of the model parameters (θ_x and θ_z) is given by

$$\log \mathscr{L}(\theta_x, \theta_z, \xi) = \sum_{i=1}^{I} \sum_{j=1}^{m_i} \Big[\log\{c(F_{\Delta X_t}(\Delta x_{ij}; \theta_x), F_{\Delta Z_t}(\Delta z_{ij}; \theta_z); \xi)\} + \log\{f_{\Delta X_t}(\Delta x_{ij}; \theta_x)\} + \log\{f_{\Delta Z_t}(\Delta z_{ij}; \theta_z)\} \Big]. \quad (3.4)$$

The MLE of θ_x, θ_z, and ξ can be obtained by maximizing the log-likelihood function in Eq. (3.4) with respect to θ_x, θ_z, and ξ. A two-stage procedure, called the inference function for margin (IFM) method, proposed by Joe and Xu (1996) can be used to obtain the MLEs. The IFM method estimates parameters in the marginal distributions in the first stage and then estimate the copula parameter using the estimated marginal distributions in the second stage. The IFM method is summarized as follows:

Stage 1.1: $\widehat{\theta}_x = \text{argmax}_{\theta_x} \sum_{i=1}^{I} \sum_{j=1}^{m_i} \log\{f_{\Delta X_t}(\Delta x_{ij}; \theta_x)\}$;

Stage 1.2: $\widehat{\theta}_z = \text{argmax}_{\theta_z} \sum_{i=1}^{I} \sum_{j=1}^{m_i} \log\{f_{\Delta Z_t}(\Delta z_{ij}; \theta_z)\}$;

Stage 2: $\hat{\xi} = \text{argmax}_{\xi} \sum_{i=1}^{I} \sum_{j=1}^{m_i} \log\{c(F_{\Delta X_t}(\Delta x_{ij}; \widehat{\theta}_x), F_{\Delta Z_t}(\Delta z_{ij}; \widehat{\theta}_z); \xi)\}$.

It has been shown that the IFM method is asymptotically efficient (Pham, 2006, Part F, Section 51.3.2).

After obtaining the MLEs of the model parameters, the marginal FPT distributions of X_t and Z_t can be estimated based on the MLEs as $\widehat{\Pr}(T_{c_x} > t) = F_{X_t}(c_x; \widehat{\theta}_x)$ and $\widehat{\Pr}(T_{c_z} > t) = F_{Z_t}(c_z; \widehat{\theta}_z)$, respectively. Then, the joint survival function of (X_t, Z_t) is $C(\widehat{\Pr}(T_{c_x} > t), \widehat{\Pr}(T_{c_z} > t, \hat{x}i)$. Hence, the system survival function of two-component series system can be estimated as

$$\hat{R}_s(t) = \widehat{\Pr}(T_{\min} > t) = C(\widehat{\Pr}(T_{c_x} > t), \widehat{\Pr}(T_{c_z} > t); \hat{\xi}). \quad (3.5)$$

Furthermore, the system survival function of two-component parallel system can be estimated as

$$\hat{R}_p(t) = \widehat{\Pr}(T_{\max} > t) = 1 - \tilde{C}(\widehat{\Pr}(T_{c_x} > t), \widehat{\Pr}(T_{c_z} > t); \hat{\xi}), \tag{3.6}$$

where $\tilde{C}(\cdot,\cdot)$ is the survival copula in Eq. (1.19).

When the underlying distributions of the degradation processes and the copula functions are known and correctly specified the estimation results based on the fully parametric approach can be used as a benchmark to compare with the semi-parametric and nonparametric approaches proposed in the subsequent sections.

Bivariate Birnbaum–Saunders distribution approach: As an alternative approach to using of copula functions, Pan and Balakrishnan (2011b) proposed to approximate the FPT distribution of a bivariate gamma process from the bivariate Birnbaum-Saunders (BVBS) distribution (Kundu et al., 2010). Suppose X_t and Z_t follows a gamma degradation process such that $X_t \sim gamma(\alpha_x, \beta_x)$ and $Z_t \sim gamma(\alpha_z, \beta_z)$ and their marginal FPT random variables with threshold levels c_x and c_z are denoted as T_{c_x} and T_{c_z}, respectively. Furthermore, suppose the correlation between two degradation processes is denoted by ρ. Then, the FPT distribution for a series system is given by

$$\begin{aligned} R_s(t) &= \Pr(T_{\min} > t) = \Pr(T_{c_x} > t, T_{c_z} > t; \rho) \\ &= 1 - \Phi[U(t)] - \Phi[V(t)] + \Phi_2[U(t), V(t); \rho], \end{aligned} \tag{3.7}$$

where Φ is the standard normal CDF and Φ_2 is the standard bivariate normal CDF. Moreover,

$$U(t) = \frac{1}{\alpha_x}\left(\sqrt{\frac{t}{\beta_x}} - \sqrt{\frac{\beta_x}{t}}\right); \quad V(t) = \frac{1}{\alpha_z}\left(\sqrt{\frac{t}{\beta_z}} - \sqrt{\frac{\beta_z}{t}}\right).$$

For a two-component parallel system, the reliability function is derived as

$$R_p(t) = \Pr(T_{\max} > t) = 1 - \Phi_2[U(t), V(t); \rho] \tag{3.8}$$

We considered the BVBS distribution to compare the proposed semiparametric and non-parametric methods. Pan and Balakrishnan (2011b) proposed to use Bayesian Monte Carlo Markov Chain (MCMC) to estimate the parameters $\{\alpha_x, \beta_x, \alpha_z, \beta_z, \rho\}$. However, for this analysis, we consider maximum likelihood method to estimate those parameters.

3.2.2. Semi-parametric approach (Semi1): Empirical marginals with a known copula function

In this proposed semi-parametric approach, we do not make any distributional assumptions on the degradation processes, X_t and Z_t, yet the joint distribution (X_t, Z_t) is modeled by a known parametric copula function. We assume that X_t and Z_t follow a Lévy process and they are increasing with probability one.

In this setting, the parametric form of copula function is known but the dependency parameter (ξ) is assumed to be unknown. To estimate ξ based on the observed degradation measurements, $(\Delta x_{ij}, \Delta z_{ij}), i = 1, \ldots, I; j = 1, \ldots, m_i$, the empirical CDFs of ΔX_t and ΔZ_t can be obtained as

$$\widehat{F}_{\Delta X_t}(x) = \frac{1}{M} \sum_{i=1}^{I} \sum_{j=1}^{m_i} \mathbf{1}(\Delta x_{ij} \leq x) \text{ and } \widehat{F}_{\Delta Z_t}(z) = \frac{1}{M} \sum_{i=1}^{I} \sum_{j=1}^{m_i} \mathbf{1}(\Delta z_{ij} \leq z), \tag{3.9}$$

where $M = \sum_{i=1}^{I} m_i$ and using those empirical CDFs of the marginals, the copula parameter can be obtained using the maximum likelihood approach by

$$\hat{\xi} = \text{argmax}_{\xi} \sum_{i=1}^{I} \sum_{j=1}^{m_i} \log\{c(\widehat{F}_{\Delta X_t}(\Delta x_{ij}), \widehat{F}_{\Delta Z_t}(\Delta z_{ij}); \xi)\}.$$

Estimating the copula parameter using empirical CDFs of the marginals is called the canonical maximum likelihood (CML) method. It has been shown that the copula parameter estimate obtained from the CML method is consistent, asymptotically normal and efficient (Pham, 2006, Part F, Section 51.3.3).

In order to obtain the joint survival function of two component series or parallel system, we need to estimate the marginal FPT distributions of degradation processes X_t ad Z_t. Here, the ESA approach presented in Section 2.3.1 is used to estimate the marginal FPT distributions of the degradation processes nonparametrically. Specifically, ESA of the marginal FPT distributions of X_t and Z_t are denoted as $\widehat{\Pr}_{ESA}(T_{c_x} > t)$ and $\widehat{\Pr}_{ESA}(T_{c_z} > t)$, respectively, can be obtained by evaluating empirical CGF in Eq. (2.10) from data and applying in the LR saddlepoint approximation equation in Eq. (2.7).

Using this method, the joint reliability function for two degradation processes can be determined by

$$\hat{R}_s(t) = \widehat{\Pr}_{Semi1}(T_{\min} > t) = C(\widehat{\Pr}_{ESA}(T_{c_x} > t), \widehat{\Pr}_{ESA}(T_{c_z} > t); \hat{\xi}). \tag{3.10}$$

Furthermore, the system survival function of two-component parallel system can be estimated as

$$\hat{R}_p(t) = \widehat{\Pr}_{Semi1}(T_{\max} > t) = 1 - \tilde{C}(\widehat{\Pr}_{ESA}(T_{c_x} > t), \widehat{\Pr}_{ESA}(T_{c_z} > t); \hat{\xi}). \tag{3.11}$$

where $\tilde{C}(\cdot,\cdot)$ is the survival copula in Eq. (1.19).

3.2.3. Semi-parametric approach (Semi2): Parametric marginals with empirical copula function

For this semi-parametric approach, we assume the parametric form of the underlying

distributions of the degradation processes X_t and Z_t are known (with unknown parameters); however, the empirical copula function for the dependency of X_t and Z_t is not specified.

Based on the bivariate degradation measurements, $(\Delta x_{ij}, \Delta z_{ij}), i = 1, \ldots, I, j = 1, \ldots, m_i$, we estimate the parameters in the marginal distributions of X_t and Z_t using the maximum likelihood estimation method without considering the dependency. In other words, we estimate θ_x and θ_z by maximizing the log-likelihood function

$$\log \mathscr{L}(\theta_x, \theta_z) = \sum_{i=1}^{I} \sum_{j=1}^{m_i} \Big[\log\{f_{\Delta X_t}(\Delta x_{ij}; \theta_x)\} + \log\{f_{\Delta Z_t}(\Delta z_{ij}; \theta_z)\} \Big], \tag{3.12}$$

with respect to θ_x and θ_z. Using these parameter estimates, $\widehat{\theta}_x$ and $\widehat{\theta}_z$, the marginal FPT distributions of X_t and Z_t can be estimated as $\widehat{\Pr}(T_{c_x} > t) = F_{X_t}(c_x; \widehat{\theta}_x)$ and $\widehat{\Pr}(T_{c_z} > t) = F_{Z_t}(c_z; \widehat{\theta}_z)$, respectively.

Here, we estimate the copula function nonparametrically using the empirical copula in Eq. (1.25). Specifically, suppose $\Delta x^{(ij)}$ be the rank of Δx_{ij} in the sample $\{\Delta x_{11}, \Delta x_{12}, \ldots, \Delta x_{1m_1}, \ldots, \Delta x_{I1}, \Delta x_{I2}, \ldots, \Delta x_{Im_I}\}$ and $\Delta z^{(ij)}$ be the rank of Δz_{ij} in the sample $\{\Delta z_{11}, \Delta z_{12}, \ldots, \Delta z_{1m_1}, \ldots, \Delta z_{I1}, \Delta z_{I2}, \ldots, \Delta z_{Im_I}\}$ for $i = 1, 2, \ldots, I$ and $j = 1, \ldots, m_i$, then the empirical copula function, $\hat{C}_M$, is given by

$$\hat{C}_M(\hat{u}, \hat{v}) = \frac{1}{M} \sum_{i=1}^{I} \sum_{j=1}^{m_i} \mathbf{1} \left(\frac{\left[\Delta x^{(ij)} - \frac{1}{2}\right]}{M} \leq \hat{u}, \frac{\left[\Delta z^{(ij)} - \frac{1}{2}\right]}{M} \leq \hat{v} \right), \tag{3.13}$$

where $\hat{u} \in [0,\ 1]$ and $\hat{v} \in [0,\ 1]$ are the evaluation points of the empirical copula function, which can be obtained as $\hat{u} = 1 - F_{X_t}(c_x; \widehat{\theta}_x)$ and $\hat{v} = 1 - F_{Z_t}(c_z; \widehat{\theta}_z)$. For simplicity, the relationship in Eq. (3.13) can be modified using the empirical CDFs in Eq. (3.9) and a semi-parametric estimate of the probability distribution of a parallel two-component sys-

tem can be obtained as

$$\widehat{\Pr}_{Semi2}(T_{\max} < t) = \hat{C}_M(\hat{u}(t), \hat{v}(t)) = \frac{1}{M}\sum_{i=1}^{I}\sum_{j=1}^{m_i} \mathbf{1}\left(\widehat{F}_{\Delta X_t}(\Delta x_{ij}) \leq \hat{u}(t), \widehat{F}_{\Delta Z_t}(\Delta z_{ij}) \leq \hat{v}(t)\right), \quad (3.14)$$

where $\hat{u}(t) = \widehat{\Pr}(T_{c_x} < t) = 1 - F_{X_t}(c_x; \widehat{\theta}_x)$ and $\hat{v}(t) = \widehat{\Pr}(T_{c_z} < t) = 1 - F_{Z_t}(c_z; \widehat{\theta}_z)$. Similarly, the survival function of $T_{\max}$ can be evaluated as $\hat{R}_p(t) = 1 - \widehat{\Pr}_{Semi2}(T_{\max} < t)$. Furthermore, using copula relationships, the survival function of a series two-component system, $T_{\min}$, is determined as

$$\hat{R}_s(t) = \widehat{\Pr}_{Semi2}(T_{\min} > t) = \hat{u}(t) + \hat{v}(t) - \hat{C}_M(\hat{u}(t), \hat{v}(t)). \quad (3.15)$$

3.2.4. Nonparametric saddlepoint approach (NP1): Empirical marginals and empirical copula

For a fully nonparametric approach, the distributional assumptions for Lévy processes X_t and Z_t and the functional form of the copula function are not required. In this case, we propose using the EPA method to estimate the marginal FPT distributions of X_t and Z_t and using the empirical copula function to approximate the joint distribution of X_t and Z_t.

Following Eq. (2.10), we use the ESA to estimate the FPT distributions of X_t and Z_t for given threshold levels c_x and c_z, denoted as $\widehat{\Pr}_{ESA}(T_{c_x} > t)$ and $\widehat{\Pr}_{ESA}(T_{c_z} > t)$, respectively. To obtain the empirical copula, the empirical marginal distributions of ΔX and ΔZ are estimated from Eq. (3.9) as

$$\widehat{\Pr}_{NP1}(T_{\max} < t) = \hat{C}_M(\hat{u}(t), \hat{v}(t)) = \frac{1}{M}\sum_{i=1}^{I}\sum_{j=1}^{m_i} \mathbf{1}\left(\widehat{F}_{\Delta X_t}(\Delta x_{ij}) \leq \hat{u}(t), \widehat{F}_{\Delta Z_t}(\Delta z_{ij}) \leq \hat{v}(t)\right), \quad (3.16)$$

where

$$\hat{u}(t) = \widehat{\Pr}_{ESA}(T_{c_x} < t) \text{ and } \hat{v}(t) = \widehat{\Pr}_{ESA}(T_{c_z} < t).$$

Hence, the survival function of $T_{\max}$ can be evaluated as $\hat{R}_p(t) = 1 - \widehat{\Pr}_{NP1}(T_{\max} < t)$. Furthermore, using copula relationships, the survival function of $T_{\min}$ is determined as

$$\hat{R}_s(t) = \widehat{\Pr}_{NP1}(T_{\min} > t) = 1 - \hat{u}(t) - \hat{v}(t) + \hat{C}_M(\hat{u}(t), \hat{v}(t)). \tag{3.17}$$

3.2.5. Nonparametric bootstrap approach (NP2)

In this subsection, we generalize the bootstrap approach for estimating the FPT distribution of degradation data in the univariate case proposed by Balakrishnan and Qin (2019) to the case with bivariate degradation processes. Without loss of generality, we assume the time increments are $\Delta t = 1$.

Based on the bivariate degradation measurements, $(\Delta x_{ij}, \Delta z_{ij}), i = 1, \ldots, I, j = 1, \ldots, m_i$, the following bootstrap procedure can be used to obtain bootstrap samples of $T_{\min}$ and $T_{\max}$ of size B (denotes as $(T_{\min}^{(1)}, T_{\min}^{(2)}, \ldots, T_{\min}^{(B)})$ and $(T_{\max}^{(1)}, T_{\max}^{(2)}, \ldots, T_{\max}^{(B)})$, respectively):

Step 1: Set $k = 1$ and $b = 1$.

Step 2: Set $T_{\min}^{(b)} = \infty$.

Step 3: Draw a random pair of degradation measurements, denoted as $(\Delta x_k^*, \Delta z_k^*)$, with replacement from $\{(\Delta x_{ij}, \Delta z_{ij}), i = 1, \ldots, I, j = 1, \ldots, m_i\}$.

Step 4: Compute $X_k = \sum_{\ell=1}^{k} \Delta x_\ell^*$ and $Z_k = \sum_{\ell=1}^{k} \Delta z_\ell^*$.

Step 5: If $X_k < c_x$ and $Z_k < c_z$, then set $k = k + 1$ and return to Step 3.

Step 6: If $X_k > c_x$ and $Z_k < c_z$, then set $T_{\min}^{(b)} = \min\{T_{\min}^{(b)}, k\}$, set $k = k + 1$ and return to Step 3.

Step 7: If $X_k < c_x$ and $Z_k > c_z$, then set $T_{\min}^{(b)} = \min\{T_{\min}^{(b)}, k\}$, set $k = k + 1$ and return to Step 3.

Step 8: If $X_k > c_x$ and $Z_k > c_z$, then set $T_{\min}^{(b)} = \min\{T_{\min}^{(b)}, k\}$ and $T_{\max}^{(b)} = k$; if $b < B$, set $b = b+1$, $k = 1$ and return to Step 2.

Once the bootstrap samples of size B are obtained, empirical distributions of $T_{\max}$ and $T_{\min}$ can be obtained by

$$\begin{aligned} \widehat{\Pr}_{NP2}(T_{\min} < t) &= \widehat{F}_{T_{\min}}(t) = \frac{1}{B}\sum_{b=1}^{B} \mathbf{1}(T_{\min}^{(b)} \le t) \\ \text{and } \widehat{\Pr}_{NP2}(T_{\max} < t) &= \widehat{F}_{T_{\max}}(t) = \frac{1}{B}\sum_{b=1}^{B} \mathbf{1}(T_{\max}^{(b)} \le t). \end{aligned}$$

3.3. Monte Carlo Simulation Study

A Monte Carlo simulation study is carried out to evaluate the performance of the methods proposed in Section 3.2. In the simulation study, we generate the bivariate degradation measurements, $(\Delta x_{ij}, \Delta z_{ij}), i = 1,\ldots,I, j = 1,\ldots,m_i$, from the gamma process with a specified copula function. Specifically, we assume both X_t and Z_t follow gamma degradation processes with $X_t \sim Gamma(2,1)$ and $Z_t \sim Gamma(1,2)$. To establish the joint distribution between the two degradation processes, we consider the Frank copula, Clayton copula and Gumbel copula presented in Sections 1.3.4.1, 1.3.4.2 and 1.3.4.3, respectively. For each copula function, we consider the dependence parameters that give the Kendall's tau correlation $\tau = 0.3$ and $\tau = 0.8$ (see Table 3.1). Furthermore, we also consider the situation that the two degradation processes, X_t and Z_t, are independent. For each simulation, 10 bivariate degradation paths ($I = 10$) with 50 measurements ($m_i = 50$ for $i = 1,2,\ldots,10$) are generated. The degradation measurements are taken at the equal-width time intervals with the time increment $\Delta t = 1$. The threshold levels for the two degra-

Table 3.1: Dependence parameters for different copula function considered in the simulation study

Copula Function	**Dependence Parameter**	
Frank	$\xi_F = 2.92$ ($\tau_F = 0.30$)	$\xi_F = 18.2$ ($\tau_F = 0.80$)
Clayton	$\xi_C = 0.86$ ($\tau_C = 0.30$)	$\xi_C = 8.0$ ($\tau_C = 0.80$)
Gumbel	$\xi_G = 1.43$ ($\tau_G = 0.30$)	$\xi_G = 5.0$ ($\tau_G = 0.80$)

dation processes are set to be the same as 100 (i.e., $c_x = c_z = 100$). Using the parametric, semi-parametric and nonparametric methods discussed in Section 3.2, the FPT distributions of the two degradation processes are approximated based on the generated bivariate degradation data. We repeated the simulation 10000 times for each setting. The performance of different estimation methods for the distributions of $T_{\max}$ and $T_{\min}$ are evaluated by mean squared errors (MSEs) for estimating the 1-st, 10-th, 50-th, 90-th and 99-th percentiles of the distributions. Note that we also consider settings with different number of degradation paths and different number of measurements. In particular, we considered $I = 10$ and $m_i = 200$, and $I = 50$ and $m_i = 50$. Since the conclusions based on these settings are similar, for the sake of saving space, we only present the simulation results for $I = 10$ and $m_i = 50$ here.

To study the robustness of the proposed estimation approaches, the FPT distributions of $T_{\max}$ and $T_{\min}$ are evaluated for each simulated bivariate degradation data based on different parametric assumptions. The parametric assumptions for the parametric and semiparametric methods are summarized as follows:

- G-f: Parametric approach (MLE) by assuming $\{X_t, Z_t; t \geq 0\}$ follows a bivariate gamma process with Frank copula
- G-c: Parametric approach (MLE) by assuming $\{X_t, Z_t; t \geq 0\}$ follows a bivariate gamma process with Clayton copula
- G-g: Parametric approach (MLE) by assuming $\{X_t, Z_t; t \geq 0\}$ follows a bivariate gamma process with Gumbel copula

- IG-f: Parametric approach (MLE) by assuming $\{X_t, Z_t; t \geq 0\}$ follows a bivariate IG process with Frank copula
- IG-c: Parametric approach (MLE) by assuming $\{X_t, Z_t; t \geq 0\}$ follows a bivariate IG process with Clayton copula
- IG-g: Parametric approach (MLE) by assuming $\{X_t, Z_t; t \geq 0\}$ follows a bivariate IG process with Gumbel copula
- G-BVBS: Parametric approach (MLE) by assuming $\{X_t, Z_t; t \geq 0\}$ follows a bivariate gamma process and modeled the FPT distribution with the BVBS distribution
- f: Semi1 approach by assuming $\{X_t, Z_t; t \geq 0\}$ follows a bivariate degradation process with Frank copula
- c: Semi1 approach by assuming $\{X_t, Z_t; t \geq 0\}$ follows a bivariate degradation process with Clayton copula
- g: Semi1 approach by assuming $\{X_t, Z_t; t \geq 0\}$ follows a bivariate degradation process with Gumbel copula
- G: Semi2 approach by assuming $\{X_t, Z_t; t \geq 0\}$ follows a bivariate gamma process with nonparametric copula
- IG: Semi2 approach by assuming $\{X_t, Z_t; t \geq 0\}$ follows a bivariate IG process with nonparametric copula

The simulated MSEs of different estimation methods when the two marginal degradation processes are independent are presented in Table 3.2. Furthermore, the simulated MSEs with different copula functions are presented in Tables 3.3, 3.4 and 3.5. In Tables 3.3, 3.4 and 3.5, the simulated MSEs under the correct model assumptions are highlighted in bold, which can be served as the benchmark for comparative purposes. In general, there is a noticeable deviation in the lower and higher percentiles (1-st and 99-th) of the MSEs obtained from BVBS approximation compared to the correctly specified

model. This indicates that the tail probability estimates through BVBS approximation may not accurate when bivariate data generated through Archimedean copulas.

The situation that the two degradation processes are independent is a special case of the Frank, Clayton and Gumbel copula functions; therefore, from Table 3.2, we observe that the MSEs of the parametric approach and the semiparametric approach (Semi1) based on different copula functions are similar.

In comparing the parametric and semiparametric approaches, from Tables 3.2 – 3.5, we observe that when the underlying model is misspecified as a bivariate IG degradation process for the parametric approach and the Semi2 approach, the MSEs are substantially larger than the MSEs when the underlying degradation model is correctly specified. This observation agrees with the conclusion in Chapter 2 for the univariate case. From Tables 3.3, 3.4 and 3.5, the parametric approaches with the correctly specified degradation processes and correctly specified copula (i.e., those values highlighted in bold) give the smallest MSEs in most cases as expected. The Semi2 approach with correctly specified degradation processes provides MSEs comparable to the values highlighted in bold. Once again, this indicates that the effect of misspecifying the underlying degradation processes on the performance of the estimation methods can be severe. In contrast, there are no substantial differences in the MSEs when the copula function is misspecified for the parametric approach and Semi1 approach. This indicates that misspecifying the underlying copula function may not affect much on the performance of the estimation methods.

For the nonparametric approaches, NP1 and NP2, from Tables 3.2 – 3.5, we observe that the two proposed nonparametric approaches perform well compared to the parametric approach with correctly specified degradation processes and copula function. Among the two proposed nonparametric approaches, NP1 gives smaller MSEs compared to NP2 in most cases. It is also noticeable that increasing in dependency slightly increasing the MSEs. The MSEs are increasing for higher percentiles for $T_{\max}$ distribution, whereas for

Table 3.2: Simulated MSEs of different percentiles of the FPT distribution when the data are generated from two independent gamma process

Percentile	Series System ($T_{\min}$) **Independent**														
	MLE							Semi1			Semi2		NP	
	G-f	G-c	G-g	IG-f	IG-c	IG-g	G-BVBS	f	c	g	G	IG	NP1	NP2
1-st	2.81	2.82	2.81	435.55	435.54	435.55	25.23	3.09	3.09	3.09	2.81	435.55	3.09	4.03
10-th	2.11	2.11	2.11	116.30	116.25	116.25	8.45	2.19	2.19	2.19	2.12	116.41	2.19	2.46
50-th	2.06	2.10	2.08	3.65	4.75	3.88	1.89	2.07	2.11	2.08	2.08	4.58	2.09	1.76
90-th	2.10	2.16	2.11	11.00	9.30	11.42	5.18	2.11	2.18	2.12	2.19	8.06	2.20	1.90
99-th	2.24	2.17	2.35	43.22	38.98	52.27	7.43	2.25	2.19	2.39	2.57	37.22	2.58	2.81
Percentile	Series System ($T_{\max}$) **Independent**														
	MLE							Semi1			Semi2		NP	
	G-f	G-c	G-g	IG-f	IG-c	IG-g	G-BVBS	f	c	g	G	IG	NP1	NP2
1-st	1.89	2.21	1.91	18.67	16.13	18.10	8.68	1.91	2.25	1.92	2.29	14.63	2.31	3.33
10-th	1.77	1.81	1.78	4.29	4.12	3.88	2.67	1.78	1.82	1.78	1.83	2.93	1.83	2.17
50-th	2.20	2.21	2.20	52.42	54.01	51.94	3.26	2.20	2.20	2.20	2.22	54.58	2.21	2.62
90-th	3.65	3.65	3.65	476.81	476.83	476.28	8.73	3.70	3.70	3.69	3.65	476.92	3.69	4.38
99-th	5.98	5.98	6.00	1040.12	1040.11	1040.04	18.53	6.17	6.17	6.18	5.99	1040.12	6.17	7.21

$T_{\min}$ the MSEs are in a similar range.

Overall, unless one is certain about the parametric form of the underlying bivariate degradation process, the parametric approach based on MLEs and the semiparametric approach Semi2 are not recommended. When both the underlying degradation process and copula function are unknown, we would recommend using either the novel nonparametric approach NP1 (empirical saddlepoint with empirical copula) or the semiparametric approach Semi1. Furthermore, the BVBS approximation may not be a better option when estimating the tail probabilities of the FPT distribution. However, in this study, we only consider copula functions in the family of Archimedean copulas and it would be important to investigate the effect of misspecification of copula for other families of copula. Hence, the proposed nonparametric approach NP1 is recommended in general.

3.3.1. Monte Carlo simulation when data generated from generalized Kibble's bivariate gamma distribution

In this section, we evaluate the proposed methods in this study by generating the degradation data from a bivariate gamma distribution without using a copula. Kibble (1941) introduced the Kibble's bivariate gamma distribution, which can be obtained using

Table 3.3: Simulated MSEs of different percentiles of the FPT distribution when the data are generated from bivariate gamma process with Frank copula with different dependent structure

Percentile	MLE							Semi1			Semi2		NP	
	G-f	G-c	G-g	IG-f	IG-c	IG-g	G-BVBS	f	c	g	G	IG	NP1	NP2
1-st	**3.04**	3.27	3.05	442.24	442.23	442.21	26.17	3.33	3.57	3.34	3.05	442.24	3.33	4.39
10-th	**2.60**	2.82	2.60	117.06	117.54	116.65	9.75	2.61	2.86	2.60	2.60	117.15	2.62	3.13
50-th	**2.48**	2.39	2.38	2.21	4.53	2.36	2.75	2.50	2.39	2.39	2.47	2.27	2.48	2.70
90-th	**2.55**	3.12	2.57	14.43	5.16	17.79	6.38	2.59	3.09	2.63	2.65	14.52	2.70	2.69
99-th	**2.84**	3.83	5.26	36.00	19.14	53.33	11.53	2.91	3.87	5.42	3.24	36.28	3.35	3.66
Parallel System ($T_{\max}$) $\xi_F = 2.92$ ($\tau_F = 0.30$)														
Percentile	MLE							Semi1			Semi2		NP	
	G-f	G-c	G-g	IG-f	IG-c	IG-g	G-BVBS	f	c	g	G	IG	NP1	NP2
1-st	**2.07**	3.43	2.16	23.54	11.84	25.56	8.64	2.10	3.55	2.18	2.36	24.43	2.37	2.67
10-th	**2.36**	2.42	2.28	8.05	3.17	7.07	3.44	2.36	2.44	2.26	2.45	8.12	2.44	2.48
50-th	**3.01**	3.49	3.03	64.01	74.65	62.14	3.21	3.00	3.49	3.02	2.98	63.65	2.98	3.93
90-th	**4.27**	4.24	4.39	493.04	493.39	491.85	10.64	4.36	4.35	4.52	4.25	493.09	4.35	4.80
99-th	**6.43**	6.43	6.63	1065.99	1066.00	1065.91	20.33	6.67	6.67	6.90	6.43	1066.00	6.67	7.70
Series System ($T_{\min}$) $\xi_F = 18.2$ ($\tau_F = 0.80$)														
Percentile	MLE							Semi1			Semi2		NP	
	G-f	G-c	G-g	IG-f	IG-c	IG-g	G-BVBS	f	c	g	G	IG	NP1	NP2
1-st	**3.67**	4.05	3.84	438.91	438.80	438.83	27.83	3.93	4.49	4.16	3.67	438.92	3.94	5.58
10-th	**3.76**	4.11	3.73	134.53	134.03	133.37	7.49	3.79	4.13	3.78	3.72	133.58	3.75	3.91
50-th	**3.40**	3.48	3.53	3.23	8.19	3.53	3.68	3.36	3.49	3.53	3.38	3.27	3.34	3.41
90-th	**3.30**	4.83	3.19	11.39	6.54	12.24	10.19	3.35	4.80	3.23	3.40	12.81	3.46	3.50
99-th	**3.80**	6.20	4.03	30.01	17.09	34.15	15.04	3.91	6.21	4.08	4.18	33.15	4.33	4.89
Parallel System ($T_{\max}$) $\xi_F = 18.2$ ($\tau_F = 0.80$)														
Percentile	MLE							Semi1			Semi2		NP	
	G-f	G-c	G-g	IG-f	IG-c	IG-g	G-BVBS	f	c	g	G	IG	NP1	NP2
1-st	**2.73**	2.42	2.39	21.14	21.59	24.6	13.10	2.75	2.49	2.43	2.93	27.03	2.95	2.98
10-th	**2.71**	2.70	2.74	8.35	6.58	7.69	6.14	2.71	2.72	2.72	2.78	10.93	2.78	3.15
50-th	**4.23**	5.84	4.58	65.54	82.11	65.42	4.23	4.30	5.70	4.51	4.25	60.53	4.31	6.35
90-th	**6.03**	6.38	6.19	517.27	518.15	516.76	9.61	6.13	6.48	6.30	5.90	517.09	6.01	6.76
99-th	**7.16**	7.14	7.43	1056.59	1056.6	1056.54	23.63	7.38	7.38	7.63	7.17	1056.60	7.38	8.54

the sums of squares of the bivariate normal data. Krishnaiah and Rao (1961) expanded the Kibble's bivariate gamma distribution for higher dimensions. Suppose the $Y = \{Y_1, Y_2\}$ be a bivariate normal random variable with mean $\mathbf{0}$ and covariance matrix

$$\Sigma = \begin{pmatrix} {\sigma_1}^2 & \rho_0\sigma_1\sigma_2 \\ \rho_0\sigma_1\sigma_2 & {\sigma_2}^2 \end{pmatrix},$$

where ρ_0 is the correlation coefficient and σ_1^2 and σ_2^2 are the variances of Y_1 and Y_2, respectively. Let $Y_1 = \{Y_{11}, Y_{12}, \ldots, Y_{1n}\}$ and $Y_2 = \{Y_{21}, Y_{22}, \ldots, Y_{2n}\}$; thus, the sum of squares of $\{Y_1, Y_2\}$ can be evaluated by $X = \sum_{j=1}^{n} Y_{1j}^2$ and $Z = \sum_{j=1}^{n} Y_{2j}^2$. Then, $\{X, Z\}$ has a bivariate gamma distribution with marginals $X \sim gamma(n/2, 2\sigma_1^2)$ and $Z \sim gamma(n/2, 2\sigma_2^2)$ correlation coefficient $\rho = \rho_0^2$.

Table 3.4: Simulated MSEs of different percentiles of the FPT distribution when the data are generated from bivariate gamma process with Clayton copula with different dependent structure

Percentile	MLE							Semi1			Semi2		NP	
	G-f	**G-c**	G-g	IG-f	IG-c	IG-g	G-BVBS	f	c	g	G	IG	NP1	NP2
Series System ($T_{\min}$) $\xi_C = 0.86$ ($\tau_C = 0.30$)														
1-st	2.99	**3.39**	3.01	437.25	437.20	437.25	26.14	3.29	3.72	3.30	3.27	437.21	3.60	4.34
10-th	3.30	**2.96**	3.22	137.27	135.32	135.73	4.92	3.32	3.01	3.25	2.96	133.25	3.02	2.62
50-th	3.81	**2.65**	3.24	7.04	6.29	3.33	2.67	3.81	2.67	3.25	2.66	3.17	2.70	2.56
90-th	3.36	**2.75**	2.64	8.07	7.43	21.13	6.85	3.39	2.75	2.66	2.82	12.25	2.83	2.56
99-th	2.74	**2.92**	9.30	36.19	33.74	71.46	7.97	2.78	2.95	9.48	3.26	43.06	3.28	5.01
Parallel System ($T_{\max}$) $\xi_C = 0.86$ ($\tau_C = 0.30$)														
1-st	11.67	**1.90**	7.57	4.18	11.46	13.32	24.82	11.74	1.98	7.53	2.11	26.42	2.16	11.48
10-th	4.86	**2.04**	3.37	3.02	3.09	4.92	6.98	4.86	2.06	3.32	2.11	8.00	2.11	5.24
50-th	3.69	**3.15**	2.95	60.34	61.26	48.09	3.01	3.67	3.12	2.91	3.14	55.49	3.13	4.16
90-th	4.26	**4.25**	4.40	483.49	483.51	482.36	9.93	4.32	4.33	4.46	4.26	483.44	4.32	4.81
99-th	6.57	**6.58**	6.78	1054.50	1054.50	1054.50	19.66	6.76	6.76	6.98	6.58	1054.50	6.75	7.80

Percentile	MLE							Semi1			Semi2		NP	
	G-f	**G-c**	G-g	IG-f	IG-c	IG-g	G-BVBS	f	c	g	G	IG	NP1	NP2
Series System ($T_{\min}$) $\xi_C = 8$ ($\tau_C = 0.80$)														
1-st	3.51	**4.01**	3.69	439.14	439.13	439.13	27.61	3.71	4.40	3.93	3.94	439.13	4.28	5.18
10-th	3.65	**4.13**	3.60	134.40	132.23	133.18	6.97	3.63	4.11	3.59	4.07	132.21	4.04	3.48
50-th	3.34	**3.33**	3.53	3.01	4.25	3.18	3.77	3.35	3.32	3.61	3.32	3.32	3.31	3.36
90-th	3.30	**3.59**	3.20	11.45	8.79	12.30	11.12	3.35	3.68	3.27	3.71	12.39	3.79	3.46
99-th	4.63	**3.96**	6.57	41.70	33.04	45.82	11.09	4.73	4.10	6.61	4.28	42.87	4.42	7.07
Parallel System ($T_{\max}$) $\xi_C = 8$ ($\tau_C = 0.80$)														
1-st	4.44	**2.55**	3.69	13.31	20.62	16.14	21.92	4.56	2.67	3.73	2.57	20.96	2.69	6.69
10-th	3.29	**2.73**	4.09	3.96	5.04	3.93	11.58	3.32	2.78	4.05	2.77	6.25	2.81	6.82
50-th	4.13	**4.21**	4.63	70.03	77.66	69.55	4.43	4.25	4.30	4.58	4.23	66.06	4.31	7.32
90-th	5.58	**5.24**	6.29	481.17	481.54	480.91	14.07	5.72	5.37	6.44	5.20	481.28	5.33	5.59
99-th	7.07	**7.06**	7.37	1058.82	1058.82	1058.82	22.99	7.33	7.32	7.64	7.06	1058.82	7.31	8.47

Using above approach, we generated bivariate gamma degradation process $\{X_t, Z_t\}$ such that the marginal degradation processes follows $X_t \sim Gamma(2, 0.5)$, $Z_t \sim Gamma(2, 1)$ with correlation coefficients $(0.3, 0.8)$. The threshold levels are considered as $c_x = 100$ and $c_z = 200$, respectively. In this simulation, we choose different threshold levels in two marginal degradation processes to ensure the mean failure time of two processes to be similar. As it is difficult to obtain the exact FPT distribution for this bivariate gamma process, we considered to apply parametric bootstrap method to estimate the exact distribution for $T_{\max}$ and $T_{\min}$.

Step 1: Set $k = 1$ and $b = 1$.

Step 2: Set $T_{\min}^{(b)} = \infty$.

Step 3: Generate bivariate gamma sample $\{\Delta x_k^*, \Delta z_k^*\}$ with marginal distributions $\Delta X \sim$

Table 3.5: Simulated MSEs of different percentiles of the FPT distribution when the data are generated from bivariate gamma process with Gumbel copula with different dependent structure

Percentile	MLE							Semi1			Semi2		NP	
	G-f	G-c	**G-g**	IG-f	IG-c	IG-g	G-BVBS	f	c	g	G	IG	NP1	NP2
Series System ($T_{\min}$) $\xi_G = 1.43$ ($\tau_G = 0.30$)														
1-st	3.11	3.29	**3.12**	440.38	440.38	440.36	26.44	3.54	3.75	3.55	3.13	440.38	3.56	4.82
10-th	2.75	2.93	**2.77**	116.44	116.80	115.92	10.40	2.87	3.12	2.88	2.77	116.18	2.91	3.72
50-th	2.63	2.52	**2.53**	2.33	4.60	2.36	3.17	2.63	2.55	2.54	2.55	2.57	2.57	3.35
90-th	2.62	3.27	**2.77**	14.08	5.30	18.33	5.28	2.61	3.26	2.76	2.78	17.14	2.78	3.08
99-th	7.35	12.21	**2.94**	17.49	7.93	30.02	20.94	7.48	12.22	2.98	3.19	28.59	3.26	3.94
Parallel System ($T_{\max}$) $\xi_G = 1.43$ ($\tau_G = 0.30$)														
1-st	2.29	3.51	**2.29**	23.32	12.24	26.70	6.79	2.39	3.64	2.41	2.50	25.42	2.57	2.84
10-th	2.64	2.61	**2.53**	7.88	3.17	7.54	3.15	2.64	2.63	2.55	2.51	6.81	2.52	2.62
50-th	3.17	3.65	**3.12**	59.15	69.42	56.41	3.72	3.14	3.58	3.11	3.12	57.24	3.10	3.59
90-th	4.32	4.29	**4.59**	489.95	490.25	488.70	11.72	4.38	4.36	4.63	4.61	488.92	4.64	4.77
99-th	6.39	6.38	**6.66**	1062.58	1062.59	1062.50	21.34	6.58	6.57	6.84	6.59	1062.54	6.76	7.62

Percentile	MLE							Semi1			Semi2		NP	
	G-f	G-c	**G-g**	IG-f	IG-c	IG-g	G-BVBS	f	c	g	G	IG	NP1	NP2
Series System ($T_{\min}$) $\xi_G = 5$ ($\tau_G = 0.80$)														
1-st	3.61	3.91	**3.82**	437.32	437.24	437.27	28.8	4.05	4.36	4.26	3.77	437.28	4.20	5.93
10-th	3.70	4.11	**3.81**	133.36	131.73	132.03	8.09	3.75	4.20	3.85	3.80	131.53	3.86	4.60
50-th	3.35	3.40	**3.33**	3.10	6.19	3.19	3.48	3.17	3.48	3.19	3.35	3.07	3.24	3.66
90-th	3.21	4.49	**3.04**	11.75	7.71	12.78	8.96	3.22	4.50	3.07	3.06	13.37	3.09	3.49
99-th	4.88	9.62	**3.35**	21.93	14.69	25.04	19.59	4.96	9.65	3.41	3.37	25.18	3.43	3.74
Parallel System ($T_{\max}$) $\xi_G = 5$ ($\tau_G = 0.80$)														
1-st	2.82	2.30	**2.36**	20.84	26.77	25.19	12.22	2.95	2.37	2.49	2.40	29.47	2.50	2.52
10-th	2.74	2.65	**2.72**	7.95	7.39	7.97	5.48	2.76	2.67	2.75	2.70	10.63	2.72	2.55
50-th	4.15	5.41	**4.24**	69.02	82.77	67.92	3.94	4.16	5.30	4.23	4.28	64.39	4.25	5.07
90-th	5.94	6.23	**6.11**	521.98	522.45	521.61	10.22	6.03	6.31	6.21	6.08	521.61	6.17	6.65
99-th	6.96	6.94	**7.17**	1056.10	1056.10	1056.09	23.53	7.18	7.17	7.41	7.15	1056.09	7.39	8.47

$gamma(\alpha_x, \beta_x)$ and $\Delta Z \sim gamma(\alpha_z, \beta_z)$ and correlation coefficient of ρ.

Step 4: Compute $X_k = \sum_{\ell=1}^{k} \Delta x_\ell^*$ and $Z_k = \sum_{\ell=1}^{k} \Delta z_\ell^*$.

Step 5: If $X_k < c_x$ and $Z_k < c_z$, then set $k = k+1$ and return to Step 3.

Step 6: If $X_k > c_x$ and $Z_k < c_z$, then set $T_{\min}^{(b)} = \min\{T_{\min}^{(b)}, k\}$, set $k = k+1$ and return to Step 3.

Step 7: If $X_k < c_x$ and $Z_k > c_z$, then set $T_{\min}^{(b)} = \min\{T_{\min}^{(b)}, k\}$, set $k = k+1$ and return to Step 3.

Step 8: If $X_k > c_x$ and $Z_k > c_z$, then set $T_{\min}^{(b)} = \min\{T_{\min}^{(b)}, k\}$ and $T_{\max}^{(b)} = k$; if $b < B$, set $b = b+1$, $k = 1$ and return to Step 2.

Once the bootstrap samples of size B are obtained, the exact distributions of $T_{\max}$ and

$T_{\min}$ can be obtained by

$$\begin{aligned} \widehat{\Pr}_{exact}(T_{\min} < t) &= \frac{1}{B}\sum_{b=1}^{B} \mathbf{1}(T_{\max}^{(b)} \leq t) \\ \text{and } \widehat{\Pr}_{exact}(T_{\max} < t) &= \frac{1}{B}\sum_{b=1}^{B} \mathbf{1}(T_{\min}^{(b)} \leq t). \end{aligned}$$

For Monte Carlo simulation, we generate 10 bivariate degradation paths ($I = 10$) with 50 measurements ($m_i = 50$ for $i = 1, 2, \ldots, 10$) following the Kibble's bivariate gamma distribution. The degradation measurements are taken at the equal-width time intervals with the time increment $\Delta t = 1$. Using the BVBS approximation, parametric copula, semiparametric and nonparametric methods discussed in Section 3.2, the distributions for T_{min} and T_{max} are estimated. However, for this simulation, we do not consider the misspecification with the IG distribution. The simulation is repeated 1000 times for each setting. Table 3.6 shows the performance of different estimation methods for the distributions of $T_{\max}$ and $T_{\min}$, which are evaluated by MSEs for estimating the 1-st, 10-th, 50-th, 90-th and 99-th percentiles of the distributions.

Based on Table 3.6, we can clearly see that the BVBS approximation performs poorly when estimating the lower tail probabilities of T_{min} and upper tail probabilities of T_{max}. On the other hand, all other parametric, semiparametric and nonparametric methods proposed in this paper have relatively lower MSEs. Except with the BVBS, the MSEs increase with the percentile for all the proposed methods. Furthermore, parametric and semiparametric methods with the Gumbel copula (G-g and g) provides relatively lower MSEs compared to all other approaches. Both nonparametric methods (NP1 and NP2) appears to be robust in both correlation settings. This implies the clear advantage of using of nonparametric methods as the results are consistent irrespective of the way in which

Table 3.6: Simulated MSEs of different percentiles of the FPT distribution when the data are generated from generalized Kibble's bivariate gamma distribution

Percentile	MLE				Semi1			Semi2	NP	
	G-BVBS	G-f	G-c	G-g	f	c	g	G	NP1	NP2
Series System ($T_{\min}$) $\rho = 0.3$										
1-st	131.32	7.55	7.29	7.54	7.69	7.55	7.69	7.54	7.71	6.66
10-th	46.48	7.12	6.83	7.00	7.22	6.85	7.08	7.04	7.19	6.28
50-th	9.19	7.45	6.95	6.93	7.79	7.34	7.38	6.93	7.32	6.48
90-th	9.99	8.46	7.80	6.92	8.31	7.68	6.96	7.01	6.98	7.07
99-th	26.57	9.01	8.50	10.09	9.04	8.61	10.15	8.72	8.79	8.31
Parallel System ($T_{\max}$) $\rho = 0.3$										
1-st	12.87	7.89	7.16	6.55	7.91	7.21	6.68	7.20	7.22	7.08
10-th	9.07	7.29	6.82	6.82	7.25	6.82	6.81	6.72	6.80	7.00
50-th	9.48	7.48	7.37	7.30	7.64	7.59	7.58	7.30	7.51	7.70
90-th	103.58	9.21	9.23	8.69	9.21	9.23	8.76	8.82	8.95	10.27
99-th	491.72	12.85	12.85	12.07	12.77	12.77	12.17	12.65	12.66	14.59
Series System ($T_{\min}$) $\rho = 0.8$										
1-st	133.10	8.17	7.26	7.82	8.21	7.42	7.92	8.08	8.14	7.83
10-th	50.16	9.22	7.68	8.03	9.24	7.74	8.22	8.16	8.17	7.70
50-th	9.80	13.47	9.31	8.93	13.52	10.07	9.92	8.79	9.89	8.23
90-th	12.17	24.90	17.09	9.68	24.96	17.09	9.72	10.08	10.20	9.54
99-th	17.61	47.42	37.03	10.66	47.36	36.75	10.82	12.43	12.60	12.25
Parallel System ($T_{\max}$) $\rho = 0.8$										
1-st	11.89	18.77	10.48	7.91	18.95	10.54	8.00	8.11	8.20	8.61
10-th	11.33	13.92	8.52	8.26	13.87	8.60	8.30	8.31	8.22	8.35
50-th	9.48	10.91	9.46	9.00	10.95	9.46	9.07	9.08	9.15	9.05
90-th	82.89	9.97	9.92	10.94	9.88	9.80	11.04	10.61	10.61	10.14
99-th	429.08	10.83	10.81	11.10	11.08	11.04	11.31	11.07	11.00	11.41

the data are generated.

3.4. Numerical Example

To illustrate the methods proposed in this study, we consider the LED degradation data set with 24 samples in Chaluvadi (2008). The lumen maintenance was inspected at every 50 hours up to 250 hours. Fang et al. (2018) used the same data set and estimated the FPT distribution using bivariate degradation models alone with the Frank copula. For our analysis, using the bivariate degradation data presented in Fang et al. (2018, Table 1), we assume that the lumen maintenance of the first 6 LEDs (PC 1) and next 6 LEDs (PC 2) under the current level 40 mA are dependent and consider the threshold level as 50% from the initial light level for both PCs. Figure 3.1 shows the bivariate degradation

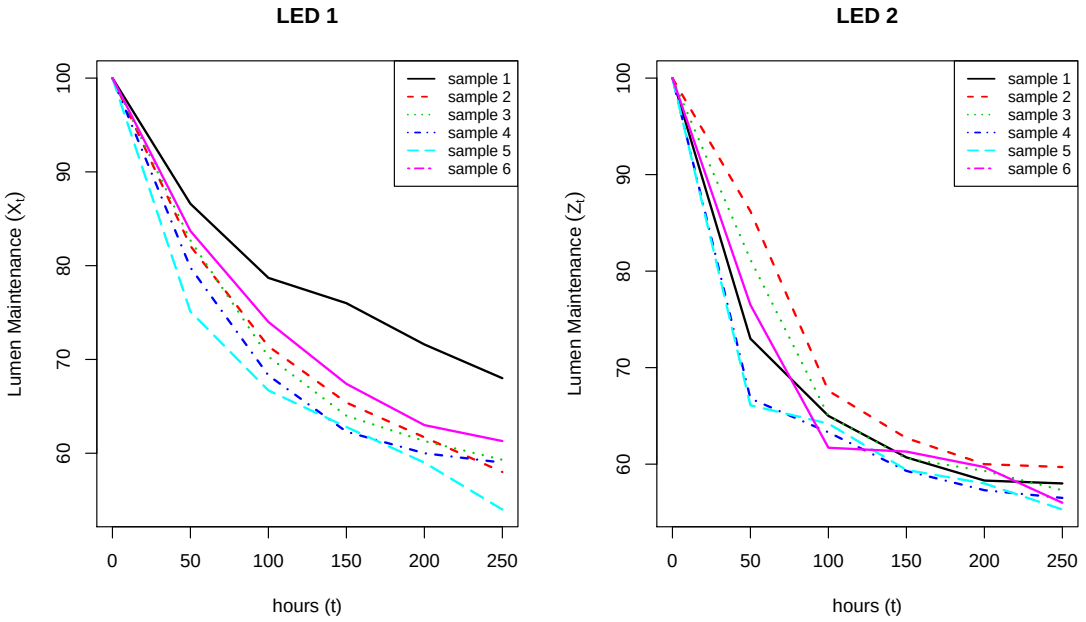

Figure 3.1: Bivariate LED degradation data for 6 samples with 5 inspection points at $t = 50, 100, 150, 200$ and 250 hours

data with $I = 6$ and $m_i = 5$, $i = 1, 2, \ldots, 6$. Fang et al. (2018) fitted the data with degradation processes such as Wiener, gamma, and IG with the Frank copula and showed that gamma degradation process has the lowest Akaike information criterion (AIC) among all. In addition, for the same data set, Hao et al. (2015) constructed a bivariate model with gamma degradation process with the Frank copula. Since all previous studies on this data set are based on a fully parametric approaches, here we apply the semiparametric and nonparametric approaches proposed in this paper to determine the FPT distribution for series connection ($T_{\min}$) and parallel connection ($T_{\max}$) of two PCs.

Assuming each PC follows a gamma process, the FPT distributions of $T_{\min}$ and $T_{\max}$ are estimated based on Clayton, Frank and Gumbel copula functions. Figures 3.2, 3.3, and 3.4 plot the estimated survival functions of $T_{\min}$ and $T_{\max}$ based on the five estimation methods presented in Section 3.2 (i.e., bivariate gamma, Semi1, Semi2, NP1 and NP2) with Clayton, Frank and Gumbel copula functions, respectively, for the parametric and Semi2 approaches. Additionally, for comparative purpose, BVBS approximation is also

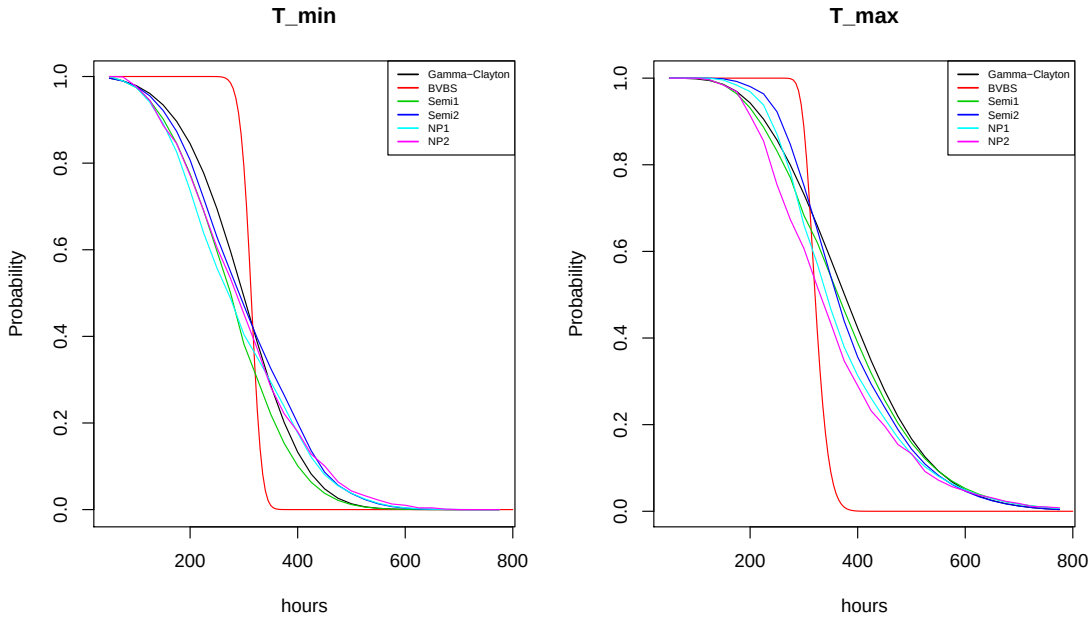

Figure 3.2: Estimated survival function of the FPT distributions based on Clayton copula

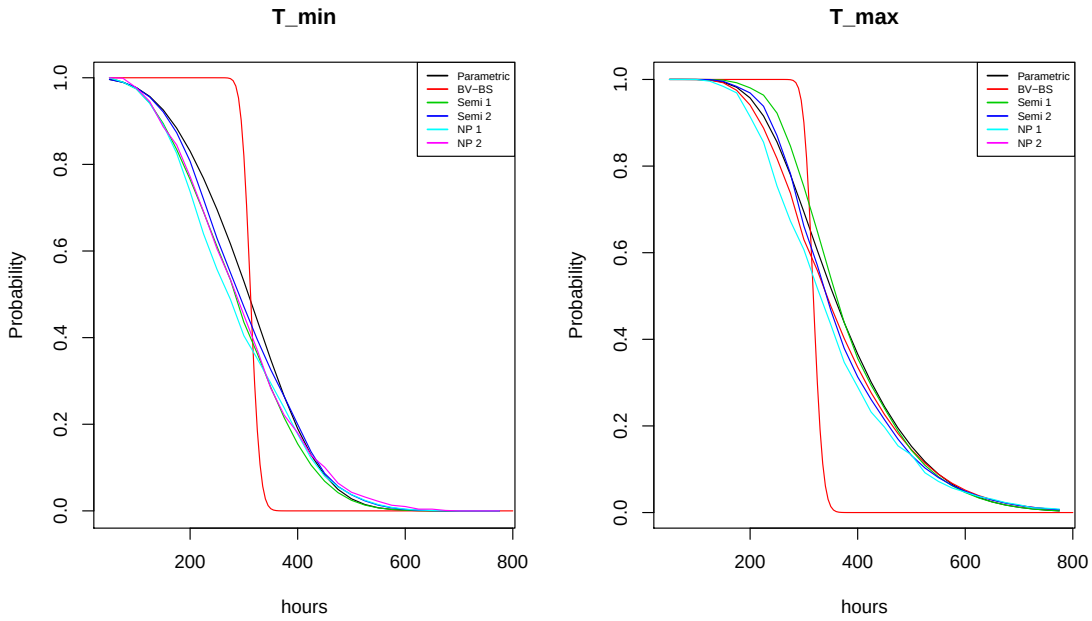

Figure 3.3: Estimated survival function of the FPT distributions based on Frank copula

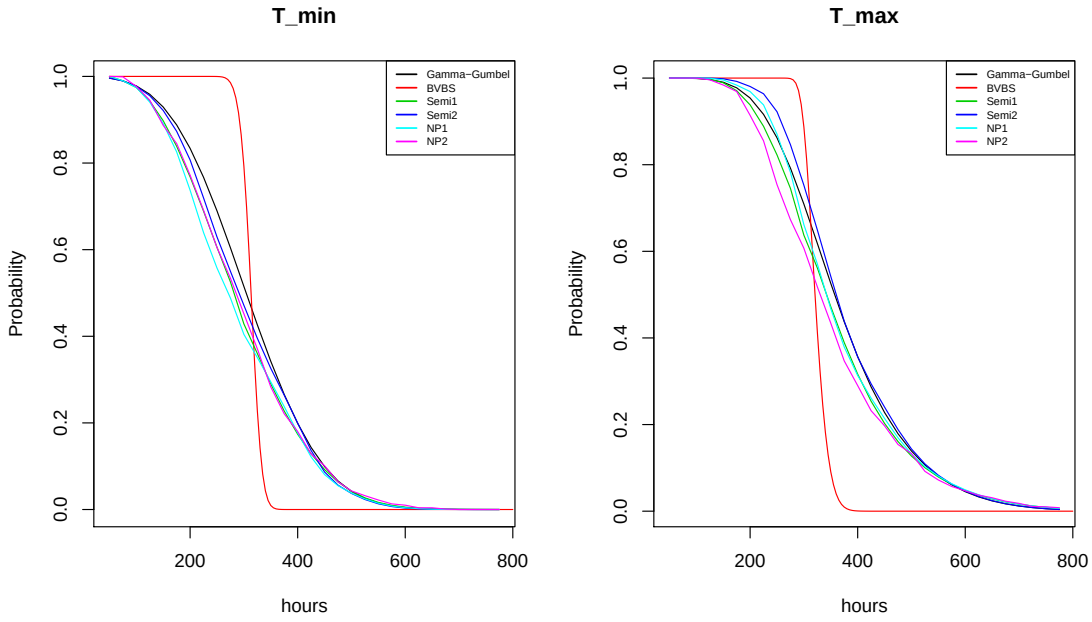

Figure 3.4: Estimated survival function of the FPT distributions based on Gumbel copula

considered to estimate the the distributions of $T_{\min}$ and $T_{\max}$. We can see that the proposed semiparametric and nonparametric approaches provide similar estimated survival curves compared to the fully parametric copula methods. It should be emphasized that the semiparametric and nonparametric approaches proposed here make less or no assumption on the underlying model. Furthermore, the FPT distribution estimated with the BVBS approximation appears to have relatively lower variability with similar mean compared to the other methods. However, it is not certain why the lower variance occurs in the BVBS approximation compared to other proposed methods since the sample size in the data set is relatively small.

3.5. Concluding Remarks

In this chapter, we proposed different semiparametric and nonparametric methods to estimate the FPT distribution of dependence bivariate degradation data. The ESA and

bootstrap methods are used to estimate the marginal FPT distributions nonparametrically, whereas the empirical copula is used to estimate the joint distribution of two dependence degradation processes nonparametrically. We have demonstrated with simulations and a numerical example that the proposed semiparametric and nonparametric approaches can provide reasonable approximation of the FPT distribution of the system when the subsystems are connected in series or in parallel. In general, when the underlying degradation process and dependence structure are unknown, we would recommend to use of the nonparamertic approach NP1 (ESA with empirical copula).

As shown in the simulation study, the proposed methodologies work well when the measured time intervals are equal; however, the ESA (Semi1 and NP1) can be inaccurate when the measured time intervals are unequal, and thereby, suitable adjustments are needed. The imputation techniques proposed in Section 2.4.2 for univariate degradation process can be generalized to the bivariate degradation process to overcome this issue. Wang (1990) proposed a saddlepoint approximation method to estimate the bivariate CDF; in addition, Kolassa et al. (2003) expanded the study by Wang (1990) for multivariate scale. For future study, the techniques presented in Wang (1990) and Kolassa et al. (2003) can be applied along with the empirical CGF to obtain nonparametric estimate the joint FPT distribution of two or more correlated degradation processes.

Chapter 4

Evaluation of Mean-Time-To-Failure based on Nonlinear Degradation Data with Applications

4.1. Introduction

With advances in technology, both manufacturer and consumer have demanded greater product reliability. As a result, to improve customer satisfaction, accurate evaluation of the reliability of products plays an important role in product design, development, and management of any warranty. Obtaining lifetime information for highly reliable products is a challenging problem in reliability engineering. The estimation of lifetime characteristics for those highly reliable products is often performed using degradation data, as it would be extremely expensive to obtain lifetime data for a long period of time. The lifetime distribution of products subjected to degradation is also called the first-passage time (FPT) distribution since it is designated as a failure when the degradation measurements reach a particular threshold level. In addition, the mean-time-to-failure (MTTF), which is the expected failure time, is one of the critical reliability characteristics to be estimated from the degradation data. To estimate the FPT distribution and the MTTF, general path models, stochastic processes and data-driven approaches such as particle filtering have been developed in the literature (see, for example, Meeker and Escobar, 1998; Chen et al., 2017).

For the Lévy process models, the linearity of degradation data (i.e., the degradation measurements are linearly related to time) is a key assumption. However, in practical applications, the degradation data may not be linearly related with time. Therefore, a suitable

transformation on the data may be required before applying a Lévy process model. For instance, residual life estimation with the time-transformed Wiener process was studied by Whitmore and Schenkelberg (1997); Si et al. (2012) and Wang et al. (2014). Nonlinear degradation data modeling with general path models were studied by Lu and Meeker (1993); Meeker et al. (1998) and Xu et al. (2016). Moreover, Bae and Kvam (2004) proposed a general path model with random coefficients for nonlinear degradation data and applied the model to analyze a vacuum fluorescent display (VFD) data set. Si (2015) extended the study in Si et al. (2012) to estimate the FPT distribution by using a general nonlinear stochastic process with time-dependent drift. Si (2015) also applied state-space models with the Kalman filter to model the degradation data with adaptive parameter estimation and applied the proposed technique to analyze the NASA lithium-ion battery data (Saha and Goebel, 2007). Miao et al. (2013) and Feng et al. (2013) used particle filtering to accommodate the nonlinearity of the degradation data and applied such methods to analyze of a lithium-ion battery data set.

Another approach to model the non-linear failure time data was proposed by Lindqvist et al. (2003) using a trend-renewal-process (TRP) model to transform a non-homogeneous Poisson process (NHPP) to a homogeneous Poisson process using a time transformation function. The TRP model transforms the failure time data to a linear scale using a suitable trend function. Following this approach, Wang et al. (2019) proposed another TRP-type model and applied the model to analyze a nonlinear lithium-ion battery degradation data set. However, the model and formulas studied by Wang et al. (2019) were developed for some specific conditions such as when the transformed degradation data are assumed to follow a normal distribution. In addition, Wang et al. (2019) took the cumulative summation of the degradation measurements before applying the TRP model, which may not be appropriate. Thus, it is desired to consider some innovative and more flexible approaches to model the degradation data with the TRP model following the methodologies proposed in Lindqvist et al. (2003) and Wang et al. (2019). In this chapter, we aim to propose some generalized parametric and semiparametric approaches, which require less restrictive as-

sumptions, to estimate the MTTF based on degradation data.

The rest of this chapter is organized as follows. In Section 4.2, following the TRP-type model proposed by Lindqvist et al. (2003), we propose the parametric and semiparametric approaches to estimate the MTTF of the degradation data. In Section 4.3, we consider the TRP model proposed by Wang et al. (2019), namely the cumulative-sum-trend-renewal-process (CTRP), and propose the corresponding parametric and semiparametric approaches to estimate the MTTF. A Monte Carlo simulation study is used to evaluate the performance of the proposed methodologies under different settings in Section 4.4. From the simulation results, we found that misspecifying the underlying model may have a severe negative effect on the estimation procedures; therefore, we propose a model selection procedure to select among the Lévy process, TRP and CTRP models in Section 4.5. The effectiveness of the proposed model selection procedure is demonstrated by means of a Monte Carlo simulation study. In Section 4.6, two lithium-ion battery degradation data sets are used to illustrate the proposed models, estimation methods and model selection procedure. Finally, some concluding remarks are provided in Section 4.7.

4.2. Trend-Renewal-Process Model

The-trend-renewal-process (TRP) is generally applicable to transform a non–homogeneous Poisson process (NHPP) to a homogeneous Poisson process using a time transformation function $\Lambda(t)$, where $\Lambda(t)$ is an increasing function in t. Here, $\Lambda(t) = \int_0^t \lambda(u)du < \infty$, where $\lambda(t)$ is a non-negative function of $t > 0$ called the trend function. Suppose $T_j,\ j = 1,2,\ldots,$ are the successive event times, Lindqvist et al. (2003) defined the TRP to be $\Delta\Lambda(T_j) = \Lambda(T_j) - \Lambda(T_{j-1}),\ j = 1,2,\ldots$ which are independent and identically distributed (i.i.d.) with a PDF, $\mathfrak{F}$, with expected value 1.

Recently, Wang et al. (2019) applied the idea of the TRP to analyze a lithium-ion battery degradation data set. Wang et al. (2019) considered the log-linear trend func-

tion, $\lambda(t) = ae^{bt}$, and the power-law trend function, $\lambda(t) = abt^{b-1}$. For the distribution of $\Delta\Lambda(T_j)$, Wang et al. (2019) considered the two-parameter lognormal distribution, the two-parameter Weibull distribution and the normal distribution. All these distributions are assumed to have an expected value of 1; therefore, there is only one parameter that needs to be estimated for the PDF, $\mathfrak{F}$, and we denote this parameter as ω.

In this study, we propose a generalized TRP approach for degradation data. We consider the cases that the parametric form of the PDF $\mathfrak{F}$ is specified and non-specified. Moreover, we proposed different point and interval estimation approaches to estimate the MTTF.

4.2.1. TRP model with specific distribution

Following the TRP model proposed by Lindqvist et al. (2003), we focus on the point and interval estimation of the MTTF based on degradation data with the TRP model.

4.2.1.1. Model and point estimation of the MTTF

We denote the degradation measurements at time t_j as X_j, $j = 1,2,\ldots,m$. Without loss of generality, we assume that the degradation measurements are taken at equal time intervals and the time is scaled to unit increments (i.e., $t_j = j$). Suppose the trend function transformation at time t_j is $\Lambda(X_j|\theta)$, and we assume that $\Delta\Lambda(X_j|\theta) = \Lambda(X_j|\theta) - \Lambda(X_{j-1}|\theta)$ follows a Lévy process with a known PDF $\mathfrak{F}$ with an expected value of 1, where θ is the parameter vector associate with the trend function. Note that the assumption for the distribution of $\Delta\Lambda(X_j|\theta)$ with mean equal to 1 (i.e., $E[\Delta\Lambda(X_j|\theta)] = 1$) is mainly for computational convenience. We denote the PDF of $\Delta\Lambda(X_j|\theta)$ as $\mathfrak{F}(\Delta\Lambda(X_j|\theta);\omega)$, where ω is the standard deviation of the Lévy process of X_j. We consider that the link function

$\lambda(t|\theta)$ satisfies

$$\Lambda(X_j|\theta) = \int_0^{X_j} \lambda(u|\theta)du.$$

For example, for the log-linear link function $\lambda(t|\theta) = ae^{bt}$, $\Lambda(X_j|\theta)$ is defined as

$$\Lambda(X_j|\theta) = \int_0^{X_j} a\exp(bu)du = \frac{a}{b}\left\{\exp(bX_j) - 1\right\}, \tag{4.1}$$

where $\theta = (a,b)$.

Let $W_j = \Lambda(X_j|\theta) = \sum_{k=1}^{j} \Delta\Lambda(X_k|\theta)$, if $\Delta\Lambda(X_j|\theta)$ is a Wiener process, then $W_j \sim N(t_j, t_j\sigma^2)$; and if $\Delta\Lambda(X_j|\theta)$ is a gamma process, then $W_j \sim Gamma(\alpha t_j, 1/\alpha)$. Based on the degradation data, we determine the trend function $\Lambda(X_j|\theta)$ by estimating the parameter vector θ, then we take the inverse of the transformation of X_j with respect to W_j, i.e., $X_j = \Lambda^{-1}(W_j|\theta)$.

Thereby, using Taylor series expansion at the mean of W_j, X_j can be approximated as

$$\begin{aligned}\tilde{X_j} \approx \Lambda^{-1}(\mu_{W_j}|\theta) + \left.\frac{d[\Lambda^{-1}(W_j|\theta)]}{dW_j}\right|_{W_j=\mu_{W_j}} (W_j - \mu_{W_j}) \quad + \\ \frac{1}{2}\left.\frac{d^2[\Lambda^{-1}(W_j|\theta)]}{dW_j^2}\right|_{W_j=\mu_{W_j}} (W_j - \mu_{W_j})^2 \quad + \quad \ldots,\end{aligned} \tag{4.2}$$

where $\mu_{W_j} = \mathbb{E}(W_j) = t_j$ since W_j is the cumulative sum from the data of a Lévy process. Furthermore, the variance of W_j is $t_j\omega^2$, denoted as $\mathbb{V}(W_j) = t_j\omega^2$. Therefore, the expected value of $\tilde{X_j}$ can be approximated as

$$\mathbb{E}[\tilde{X_j}|t_j,\theta,\omega] \approx \Lambda^{-1}(t_j|\theta) + \frac{1}{2}\left.\frac{d^2[\Lambda^{-1}(W_j|\theta)]}{dW_j^2}\right|_{W_j=t_j} t_j\omega^2. \tag{4.3}$$

For a given degradation data set and a specific parametric PDF $\mathfrak{F}$, the parameters θ and ω in Eq. (4.3) can be estimated by the maximum likelihood estimation method. Suppose

degradation data are measured for I units with m measurements, $\mathbf{X} = x_{ij}, i = 1,2,\ldots,I\ j = 1,2,\ldots,m$, and the corresponding PDF of the Lévy process is $\mathfrak{F}(\Delta\Lambda(x|\theta);\omega)$, then the likelihood function for the parameter vector θ and the parameter ω is

$$\mathfrak{L}(\theta,\omega|x) = \prod_{i=1}^{I}\prod_{j=1}^{m}\mathfrak{F}\{\Delta\Lambda(x_{ij}|\theta);\omega\}\lambda(x_{ij}|\theta), \tag{4.4}$$

where $\Delta\Lambda(x_{ij}|\theta) = \Lambda(x_{ij}|\theta) - \Lambda(x_{i(j-1)}|\theta)$ and $\Lambda(x_{ij}|\theta) = \int_0^{x_{ij}}\lambda(u|\theta)du$. The MLEs of θ and ω can be obtained by maximizing the likelihood function $\mathfrak{L}(\theta,\omega|x)$ w.r.t. θ and ω. Therefore, the MTTF for a given threshold c is obtained using the estimated parameters by

$$\widehat{T} = \sup\left\{t_j : \mathbb{E}\left[\tilde{X}_j|\hat{\theta},\hat{\omega}\right] < c\right\}. \tag{4.5}$$

Example 1. Consider the log-linear trend function as in Eq. (4.1), X_j can be expressed in terms of W_j as

$$X_j = \frac{1}{b}\log\left(1+\frac{b}{a}W_j\right) = \frac{1}{b}\log\left(U_j\right), \tag{4.6}$$

where $U_j = 1+\frac{b}{a}W_j$, which implies $\mathbb{E}(U_j) = \mu_U = 1+\frac{b}{a}t_j$ and $\mathbb{V}(U_j) = \sigma^2{}_U = \frac{b^2}{a^2}t_j\sigma^2$. The expression of X_j in Eq.(4.6) can be approximated using the Taylor series expansion at the mean of U_j as

$$\tilde{X}_j \approx \frac{1}{b}\left[\ln\mu_U + \frac{(U_j-\mu_U)}{\mu_U} - \frac{(U_j-\mu_U)^2}{2\mu_U^2}\right],$$

where μ_U is the mean of U_j. Hence, if $W_j \sim Normal(t_j, t_j\sigma^2)$, then $\omega = \sigma$ and the expected value of $\tilde{X}_j$ can be approximated with respect to t_j by

$$\mathbb{E}[\tilde{X}_j|t_j,a,b,\sigma] \approx \frac{1}{b}\left\{\log\left(1+\frac{b}{a}t_j\right) - t_j\frac{\frac{b^2}{a^2}\sigma^2}{2(1+\frac{b}{a}t_j)^2}\right\}. \tag{4.7}$$

Similarly, if $W_j \sim Gamma(\alpha t_j, 1/\alpha)$, then $\omega = 1/\sqrt{\alpha}$ and the expected value of $\tilde{X}_j$ is approximated by

$$\mathbb{E}[\tilde{X}_j|t_j,a,b,\alpha] \approx \frac{1}{b}\left\{\log\left(1+\frac{b}{a}t_j\right) - t_j\frac{\frac{b^2}{a^2}}{2\alpha(1+\frac{b}{a}t_j)^2}\right\}.\blacksquare \tag{4.8}$$

4.2.1.2. *Interval estimation of the MTTF based on parametric bootstrap*

To evaluate the standard error of the MTTF estimate in Eq. (4.5) and to a construct confidence interval of the MTTF, we propose a parametric bootstrap procedure. Suppose the parameters of Eq. (4.5), $\hat{\theta}$ and $\hat{\omega}$, are estimated from the maximum likelihood approach. The bootstrap procedure is presented as follows:

A1. Generate a random sample $\{\Delta\Lambda(x_{ij})^{(1)};\ i = 1,2,\ldots,I; j = 1,2,\ldots,m\}$ from the parametric distribution corresponds to the PDF $\mathfrak{F}(\Delta\Lambda(x|\hat{\theta});\hat{\omega})$, where $\hat{\theta}$ and $\hat{\omega}$ are the MLEs of θ and ω. Then, set $W^{(1)} = \{w_{ij}^{(1)}\} = \{\Lambda(x_{ij})^{(1)}\} = \{\sum_{k=1}^{j}\Delta\Lambda(x_{ik})^{(1)}\}$;

A2. Maximize the likelihood function in Eq. (4.4) w.r.t. to θ and ω based on the simulated sample to obtain the MLEs as $\hat{\theta}^{(1)}$ and $\hat{\omega}^{(1)}$;

A3. Evaluate the expected value of X_j by Eq. (4.3) and estimate the MTTF by Eq. (4.5). The bootstrap estimate of MTTF with a threshold level c is denoted by $\widehat{T^{(1)}}$;

A4. Repeat Steps A1–A3 B times and obtain B bootstrap estimates of MTTF, i.e., $\widehat{T^{(1)}}, \widehat{T^{(2)}}, \ldots, \widehat{T^{(B)}}$.

Based on the B bootstrap estimates of MTTF, the $100(1-\delta)\%$ confidence interval of MTTF can be obtained by the bootstrap percentile method . Specifically, after ordering the B bootstrap estimates of the MTTF in ascending order as $\widehat{T^{[1]}} < \widehat{T^{[2]}} < \ldots < \widehat{T^{[B]}}$, a $100(1-\delta)\%$ the bootstrap percentile confidence interval of the MTTF can be obtained as $(\widehat{T}^{[B(\delta/2)]}, \widehat{T}^{[B(1-\delta/2)]})$.

4.2.2. TRP model with non-specific distribution

The TRP model discussed in Section 4.2.1 assumed a Lévy process with a known PDF $\mathfrak{F}$. In this subsection, the TRP model is fitted without a distributional assumption on

$\Lambda(X_j|\theta)$. Here, we only assume $\Lambda(X_j|\theta)$ follows a Lévy process and the parameter vector θ of the trend function is estimated using the least squares method.

4.2.2.1. Least-square estimation of the parameter vector θ

If $W_j = \Lambda(X_j|\theta)$ follows a Lévy process with an expected value of 1 and a variance ω_{LS}^2, then we consider the time transformation function

$$\Lambda(x_{ij}|\theta) = t_j + \varepsilon_{ij}, \quad i = 1,\ldots,I \quad j = 1\ldots,m, \tag{4.9}$$

where x_{ij} is the j-th measurement for the i-th unit, ε_{ij} is randomly distributed with mean 0 and variance $t_j\omega_{LS}^2$. Based on the time transformation function in Eq. (4.9), the least squares function for the TRP model can be expressed as

$$Q(\theta) = \sum_{j=1}^{m}\left[t_j - \frac{1}{I}\sum_{k=1}^{I}\Lambda(x_{ij}|\theta)\right]^2, \tag{4.10}$$

where θ is the parameter vector associated with the trend function. The parameter vector θ can be estimated by minimizing $Q(\theta)$ w.r.t. θ.

4.2.2.2. MTTF estimate based on Taylor series expansion

Let $\hat{\theta}_{LS}$ be the least squares estimate of the parameter vector θ. Then $\mathbb{E}(\tilde{X}_j)$ can be estimated by

$$\hat{\mathbb{E}}[\tilde{X}_j|t_j,\hat{\theta}_{LS},\hat{\omega}_{LS}] \approx \Lambda^{-1}(t_j|\hat{\theta}_{LS}) + \frac{1}{2}\frac{d^2[\Lambda^{-1}(W_j|\hat{\theta}_{LS})]}{dW_j^2}\bigg|_{W_j=t_j}\{t_j\hat{\omega}_{LS}^2\}, \tag{4.11}$$

where $\hat{\omega}_{LS}$ is the standard deviation of $\Delta\Lambda\left(x_{ij}|\hat{\theta}_{LS}\right)$. Thereby, the MTTF for a given thresh-

old c based on the TRP model with non-specific distribution can be estimated as

$$\widehat{T_{LS_1}} = \sup\left\{t_j : \hat{\mathbb{E}}\left[\tilde{X}_j | t_j, \hat{\theta}_{LS}, \hat{\omega}_{LS}\right] < c\right\}. \tag{4.12}$$

Interval estimation based on the bootstrap method: An estimate for error term ε_{ij} is given by $\hat{\varepsilon}_{ij} = \left\{t_j - \Lambda(x_{ij}|\widehat{\theta}_{LS})\right\}$, where $\hat{\varepsilon}_{ij}$ has a distribution with mean 0 and variance $t_j\hat{\omega}^2_{LS}$. Though $\hat{\varepsilon}_{ij}$ are assumed to be independent, these estimates are not identically distributed and they are correlated. Therefore, we consider the weighted version of $\hat{\varepsilon}_{ij}$ in which the estimate is divided by $\sqrt{t_j}$, i.e., $\hat{\varepsilon}^*_{ij} = \hat{\varepsilon}_{ij}/\sqrt{t_j}$. The weighted values $\hat{\varepsilon}^*_{ij}$ have mean 0 and variance $\hat{\omega}^2_{LS}$ and they are approximately i.i.d. Suppose $\{\hat{\varepsilon}^*_{ij}, i = 1,2,\ldots,I; j = 1,2,\ldots,m\}$, a nonparametric bootstrap procedure for constructing a confidence interval of MTTF is presented as follows:

B1. Obtain a random sample of size $M = Im$ by sampling with replacement from $\{\hat{\varepsilon}^*_{ij}, i = 1,2,\ldots,I; j = 1,2,\ldots,m\}$. Denote the sample of size M as $\hat{\varepsilon}^{*(1)}_{11}, \hat{\varepsilon}^{*(1)}_{12}, \ldots, \hat{\varepsilon}^{*(1)}_{ij}, \ldots, \hat{\varepsilon}^{*(1)}_{Im}$ for $i = 1,\ldots,I$ and $j = 1\ldots,m$;

B2. Compute $\hat{\Lambda}(x_{ij})^{(1)} = t_j + \sqrt{t_j}\hat{\varepsilon}^{*(1)}_{ij}$ for $i = 1,\ldots,I$ and $j = 1\ldots,m$;

B3. Update the least squares equation as

$$Q^{(1)}(\theta) = \sum_{i=1}^{I}\sum_{j=1}^{m}\left\{\hat{\Lambda}(x_{ij})^{(1)} - \frac{1}{I}\sum_{k=1}^{I}\Lambda(x_{ij}|\theta)\right\}^2,$$

and estimate the parameter θ by minimizing $Q^{(1)}(\theta)$ w.r.t. θ, denoted by $\hat{\theta}^{(1)}_{LS}$. Then, evaluate $\hat{\omega}^2_{LS}$.

B4. Evaluate $\hat{\mathbb{E}}[\tilde{X}_j | t_j, \hat{\theta}^{(1)}_{LS}, \hat{\omega}^{(1)}_{LS}]$ by equation Eq. (4.11) and estimate the MTTF from Eq. (4.12) denoted as $\widehat{T^{(1)}_{LS_1}}$; (or estimate the MTTF from the ESA approach by Eq. (4.13))

B5. Repeat the Steps B1–B4 for B times and obtain $\widehat{T^{(1)}_{LS_1}}, \widehat{T^{(2)}_{LS_1}}, \ldots, \widehat{T^{(B)}_{LS_1}}$;

Based on the B bootstrap estimates of MTTF, a $100(1-\delta)\%$ confidence interval of MTTF can be obtained by the bootstrap percentile method.

4.2.2.3. MTTF estimate based on ESA

In this subsection, the MTTF is estimated by obtaining the failure time distribution through the ESA method. Since $\Delta\Lambda(X_j|\theta)$ follows a Lévy process, it satisfies the requirement to apply the ESA. However, we have to ensure that all $\Delta\Lambda(X_j|\theta)$ values are strictly positive (or dominated by positives) to apply this method. Once the parameter vector θ is estimated by the least squares method, ΔW_j is evaluated by

$$\Delta\hat{W}_j^{LS} = \Delta\hat{\Lambda}(X_j|\hat{\theta}_{LS}) = \hat{\Lambda}(X_j|\hat{\theta}_{LS}) - \hat{\Lambda}(X_{j-1}|\hat{\theta}_{LS}).$$

The transformed threshold level in this situation is $c_{LS} = \hat{\Lambda}(c|\hat{\theta}_{LS})$. Suppose the transformed differences (i.e., ΔW_j^{LS}) are evaluated for sample degradation data and denoted as $\Delta\hat{w}_1^{LS}, \Delta\hat{w}_2^{LS}, \ldots, \Delta\hat{w}_m^{LS}$. With a transformed threshold level of c_{LS}, the estimate for the MTTF can be obtained using the ESA method as follows.

$$\widehat{T_{LS_2}} = \frac{c_{LS}}{\bar{\hat{w}}} + \frac{s_{\Delta\hat{w}}^2}{2\bar{\hat{w}}^2}, \tag{4.13}$$

where $\bar{\hat{w}} = \sum_{j=1}^{m} \Delta\hat{w}_j^{LS}$ and $s_{\Delta\hat{w}} = \sqrt{\sum_{j=1}^{m}(\Delta\hat{w}_j^{LS} - \bar{\hat{w}})^2/(m-1)}$ are the sample mean and sample standard deviation of $\Delta\hat{w}_j^{LS},\ j = 1,2,\ldots,m$, respectively. A $100(1-\delta)\%$ confidence interval of the MTTF specifically based on the ESA estimate in Eq. (4.13) with normal approximation can be obtained as

$$\widehat{T}_{LS_2} \pm z_{\delta/2}\{c/\bar{\hat{w}}^2\}s_{\Delta\hat{w}}. \tag{4.14}$$

4.3. Cumulative Sum TRP Model (CTRP)

In this study, we name the model proposed by Wang et al. (2019) as the cumulative sum TRP (CTRP) as they took the cumulative summation of the exact measurements. At time t_j, the exact measurement is defined as $Z_j = Z_0 - X_j$, where X_j is the degradation measurement and Z_0 is the initial measurement. Similar to the TRP model, without loss of generality, we assume that the number of measurements for each unit is the same, and the number of measurements is m for each I of each units.

Suppose $D_j = \sum_{k=1}^{j} Z_k$ is the cumulative sum of the exact measurements. Using a trend function, D_j is then transformed such that $\Lambda(D_j|\theta^*) = \int_0^{D_j} \lambda(u|\theta^*)du$, where $\lambda(\cdot|\theta^*)$ is the trend function with the parameter vector θ^*. Wang et al. (2019) assume that $\Delta\Lambda(D_j|\theta^*) = \Lambda(D_j|\theta^*) - \Lambda(D_{j-1}|\theta^*)$ follows a known distribution with an expected value of 1, denoted as $\mathfrak{F}^*$. Similar to the TRP model presented in Section 4.2, we consider the cases that the parametric form of the PDF $\mathfrak{F}^*$ is specified and non-specified.

4.3.1. CTRP model with specific distribution

To obtain generalized expressions, we consider that $\Lambda(D_j|\theta^*)$ follows a Lévy process which has expected value 1 and variance ω^{*2} with PDF $\mathfrak{F}^*$. If a two-parameter parametric PDF $\mathfrak{F}^*$ is considered, then only ω^* is required to estimate. The parameter vector related to the trend function in a CTRP model, denoted as θ^* and the parameter related to the PDF $\mathfrak{F}^*$ (i.e., ω^*) can be estimated through the maximum likelihood method similar to Eq. (4.4).

4.3.1.1. Model and point estimation

Suppose the cumulative sums of the exact degradation measurements are $\mathbf{d} = \{d_{ij} :$

$i = 1,2,\ldots,I; j = 1,2,\ldots,m\}$, then the likelihood function is given by

$$\mathfrak{L}(\theta^*, \omega^* | \mathbf{d}) = \prod_{i=1}^{I} \prod_{j=1}^{m} \mathfrak{F}^*\{\Delta\Lambda(d_{ij}|\theta^*); \omega^*\} \lambda(d_{ij}|\theta^*), \tag{4.15}$$

where $\Delta\Lambda(d_{ij}|\theta^*) = \Lambda(d_{ij}|\theta^*) - \Lambda(d_{i(j-1)}|\theta^*)$ and $\Lambda(d_{ij}|\theta^*) = \int_0^{d_{ij}} \lambda(u|\theta^*)du$. The MLEs of the parameter vector θ^* and the parameter ω^*, denoted by $\hat{\theta}^*$ and $\hat{\omega}^*$, respectively, can be obtained by maximizing Eq. (4.15) w.r.t. θ^* and ω^*.

Let $Y_j = \Lambda(D_j|\theta^*)$ so that $Y_j = \sum_{k=1}^{j} \Delta\Lambda(D_k|\theta^*)$. Thus, if $\Delta\Lambda(D_j|\theta^*)$ follows a Wiener process, then $Y_j \sim N(t_j, t_j\sigma^2)$; and if $\Delta\Lambda(D_j|\theta^*)$ follows a gamma process, then $Y_j \sim gamma(\alpha t_j, 1/\alpha)$. The inverse transformation of D_j with respect to Y_j can be obtained by $D_j = \Lambda^{-1}(Y_j|\hat{\theta}^*)$ based on the MLE of the parameter vector θ^*. Hence, using the Taylor series expansion, D_j can be approximated using the Y_j as

$$\begin{aligned} \tilde{D}_j &\approx \Lambda^{-1}(\mu_{Y_j}|\theta^*) + \frac{d[\Lambda^{-1}(Y_j|\theta^*)]}{dY_j}\bigg|_{Y_j=\mu_{Y_j}} (Y_j - \mu_{Y_j}) \\ &\quad + \frac{1}{2}\frac{d^2[\Lambda^{-1}(Y_j|\theta^*)]}{dY_j^2}\bigg|_{Y_j=\mu_{Y_j}} (Y_j - \mu_{Y_j})^2 + \ldots, \end{aligned} \tag{4.16}$$

where $\mu_{Y_j} = t_j$ is the mean of Y_j and the variance of Y_j is $t_j\omega^{*2}$. Therefore, the expected value of the exact degradation measurements, Z_j, can be approximated as

$$\begin{aligned} \mathbb{E}[Z_j|t_j, \theta^*, \omega^*] &= \mathbb{E}(\tilde{D}_j|t_j, \theta^*, \omega^*) - E(\tilde{D}_{j-1}|t_{j-1}, \theta^*, \omega^*) \\ &\approx \left\{\Lambda^{-1}(t_j|\theta^*) + \frac{1}{2}\frac{d^2[\Lambda^{-1}(Y_j|\theta^*)]}{dY_j^2}\bigg|_{Y_j=t_j} t_j\omega^{*2}\right\} - \\ &\quad \left\{\Lambda^{-1}(t_{j-1}|\theta^*) + \frac{1}{2}\frac{d^2[\Lambda^{-1}(Y_{j-1}|\theta^*)]}{dY_{j-1}^2}\bigg|_{Y_{j-1}=t_{j-1}} t_{j-1}\omega^{*2}\right\}. \end{aligned} \tag{4.17}$$

In Eq. (4.17), if we only consider the first-order terms, the expected value of Z_j can be approximated as (see, for example, Wang et al., 2019)

$$\mathbb{E}[Z_j|t_j,\theta^*] \approx \left\{\Lambda^{-1}(t_j|\theta^*) - \Lambda^{-1}(t_{j-1}|\theta^*)\right\}. \tag{4.18}$$

Then, the estimate of MTTF with a threshold level c based on the CTRP is given by

$$\widehat{T^*} \approx \inf\left\{t_j : \mathbb{E}(Z_j|t_j,\theta^*) > z_c\right\}, \tag{4.19}$$

where $z_c = Z_0 - c$.

Example 2. If $\mathfrak{F}^*$ is considered as a normal PDF with mean 1 and variance σ^2 and the trend function is log-linear with parameters a and b (i.e., $\Lambda(D_j|a,b) = a/b\{\exp(bD_j) - 1\}$), then the corresponding relationship of expected exact measurements (Z_j) with respect to the time (t_j) can be evaluated by (Wang et al., 2019)

$$\begin{aligned}\mathbb{E}(Z_j|t_j,a,b,\sigma) &= \mathbb{E}(D_j|t_j,a,b,\sigma) - E(D_{j-1}|t_{j-1},a,b,\sigma)\\ &\approx \frac{1}{b}\left[\log\left(\frac{t_j+\frac{a}{b}}{(t_j-1)+\frac{a}{b}}\right) + \frac{\sigma^2}{2}\left(\frac{t_j-1}{\left(t_j-1+\frac{a}{b}\right)^2} - \frac{t_j}{\left(t_j+\frac{a}{b}\right)^2}\right)\right].\end{aligned} \tag{4.20}$$

In Eq. (4.20), when the term related to σ^2 is substantially small, the expected value can be further approximated by

$$\mathbb{E}(Z_j|t_j,a,b) \approx \frac{1}{b}\left[\log\left(\frac{t_j+\frac{a}{b}}{(t_j-1)+\frac{a}{b}}\right)\right]. \tag{4.21}$$

For this situation, the MTTF for the threshold level of the exact measurement z_c is estimated by

$$\widehat{T^*} \approx \inf\left\{t_j : \mathbb{E}(Z_j|t_j,a,b) > z_c\right\}. \tag{4.22}$$

4.3.1.2. *Interval estimation of MTTF based on parametric bootstrap*

To evaluate the confidence intervals of the MTTF estimate in Eq. (4.19) Wang et al. (2019) proposed a parametric bootstrap procedure. Suppose the CTRP parameters, θ^* and ω^*, are estimated from the maximum likelihood approach. The bootstrap procedure is presented as follows:

C1. Generate a random sample $\{\Delta\Lambda(d_{ij})^{(1)}; i = 1,2,\ldots,I; j = 1,2,\ldots,m\}$ from $\mathfrak{F}^*(\Delta\Lambda(d|\hat{\theta}^*); \hat{\omega}^*)$, where $\hat{\theta}^*$ and $\hat{\omega}^*$ are the MLEs of θ^* and ω^*.

C2. Maximize the likelihood function in Eq. (4.15) w.r.t. to θ and ω based on the simulated sample to obtain the MLEs as $\hat{\theta}^{*(1)}$ and $\hat{\omega}^{*(1)}$;

C3. For time t_j, evaluate the expected value of exact measurement, Z_j from Eq. (4.18) and estimate the MTTF by Eq. (4.19). The bootstrap estimate of MTTF with a threshold level c is denoted by $\widehat{T^{*(1)}}$;

C4. Repeat Steps C1–C3 B times and obtain B bootstrap estimates of MTTF, i.e., $\widehat{T^{*(1)}}, \widehat{T^{*(2)}}, \ldots, \widehat{T^{*(B)}}$.

Based on the B bootstrap estimates of MTTF, a $100(1-\delta)\%$ confidence interval of MTTF can be obtained by bootstrap percentile method. Specifically, after ordering the B bootstrap estimates of MTTF in ascending order as $\widehat{T^{*[1]}} < \widehat{T^{*[2]}} < \ldots < \widehat{T^{*[B]}}$, a $100(1-\delta)\%$ bootstrap percentile confidence interval of MTTF can be obtained as $(\widehat{T}^{*[B(\delta/2)]}, \widehat{T}^{*[B(1-\delta/2)]})$.

Taking the cumulative sum of the capacity ratios act as a low-pass filter since it help to remove the high frequency noise in the measurements. Moreover, the cumulative sums tend to have positive increments, which support the model assumptions in trend-renewal-process. In this study, we propose to apply the CTRP approach with any Lévy process distributions such as gamma and IG in addition to the normal distribution.

4.3.2. CTRP model with non-specific distribution

Following the CTRP model, we consider the situation that a parametric distributional assumption for $\mathfrak{F}^*$ is not required. We only assume that $\Delta\Lambda(D_j|\theta^*) = \Lambda(D_j|\theta^*) - \Lambda(D_{j-1}|\theta^*)$ follows a Lévy process with expected value of 1 and variance ω^{*2}. Therefore, $\Lambda(D_j|\theta^*)$ has a expected value of t_j with a variance of $t_j\omega^{*2}$.

4.3.2.1. Model and point estimate

Suppose we have the cumulative sums of m exact measurements measured at unit time intervals for I units denoted as $\mathbf{d} = \{d_{ij}; i = 1,2,\ldots,I\,; j = 1,2,\ldots,m\}$, then we consider the CTRP model

$$\Lambda(d_{ij}|\theta^*) = t_j + \varepsilon_{ij}, \quad i = 1,\ldots,I \quad j = 1\ldots,m, \tag{4.23}$$

where ε_{ij} is a random variable with mean 0 and variance $t_j\omega^{*2}$.

The approach to estimate the MTTF based on CTRP is similar to the approach presented in Section 4.3.1 except the parameter vector θ^* for the trend function is estimated by the least squares method. Using the relationship in Eq. (4.23), the least squares function for CTRP method can be expressed as

$$\mathbf{Q}^*(\theta^*) = \sum_{j=1}^{m}\left\{t_j - \frac{1}{I}\sum_{k=1}^{I}\Lambda(d_{ij}|\theta^*)\right\}^2. \tag{4.24}$$

The least squares estimate of the parameter vector θ^*, denoted as $\hat{\theta}^*_{LS}$, is obtained by minimizing $\mathbf{Q}^*(\theta^*)$ w.r.t. θ^*. Then, $\mathbb{E}(D_j)$ can be estimated by

$$\hat{\mathbb{E}}\left[D_j|t_j,\hat{\theta}^*_{LS},\hat{\omega}^*_{LS}\right] \approx \Lambda^{-1}\left(t_j|\hat{\theta}^*_{LS}\right) + \frac{1}{2}\frac{d^2\left[\Lambda^{-1}(Y_j|\hat{\theta}^*_{LS})\right]}{dY_j^2}\bigg|_{Y_j=t_j}\left\{t_j\hat{\omega}^{*2}_{LS}\right\} \tag{4.25}$$

and the expected value of exact measurements can be approximated by

$$\begin{aligned}\hat{\mathbb{E}}\left[Z_j|t_j,\hat{\theta}^*_{LS},\hat{\omega}^*_{LS}\right] &= \mathbb{E}\left(D_j|t_j,\hat{\theta}^*_{LS},\hat{\omega}^*_{LS}\right) - E\left(D_{j-1}|t_{j-1},\hat{\theta}^*_{LS},\hat{\omega}^*_{LS}\right) \\ &\approx \Lambda^{-1}\left(t_j|\hat{\theta}_{LS}\right) - \Lambda^{-1}\left(t_{j-1}|\hat{\theta}^*_{LS}\right).\end{aligned} \tag{4.26}$$

The estimate of the standard deviation of the Lévy process, $\hat{\omega}^*_{LS}$, is then obtained by taking the standard deviation of $\Delta\Lambda(d_{ij}|\hat{\theta}^*) = \Lambda(d_{i(j+1)}|\hat{\theta}^*) - \Lambda(d_{ij}|\hat{\theta}^*),\ i = 1,2,\cdots,I, j = 1,2,\cdots,m-1$. Hence, based on Eq. (4.26), the MTTF for a given threshold level c can be estimated by

$$\widehat{T^*_{LS}} \approx \inf\left\{t_j : \mathbb{E}(Z_j|t_j,\hat{\theta}^*_{LS}) > z_c\right\}, \tag{4.27}$$

where $z_c = Z_0 - c$. Similar to the TRP least squares approach, to construct the confidence intervals for the least squares approach of CTRP model, we propose the bootstrap method.

4.3.2.2. Interval estimation of the MTTF

The least squares error estimate for unit i at time t_j is given by

$$\hat{\varepsilon}_{ij} = \left\{t_j - \Lambda(d_{ij}|\theta^*_{LS})\right\}$$

Here, $\hat{\varepsilon}_{ij}$ has a distribution with mean 0 with variance of $t_j\hat{\omega}^{*2}_{LS}$. Though ε_{ij} are assumed to be independent, their estimates are not identically distributed and they are correlated with time. Thus, we weight $\hat{\varepsilon}_{ij}$ estimates by dividing $\sqrt{t}_j$, which will provide roughly iid estimates of error as $\hat{\varepsilon}^*_{ij} = \hat{\varepsilon}_{ij}/\sqrt{t_j} \sim .(0,\hat{\omega}^{*2}_{LS})$.

Suppose $\hat{\varepsilon}^* = \{\hat{\varepsilon}^*_{ij}\}$ and the bootstrap procedure is given as follows:

D1. Randomly select M (where $M = Im$) samples with replacement from $\hat{\varepsilon}^*$. Denote those M samples as $\hat{\varepsilon}^{*(1)}_{11}, \hat{\varepsilon}^{*(1)}_{12}, \ldots, , \hat{\varepsilon}^{*(1)}_{ij}, \ldots, \hat{\varepsilon}^{*(1)}_{Im}$ for $i = 1, \ldots, I$ and $j = 1 \ldots, m$.

D2. Estimate $\hat{\Lambda}(d_{ij})^{(1)}$ by $\hat{\Lambda}(d_{ij})^{(1)} = t_j + \sqrt{t_j}\hat{\varepsilon}^{*(1)}_{ij}$ for $i = 1, \ldots, I$ and $j = 1 \ldots, m$.

D3. Update the least squares equation as

$$\mathbf{Q}^{*(\mathbf{1})}(\theta^*) = \sum_{i=1}^{I}\sum_{j=1}^{m}\left\{\hat{\Lambda}(d_{ij})^{(1)} - \frac{1}{I}\sum_{k=1}^{I}\Lambda(d_{ij}|\theta^*)\right\}^2,$$

and estimate the parameters θ^*, denoted by by $\hat{\theta}^{(1)}_{LS}$, minimizing $\mathbf{Q}^{*(\mathbf{1})}(\theta^*)$ w.r.t. θ^*.

D4. Evaluate $\hat{\mathbb{E}}[Z_j|\hat{\theta}^*_{LS}]$ from equation Eq. (4.26) and estimate the MTTF using those estimates from Eq. (4.27) denoted by $\widehat{T^{*(1)}_{LS}}$.

D5. Repeat the steps D1–D4 for B times and obtain bootstrap samples of MTTF as $\widehat{T^{*(1)}_{LS}}$, $\widehat{T^{*(2)}_{LS}}, \ldots, \widehat{T^{*(B)}_{LS}}$.

Based on the B bootstrap estimates of MTTF the $100(1-\delta)\%$ confidence interval of MTTF can be obtained by bootstrap percentile method.

However, taking the cumulative sum of measurements does not provide a clear physical or modeling interpretation. According to the the TRP model proposed in Lindqvist et al. (2003) and Cook and Lawless (2007, Chapter 5), they considered taking the cumulative time of the failure time when the differences between failure times are known. Due to this concern, it is important to compare the CTRP model proposed by Wang et al. (2019) and TRP model proposed by Lindqvist et al. (2003).

4.4. Monte Carlo Simulation Studies

Monte Carlo simulation is used to to evaluate the performance of the proposed models and estimation methods for the MTTF. We consider four different settings in which the degradation data are generated from different models discussed in this study including the Wiener process, the gamma process, the TRP and the CTRP. The following estimation methods for the MTTF with different threshold values are considered in the Monte Carlo simulation study:

- ESA: Empirical saddlepoint approximation
- TRP$_N$: TRP model with specific PDF $\mathfrak{F} \sim Normal$
- TRP$_G$: TRP model with specific PDF $\mathfrak{F} \sim Gamma$
- TRP$_{TS}$: TRP model with non-specific PDF and MTTF estimate based on Taylor series expansion
- TRP$_{ESA}$: TRP model with non-specific PDF and MTTF estimate based on ESA
- CTRP$_N$: CTRP model with specific PDF $\mathfrak{F}^* \sim Normal$
- CTRP$_G$: CTRP model with specific PDF $\mathfrak{F}^* \sim Gamma$
- CTRP$_{TS}$: CTRP model with non-specific PDF and MTTF estimate based on Taylor series expansion (i.e., Eq. (4.27))

To compare the performance of different models and estimation methods, we compute the simulated mean square errors (MSEs) for different estimation methods based on 10,000 simulations with 10 units ($I = 10$) and 100 measurements ($m = 100$). The parameter settings for these simulations are selected ensuring that the degradation process reaches the threshold level between 100 to 500 time units, which is an arbitrarily selected range.

4.4.1. Setting 1: Degradation data are generated from a Wiener process

For this setting, the degradation data are generated from a Wiener process presented in Section 1.1.4 with parameters $\nu = 1, \sigma = 1$ (i.e., Wiener(1,1)) or $\nu = 1, \sigma = 2$ (i.e., Wiener(1,2)) with threshold values $c = 150, 200$ and 300. In addition to the aforementioned estimation methods, we also included the parametric estimates based on the known FPT distribution (i.e., the IG distribution) with the MLEs of the parameters ν and σ (denoted as MLE) obtained from Eq. (1.6). The simulated MSEs in estimating MTTF for different estimation methods are presented in Table 4.1. Note that TRP_G and CTRP_G methods are not considered for this simulation because Wiener process data contains negative increments, which do not support the gamma likelihood function.

Based on the results presented in Table 4.1, we observe that when the threshold level (c) increases, the MSEs increase. In this setting, the MSEs of the ESA method are close to the MSEs of the MLE, whereas in all other methods, the MSEs deviate substantially from the MSEs of the MLE, especially for larger threshold level c. Note that the MLE requires the assumption of the underlying degradation process, while the ESA only requires the assumption that the underlying process is a Lévy process. The performance of the ESA method is better than the other methods because it particularly supports the linear degradation data.

4.4.2. Setting 2: Degradation data are generated from a gamma process

For this setting, the degradation data are generated from a gamma process presented in Section 1.1.5 with parameters $\alpha = 1,\ \beta = 1$ (i.e., Gamma(1,1)) or $\alpha = 0.5,\ \beta = 2$ (i.e., Gamma(0.5,2)) with threshold values $c = 150, 200$ and 300. In addition to the aforementioned estimation methods, we also included the parametric estimates based on the approximate FPT distribution using BS approximation with the MLEs of the parameters α

Table 4.1: Simulated MSEs for MTTF estimates of different methods when data are generated from Wiener process

		Wiener(1, 1) Process						
c	True MTTF	MLE	ESA	TRP_N	TRP_{ESA}	TRP_{TS}	$CTRP_N$	$CTRP_{TS}$
150	150	22.3	23.0	25.9	37.5	39.0	499.4	483.7
200	200	39.7	40.5	64.4	144.2	147.8	3624.2	3494.5
300	300	90.9	92.1	319.0	1101.4	1090.5	55732.8	53446.2
		Wiener(1, 2) Process						
c	True MTTF	MLE	ESA	TRP_N	TRP_{ESA}	TRP_{TS}	$CTRP_N$	$CTRP_{TS}$
150	150	91.6	103.0	100.6	182.8	193.0	735.7	581.9
200	200	162.8	176.0	207.1	757.1	762.9	3750.3	3106.2
300	300	373.6	392.8	702.2	6965.6	6780.6	43823.7	38461.0

and β (denoted as MLE). The simulated MSEs for different estimation methods are presented in Table 4.2.

Similar to the simulation results for Setting 1, when the threshold level (c) increases, the MSEs of the estimates increase. Once again, the MSEs of the ESA method are closed to the MSEs of the MLE, whereas in all other methods, the MSEs deviate substantially from the MSEs of the MLE, especially for larger threshold level c.

4.4.3. Setting 3: Degradation data are generated from the TRP model

For this setting, we simulate the degradation data from the TRP model presented in Section 4.2.1 with the log-linear link function $\lambda(t|\theta) = ae^{bt}$, where $\theta = (a,b)$, $a = 0.4$ or 0.6 and $b = 0.002$ and 0.005, and $\mathfrak{F} \sim Normal(1,1)$ or $\mathfrak{F} \sim Gamma(1,1)$ (see, Eq. (4.7) and Eq. (4.8)). The threshold values $c = 200$ and 300 are considered for each setting. The simulated MSEs are presented in Tables 4.3 and 4.4 for $\mathfrak{F} \sim Normal(1,1)$ and $\mathfrak{F} \sim Gamma(1,1)$, respectively. Note that when data are generated from the TRP model

Table 4.2: Simulated MSEs for MTTF estimates of different methods when data are generated from gamma process

		Gamma(1, 1) Process								
c	True MTTF	MLE	ESA	TRP_N	TRP_G	TRP_{ESA}	TRP_{TS}	CTRP_N	CTRP_G	CTRP_{TS}
150	150.5	22.9	22.6	31.8	32.0	37.0	36.2	348.8	331.9	464.5
200	200.5	41.2	40.8	108.0	108.1	137.5	135.0	2934.7	2856.3	3450.3
300	300.5	91.3	90.7	782.2	838.9	1071.3	1082.9	48333.7	47653.1	52645.6
		Gamma(0.5, 2) Process								
c	True MTTF	MLE	ESA	TRP_N	TRP_G	TRP_{ESA}	TRP_{TS}	CTRP_N	CTRP_G	CTRP_{TS}
150	150.25	45.2	45.9	60.3	67.7	81.9	81.2	424.0	392.8	497.1
200	200.25	81.4	82.2	195.1	245.2	304.7	302.6	2932.1	2795.0	3226.0
300	300.25	188.8	189.8	1425.3	2066.3	2497.1	2545.5	43075.3	41994.9	45393.9

with $\mathfrak{F} \sim Normal(1,1)$, the TRP_G model is discarded as it does not support the negative increments.

From Tables 4.3 and 4.4, it appears that MSEs are larger when the threshold level increases from 200 to 300. The MTTF estimates based on the correctly specified model (i.e., TRP_N in Table 4.3 and TRP_G in Table 4.4) give the smallest MSE in most cases. We also observed that the estimates obtained under the TRP models are better than the estimates obtained under the Lévy process models and CTRP models in most cases. However, the MSE of the estimates obtained from the ESA approach substantially deviates from the MSEs of the estimates obtained based on the true model as the ESA only supports the linear data. In comparing two estimation methods under the TRP model without a specific $\mathfrak{F}$ (i.e., TRP_{ESA} and TRP_{TS} methods), the TRP_{TS} method gives smaller MSEs in most cases considered here. Therefore, if $\mathfrak{F}$ is not specified when the TRP model is used we would recommend the TRP_{TS} method for estimating the MTTF.

Table 4.3: Simulated MSEs for MTTF estimates of different methods when data are generated from TRP model with $\mathfrak{F} \sim Normal(1,1)$

				TRP(a,b) model with $\mathfrak{F} \sim Normal(1,1)$						
c	a	b	True MTTF	TRP$_N$	TRP$_{ESA}$	TRP$_{TS}$	ESA	CTRP$_N$	CTRP$_G$	CTRP$_{TS}$
200	0.4	0.002	98	10.7	11.2	14.4	9.4	12.2	12.2	13.9
300	0.4	0.002	164	36.4	84.0	76.4	238.1	40.1	39.5	43.1
200	0.4	0.005	137	21.5	34.5	32.0	156.0	122.8	124.7	176.3
300	0.4	0.005	278	196.1	733.9	690.2	8300.1	2723.9	2744.0	3233.5
200	0.6	0.002	147	26.4	52.1	46.8	62.8	65.7	63.2	71.0
300	0.6	0.002	246	155.7	646.2	605.7	1343.1	956.1	930.4	977.8
200	0.6	0.005	206	73.3	221.0	204.7	1576.2	268.2	274.2	347.8
300	0.6	0.005	418	891.5	4634.9	4494.2	28429.8	2866.8	2913.4	3425.2

Table 4.4: Simulated MSEs for MTTF estimates of different methods when data are generated from TRP model with $\mathfrak{F} \sim Gamma(1,1)$ with $I = 10$ and $m = 100$

				TRP(a,b) model with $\mathfrak{F} \sim Gamma(1,1)$							
c	a	b	True MTTF	TRP$_G$	TRP$_N$	TRP$_{ESA}$	TRP$_{TS}$	ESA	CTRP$_G$	CTRP$_N$	CTRP$_{TS}$
200	0.4	0.002	98	10.7	10.3	11.3	14.3	9.4	12.2	12.1	13.9
300	0.4	0.002	164	53.2	63.7	83.2	76.2	236.8	41.6	41.9	46.0
200	0.4	0.005	137	24.7	26.7	34.4	32.0	154.9	124.6	122.9	176.6
300	0.4	0.005	278	426.8	547.4	734.7	689.1	8317.5	2790.5	2770.6	3287.7
200	0.6	0.002	147	33.9	38.7	51.9	46.7	62.5	62.4	64.5	70.2
300	0.6	0.002	246	363.9	453.1	660.1	621.8	1348.7	916.7	940.0	966.1
200	0.6	0.005	206	128.3	165.1	211.7	194.3	1576.5	279.4	273.5	355.2
300	0.6	0.005	418	2404.0	3125.1	4400.9	4276.6	28461.6	3033.6	2986.7	3551.8

4.4.4. Setting 4: Degradation data are generated from the CTRP model

For this setting, we simulate the degradation data from the CTRP model presented in Section 4.3 with log-linear link function $\lambda(t|\theta^*) = ae^{bt}$, where $\theta^* = (a,b)$, and $a = 0.001$ and 0.0012 and $b = 1 \times 10^{-4}$ and 1.5×10^{-4} with $\mathfrak{F}^* \sim Normal(1, 0.02)$ and $b = 2 \times 10^{-5}$ and 4×10^{-5} with $\mathfrak{F}^* \sim Gamma(10000, 1/10000)$. The threshold levels $c = 500$ and 700 are considered when $\mathfrak{F}^* \sim Normal(1, 0.02)$ and $c = 300$ and 400 are considered when $\mathfrak{F}^* \sim Gamma(10000, 1/10000)$. The simulated MSEs of the MTTF estimates obtained from the different methods are presented in Table 4.5 and 4.6 for $\mathfrak{F}^* \sim Normal(1, 0.02)$ and $\mathfrak{F}^* \sim Gamma(10000, 1/10000)$, respectively. When the data are generated from CTRP with $\mathfrak{F}^* \sim Normal$, the TRP$_G$ and TRP$_{ESA}$ methods are not considered since the data do not support the assumptions due to negative increments.

From Tables 4.5 and 4.6, we observed that the MSEs are larger when the threshold level increases. The MTTF estimates based on the correctly specified model (i.e., CTRP$_N$ in Table 4.5 and CTRP$_G$ in Table 4.6) give the smallest MSE in most cases. We also observed that the performances of the MTTF estimates based on the CTRP$_N$, CTRP$_G$, and CTRP$_{TS}$ methods are similar, which suggests that these estimation methods based on CTRP models are robust to the choice of the $\mathfrak{F}^*$. When the degradation data are generated from the CTRP model from Tables 4.5 and 4.6, we can see that the MTTF estimates can performed poorly if one uses TRP or the Lévy process models. For example, in Table 4.5, when $c = 700$ $a = 0.0012$ and $b = 0.02$, the MSE for CTRP$_{TS}$ method 84.3, while MSEs of the TRP$_{TS}$ and ESA methods are 82601.1 and 204785.5.

Based on the simulation results of the four settings presented in Sections 4.4.1 to 4.4.4, we observe that the performances of the proposed semiparametric and nonparametric approaches (i.e., ESA, TRP$_{ESA}$, TRP$_{TS}$, CTRP$_{TS}$) are comparable to those parametric approaches. Note that these proposed semiparametric and nonparametric methods are less restrictive in the sense that the specification of underlying distribution of

Table 4.5: Simulated MSEs for MTTF estimates of different methods when data are generated from CTRP model with $\mathfrak{F}^* \sim Normal(1, 0.02)$

				CTRP(a,b) model with $\mathfrak{F}^* \sim Normal(1, 0.02)$					
c	a	b	True MTTF	CTRP$_N$	CTRP$_G$	CTRP$_{TS}$	TRP$_N$	TRP$_{TS}$	ESA
500	0.0010	1.0×10^{-5}	102	1.6	1.6	1.6	120.0	4.9	58.7
700	0.0010	1.0×10^{-5}	239	6.1	6.1	6.3	6304.9	1214.8	7931.9
500	0.0010	1.5×10^{-5}	69	2.0	2.0	2.1	329.7	8.2	427.4
700	0.0010	1.5×10^{-5}	161	2.6	2.6	2.7	1054.4	130.2	1398.0
500	0.0012	1.0×10^{-5}	183	3.1	3.1	3.3	1294.7	158.4	1515.6
700	0.0012	1.0×10^{-5}	650	80.1	80.1	84.3	180311.6	82601.1	204785.5
500	0.0012	1.5×10^{-5}	123	1.7	1.7	1.8	112.1	8.2	56.2
700	0.0012	1.5×10^{-5}	440	34.8	34.8	36.0	69049.3	27899.6	78646.9

the degradation data or transformed degradation data are not required. Moreover, we can conclude that the misspecifying the underlying models can lead to severe distortions estimating the MTTF. Hence, a model selection procedure is discussed in the following section.

Table 4.6: Simulated MSEs for MTTF estimates of different methods when data are generated from CTRP model with $\mathfrak{F}^* \sim Gamma(10000, 1/10000)$ with $I = 10$ and $m = 100$

				CTRP(a, b) model with $\mathfrak{F}^* \sim Gamma(10000, 1/10000)$							
c	a	b	True MTTF	CTRP$_G$	CTRP$_N$	CTRP$_{TS}$	TRP$_G$	TRP$_N$	TRP$_{ESA}$	TRP$_{TS}$	ESA
300	0.0010	2.0×10^{-6}	215	3.1	3.1	3.2	1503.3	1346.2	129068.2	89.2	57.8
400	0.0010	2.0×10^{-6}	335	8.3	8.3	7.9	3883.0	3944.0	343851.1	983.4	4180.4
300	0.0010	4.0×10^{-6}	108	1.0	1.0	0.4	4302.9	434.4	37598.4	1.8	43.4
400	0.0010	4.0×10^{-6}	168	1.6	1.6	0.9	7330.4	991.1	96381.1	18.3	347.0
300	0.0012	2.0×10^{-6}	339	10.5	10.5	10.5	4858.7	2450.2	327296.2	1311.0	2037.2
400	0.0012	2.0×10^{-6}	556	25.9	25.8	28.0	22900.2	18575.5	942143.0	10541.2	31391.5
300	0.0012	4.0×10^{-6}	170	2.0	2.0	1.0	5058.4	1130.3	94782.5	16.6	185.9
400	0.0012	4.0×10^{-6}	279	4.1	4.0	2.9	7238.9	5027.6	260953.0	419.7	5511.1

4.5. Model Selection Procedure

Based on the simulation results in Section 4.4, it is clear that misspecifying the model for degradation data analysis might cause a substantial deviation in estimating the MTTF which probably have a severe consequences in reliability evaluation and product development. Therefore, we propose a model selection procedure to select an appropriate model based on the given degradation data set.

4.5.1. Lévy process vs. TRP-type models

When the degradation data are obtained, first, we can check that the differences of the consecutive degradation measurements are independent. This step allows us to choose between the Lévy process models (Wiener process, gamma process, or ESA) and the TRP-type models (i.e. TRP or CTRP) based on the observed degradation data. If the differences of the degradation measurements are independent, then the Lévy process models are more appropriate. Therefore, we can propose the following procedure to check the independence (or randomness) of the differences between two consecutive degradation measurements.

Suppose degradation measurements $X_j,\ j=0,1,\ldots,m$ are taken at time $t_j,\ j=0,1,\ldots,m$, and we obtain the differences between two consecutive measurements as $\Delta X_j = X_j - X_{j-1}$. If all ΔX_j are strictly positive (or dominated by the positive increments) and satisfy the Lévy process assumptions, then we can obtain the FPT distribution and the MTTF using the ESA approach. To test whether ΔX_j's are independent (one of the assumptions of the Lévy process), we apply a white-noise test introduced by Box and Pierce (1970) and Ljung and Box (1978) called Ljung-Box test. This white-noise test simultaneously tests the autocorrelations for several lags. Specifically, the Ljung-Box test is used to test the hypotheses,

$$
\begin{aligned}
H_0 &: \rho_1 = \rho_2 = \cdots = \rho_k = 0 \\
\text{vs.} \quad H_a &: \text{at least one } \rho_k \neq 0 \text{ for } 1 \leq k \leq K.
\end{aligned} \tag{4.28}
$$

The test statistic for Ljung-Box test is (see for example Woodward et al., 2017, Chapter 9, Section 9.1.2)

$$
\mathscr{R} = m(m+2) \sum_{k=1}^{K} \frac{\hat{\rho}_k^2}{n-k}, \tag{4.29}
$$

where $\hat{\rho}_k^2$ is the autocorrelation estimate for the k-th lag of ΔX_j and $k = 1, 2, \ldots, K$.

The Ljung-Box test statistic in Eq. (4.29) approximately follows a χ^2-distribution with degrees of freedom (d.f.) of K (Ljung and Box, 1978; Woodward et al., 2017); thus, we reject H_0 at significance level δ if $\mathscr{R} > \chi^2_{1-\delta}(K)$, where $\chi^2_q(K)$ is the q-th percentile of the chi-square distribution with d.f. K. Furthermore, as suggested by Woodward et al. (2017, pp. 377), in this study, we considered $K = 24$. The value of K can be adjusted based on the sample size. To perform the Ljung-Box test for multiple degradation paths, we apply the Bonferroni correction (Bonferroni, 1936) by controlling the Type-I error rate of the test. Hense, the significance level of the test is δ/I, where I is the number of samples/degradation paths and δ is the family-wise error rate of the test.

If we fail to reject the null hypothesis in Eq. (4.28), then use the Lévy process models (either assume parametric form or use ESA); otherwise, we consider the TRP-type models. In following subsection, we propose to a way to distinguish the TRP and CTRP models based on the observed degradation data.

4.5.2. TRP vs. CTRP

If null hypothesis in Eq. (4.28) is rejected for at least one degradation path, then it suggests that we should consider the TRP and CTRP models, which are appropriate for the degradation data with nonlinearity in time. To select between the TRP and CTRP models, we propose to select the model that gives a small value of the sum of squared distances between the observed degradation measurements and the expected values of the degradation measurements based on a particular model. Specifically, suppose $\hat{\theta}$ and $\hat{\theta}^*$ are the estimates of the parameter vector of the trend function associated with TRP and CTRP models, then we define the loss functions corresponding to the TRP and CTRP models, respectively, as

$$\mathbf{Loss}(\mathbf{TRP}) = \sum_{i=1}^{I}\sum_{j=1}^{m}\left\{x_{ij} - \mathbb{E}\left(X_j|t_j,\hat{\theta}\right)\right\}^2, \tag{4.30}$$

$$\text{and } \mathbf{Loss}(\mathbf{CTRP}) = \sum_{i=1}^{I}\sum_{j=1}^{m}\left\{z_{ij} - \mathbb{E}\left(Z_j|t_j,\hat{\theta}^*\right)\right\}^2, \tag{4.31}$$

For a given data set, the loss functions in Eqs. (4.30) and (4.31) can be calculated for a specific trend function. If $\mathbf{Loss}(\mathbf{TRP}) < \mathbf{Loss}(\mathbf{CTRP})$, then the TRP model is selected for modeling the degradation data; otherwise, the CTRP model is selected.

4.5.3. Monte Carlo simulation for the model selection procedure

To evaluate the performance of the proposed model selection procedure, a Monte Carlo simulation study is used. We consider the cases that the distributions of the transformed degradation data (i.e., $\mathfrak{F}$ and $\mathfrak{F}^*$) are not specified. In this simulation study, the degradation data are generated from the gamma degradation process, the TRP model

and the CTRP model. For each simulated degradation data set, we compute the estimate of the MTTF using the ESA based on original degradation measurements (ESA), the MTTF estimate using Taylor series expansion based on the TRP model with non-specific distribution (TRP$_{TS}$) and the MTTF estimate using Taylor series expansion based on the CTRP model with non-specific distribution (CTRP$_{TS}$). For comparative purposes, the simulated MSEs of the estimates of the MTTF with the model selection procedure (denoted as MSP) and without the model selection procedure are computed and the estimated proportions of selecting each model (% selection) are also presented.

4.5.3.1. Degradation data generated from the gamma process

In this simulation, the degradation data are generated from the gamma process with parameters $\alpha = 0.5$ and 1, and $\beta = 1.0$ and 2. The threshold values $c = 300$ and 500 are considered. The number of units (or number of degradation paths) is $I = 10$ with number of measurements $m = 200$ and 300. Based on 10000 simulations, the simulation results are presented in Table 4.7. Since the gamma process is a Lévy process, the ESA method is considered as the method that uses the correctly specified model, and hence, the related simulation results are highlighted.

From Table 4.7, we observe that the proposed model selection procedure can correctly select the Lévy process as an appropriate model about 90% of the time. Moreover, we observe that the model selection procedure successfully reduces the risk in providing an inaccurate estimate of MTTF when the underlying model for the degradation measurements is misspecified. For example, for Gamma(0.5, 1) process with $m = 300$, $c = 300$, the MSEs based on misspecifying the model as TRP and CTRP are 1012.7 and 38862.2, respectively, while the MSE based on the proposed model selection approach is 333.1.

Table 4.7: Simulation for the model selection procedure when the data are generated from the gamma process with $I = 10$

					MSE of MTTF				% Selection		
m	c	α	β	True MTTF	**ESA**	TRP$_{TS}$	CTRP$_{TS}$	MSP	**Lévy**	TRP	CTRP
200	300	0.5	1	590.6	**360.7**	6260.4	226551.6	1837.5	**90.5**	9.0	0.5
300	300	0.5	1	594.9	**246.2**	1012.7	38862.2	333.1	**90.9**	9.0	0.1
200	500	0.5	1	1027.6	**1022.6**	92342.9	16087619.4	98154.8	**89.7**	9.7	0.6
300	500	0.5	1	986.1	**662.9**	13979.1	1217621.7	2640.6	**90.7**	9.3	0.1
200	300	0.5	2	286.5	**91.7**	167.6	2485.5	106.7	**90.1**	9.4	0.6
300	300	0.5	2	290.1	**60.7**	74.8	300.4	62.0	**90.8**	9.1	0.1
200	500	0.5	2	477.8	**252.8**	2333.5	66484.7	662.5	**90.1**	9.4	0.5
300	500	0.5	2	495.9	**166.5**	395.4	11961.8	189.6	**90.8**	9.2	0.1
200	300	1	1	305.0	**45.4**	81.1	2645.7	49.2	**90.1**	9.9	0.0
300	300	1	1	313.4	**30.0**	38.6	274.3	31.0	**91.1**	8.9	0.0
200	500	1	1	507.6	**125.5**	1276.6	75378.4	253.2	**90.4**	9.6	0.1
300	500	1	1	526.2	**85.5**	201.8	12832.9	95.7	**91.4**	8.6	0.0
200	300	1	2	143.0	**11.2**	23.9	18.9	12.6	**89.8**	10.2	0.1
300	300	1	2	149.5	**7.5**	23.8	43.6	8.9	**91.2**	8.8	0.0
200	500	1	2	262.4	**31.6**	41.6	719.7	32.9	**89.9**	10.1	0.0
300	500	1	2	245.0	**21.3**	33.3	51.2	22.1	**91.3**	8.7	0.0

4.5.3.2. Degradation data generated from the TRP model

In this simulation, the degradation data are generated from the TRP model presented in Section 4.2 with log-linear trend function $\lambda(t|\theta) = ae^{bt}$, where a = 0.4 and 0.6 and b = 0.002 and 0.0005, and $\mathfrak{F}$ is a normal PDF with mean 1 and variance 0.3. The threshold values $c = 300$ and 500 are considered. The number of units (or number of degradation paths) is $I = 10$ with number of measurements $m = 200$ and 300. Based on 10000 simulations, the simulation results are presented in Table 4.8. The related simulation results based on the correctly specified model (i.e., TRP model) are highlighted.

Table 4.8: Simulation for the model selection procedure when the data are generated from TRP with $I = 10$ and $\mathfrak{F} \sim Normal(1, 0.2)$

					MSE of MTTF				% Selection		
m	c	a	b	True MTTF	ESA	**TRP**$_{TS}$	CTRP$_{TS}$	MSP	Lévy	**TRP**	CTRP
200	300	0.4	0.002	164	92.7	**5.7**	11.4	5.7	0	**100**	0
300	300	0.4	0.002	164	1088.3	**6.2**	6.1	6.2	0	**100**	0
200	500	0.4	0.002	343	2885.4	**16.0**	780.5	16.0	0	**100**	0
300	500	0.4	0.002	343	219.5	**5.6**	637.5	5.6	0	**100**	0
200	300	0.4	0.005	278	1382.1	**5.9**	1975.0	5.9	0	**100**	0
300	300	0.4	0.005	278	153.4	**5.7**	571.2	5.7	0	**100**	0
200	500	0.4	0.005	894	242746.2	**853.5**	150798.1	853.5	0	**100**	0
300	500	0.4	0.005	894	168252.7	**180.3**	131668.4	180.3	0	**100**	0
200	300	0.6	0.002	246	115.1	**4.5**	18.5	16.8	0	**6.32**	93.68
300	300	0.6	0.002	246	202.1	**5.5**	17.8	5.5	0	**100**	0
200	500	0.6	0.002	515	15077.0	**150.9**	101.1	130.1	0	**6.92**	93.08
300	500	0.6	0.002	515	6634.9	**22.1**	1712.4	22.1	0	**100**	0
200	300	0.6	0.005	417	12086.9	**38.5**	6519.2	38.5	0	**100**	0
300	300	0.6	0.005	417	3187.2	**8.3**	4365.5	8.3	0	**100**	0
200	500	0.6	0.005	1341	687686.4	**4547.2**	295464.8	4547.2	0	**100**	0
300	500	0.6	0.005	1341	547774.2	**1071.6**	337957.1	1071.6	0	**100**	0

From Table 4.8, once again, we observe that the proposed model selection procedure can correctly select the TRP model as an appropriate model in most cases and successfully reduces the risk in providing inaccurate estimate of the MTTF when the underlying model for the degradation measurements is misspecified. Although there are two cases ($m = 200$, $a = 0.6$, $b = 0.002$ and $c = 300$ and 500) that the model selection procedure select the CTRP as the appropriate model more than 93% of the times, the performance of the estimates of the MTTF based on the model selection procedure is still comparable to the estimates of the MTTF under the correctly specified model because the accuracy of the estimates of the MTTF based on TRP and CTRP models are quite close to each other in these two cases.

4.5.3.3. Degradation data generated from the CTRP model

In this simulation, the degradation data are generated from the CTRP model presented in Section 4.3 with log-linear trend function $\lambda(t|\theta) = ae^{bt}$, where $a = 0.001$ and 0.0012 and $b = 2 \times 10^{-5}$ and 4×10^{-5}, and $\mathfrak{F}^*$ is a normal PDF with mean 1 and variance 0.3. The threshold values $c = 300$ and 500 are considered. The number of units (or number of degradation paths) is $I = 10$ with number of measurements $m = 200$ and 300. Based on 10000 simulations, the simulation results are presented in Table 4.9. From Table 4.9, we observe that the proposed model selection procedure above selects the CTRP model correctly as the appropriate model in all the cases.

Based on the simulation results of the three settings presented in Sections 4.5.3.1 to 4.5.3.3 , we observe that MSEs of the MTTF estimates based on the proposed model selection procedure are lower than the MTTF estimates based on the misspecified models in all the settings considered here. These results clearly illustrates that the proposed model selection procedure can effectively reduce the risk of using an incorrect model and obtaining an inaccurate estimate of MTTF.

Table 4.9: Simulation for model selection procedure when the data are generated from the CTRP model with $I = 10$ $\mathfrak{F}^* \sim Normal(1, 0.02)$

					MSE of MTTF				% Selection		
m	c	a	b	True MTTF	ESA	TRP$_{TS}$	**CTRP**$_{TS}$	MSP	Lévy	TRP	**CTRP**
200	300	0.001	2.0×10^{-5}	215	18804.3	34.1	**2.7**	2.7	0	0	**100**
300	300	0.001	2.0×10^{-5}	215	34883.9	48.1	**1.2**	1.2	0	0	**100**
200	500	0.001	2.0×10^{-5}	502	452.6	1706.3	**15.2**	15.2	0	0	**100**
300	500	0.001	2.0×10^{-5}	502	3794.2	610.1	**6.9**	6.9	0	0	**100**
200	300	0.001	4.0×10^{-5}	108	5347.3	13.5	**0.4**	0.4	0	0	**100**
300	300	0.001	4.0×10^{-5}	108	12860.7	14.9	**0.3**	0.3	0	0	**100**
200	500	0.001	4.0×10^{-5}	252	414.3	62.4	**2.2**	2.2	0	0	**100**
300	500	0.001	4.0×10^{-5}	252	6418.9	35.3	**1.2**	1.2	0	0	**100**
200	300	0.0012	2.0×10^{-5}	339	20997.3	155.9	**7.9**	7.9	0	0	**100**
300	300	0.0012	2.0×10^{-5}	339	41332.7	75.5	**3.4**	3.4	0	0	**100**
200	500	0.0012	2.0×10^{-5}	903	53006.1	26978.8	**68.5**	68.5	0	0	**100**
300	500	0.0012	2.0×10^{-5}	903	21373.7	14405.4	**30.1**	30.1	0	0	**100**
200	300	0.0012	4.0×10^{-5}	170	5102.6	21.7	**1.0**	1.0	0	0	**100**
300	300	0.0012	4.0×10^{-5}	170	14309.8	26.4	**0.5**	0.5	0	0	**100**
200	500	0.0012	4.0×10^{-5}	453	8424.0	2140.8	**9.1**	9.1	0	0	**100**
300	500	0.0012	4.0×10^{-5}	453	420.9	744.6	**4.7**	4.7	0	0	**100**

4.6. Application to Predict the End of Performance of Lithium-Ion Batteries

In this section, we illustrate the models and methodologies proposed in this chapter by using two different lithium-ion battery degradation data sets and compare their behavior. For the battery degradation analysis, the capacity ratio (CR) of lithium-ion batteries is subjected to degradation over number of battery recharging cycles. Thus, the CR provides information about the lifetime of lithium-ion batteries. Suppose $Z_j,\ j = 1,2,\ldots m$ are the CR measurements measured at time $t_j = 1,2,\ldots,m$ (i.e., battery recharging cycles). Therefore, the degradation measurement of the lithium-ion battery with respect to the initial measurement is defined as $X_j = Z_0 - Z_j$, where Z_0 is the initial CR measurement at each recharging cycle.

4.6.1. Lithium-ion battery data set from Wang et al. (2019)

Wang et al. (2019) carried out an experiment for three lithium-ion batteries named B18, B19, and B20. Each battery follows discharging current rates of 1C, 3C and 5C (see Figure 4.1) through a step-stress process in which batteries were charged with current rate of 1C under a constant-current/constant-voltage charge mode (Hunt, 1996) and discharged with current rates 1C, 3C and 5C, repeatedly. In each discharging current, the CR is measured.

Based on this data set, the discharge patterns of the batteries B18 and B19 are similar with three discharging currents; however, the discharge pattern of the battery B20 is largely deviates with respect to the batteries B18 and B19. Therefore, in this analysis, we only considered the data obtained from the batteries B18 and B19. Furthermore, the first 70 CR measurements are not considered in the analysis because those measurements represent the warming up state of the experiment. For this study, the failure threshold level of a battery is set to be if the CR drops to 80% from its initial value (i.e., $Z_c = 0.8$). Wang

et al. (2019) took the summation of 10 consecutive CR measurements and called it as g-cycles. Since taking summation of consecutive measurements would adversely impact on the variability of the estimates of the MTTF, in this study, the g-cycles transformation is not considered.

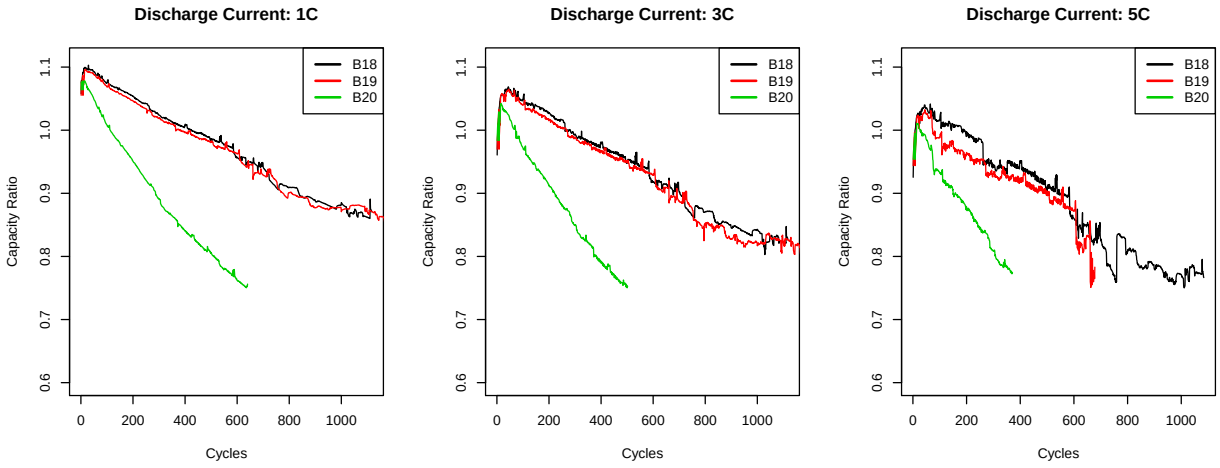

Figure 4.1: Capacity ratio plots for different discharge currents in batteries B18, B19 and B20

The autocorrelation plots for the differences of degradation measurements for batteries B18 and B19 for each discharging current level are presented in Figure 4.2. Furthermore, the Ljung-Box test described in Section 4.5.1 is carried out to test for the autocorrelation of the differences of the degradation measurements in each discharging current level and the results are presented in Table 4.11. The autocorrelation plots and Ljung-Box tests indicate that there is a significant autocorrelation in the degradation measurements, which suggests that the TRP-type models are more appropriate compared to the Lévy process models. In other words, the Lévy process related models and estimation methods may not be appropriate without proper transformation.

To select in between the TRP and CTRP models, we compute the loss functions in Eq. (4.30) and Eq. (4.31) for batteries B18 and B19 at each current level and the values are presented in Table 4.10. From Table 4.10, we observe that the TRP model provides a

better fit to the degradation data of the batteries B18 and B19. Therefore, based on the proposed model selection procedure, we recommend the use of the TRP model. Nevertheless, for illustrative purposes, we also modeled the batteries B18 and B19 data without any transformations from the ESA and the Wiener process models (see Figure 4.3). The gamma process model is not considered here because the increments of degradation measurements are not monotone.

Table 4.10: Loss of TRP and CTRP methods

Battery	**Discharge**	**TRP**$_{TS}$	**CTRP**$_{TS}$
B18	1C	0.0011	0.0153
B18	3C	0.0041	0.0150
B18	5C	0.0010	0.7912
B19	1C	0.1760	3.8665
B19	3C	0.0395	2.9733
B19	5C	0.4843	7.5844

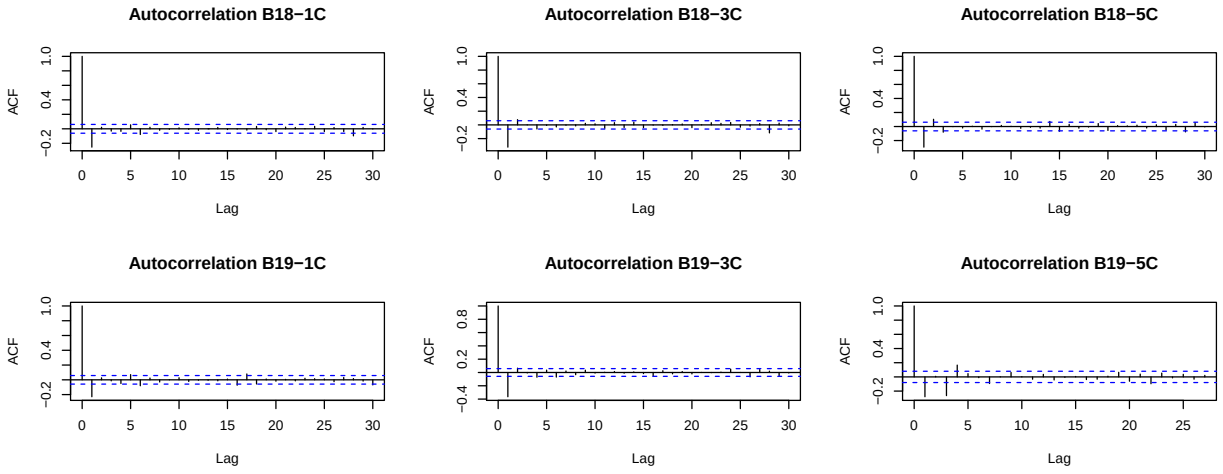

Figure 4.2: Autocorrelation plots for batteries B18 and B19 at different current levels

The predicted degradation paths of the batteries B18 and B19 obtained from the TRP model with $\mathfrak{F} \sim Normal$ (TRP$_N$) and with non-specific $\mathfrak{F}$ (TRP$_{TS}$), and from CTRP model with $\mathfrak{F}^* \sim Normal$ (CTRP$_N$) and with non-specific $\mathfrak{F}^*$ (CTRP$_{TS}$), where the log-linear trend function is used are presented in Figure 4.4.

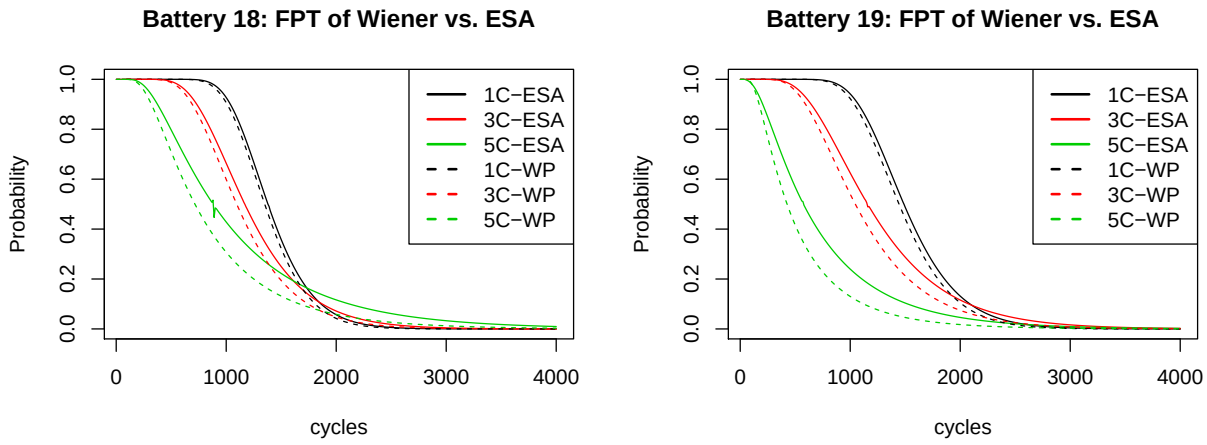

Figure 4.3: Estimated FPT distributions for the batteries B18 and B19 obtained by the ESA and the MLE based on the Wiener process

Table 4.11: Ljung-Box test for independence of the differences of degradation data

Battery	**Discharge**	**Test statistic ($\mathscr{R}$)**	p-value
B18	1C	87.15	4.25e-09
B18	3C	136.28	0
B18	5C	126.40	6.66e-16
B19	1C	99.56	3.56e-11
B19	3C	183.15	0
B19	5C	134.48	0

The point estimates and 95% confidence intervals of the MTTF obtained from different models and methods are presented in Table 4.12. For Wiener process, ESA, and TRP$_{ESA}$ methods, the standard errors of the MTTF estimates can be obtained through the method presented in Section 2.3.3 and Eq. (2.15). For some batteries, the lower confidence limit of the MTTF observed using these methods resulted in negative values; thus, we truncated those to 0. On the other hand, for TRP$_N$, TRP$_{TS}$, CTRP$_N$, and CTRP$_{TS}$ methods, the bootstrap methods presented in Sections 4.2.1.2, 4.2.2.2, 4.3.1.2 and 4.3.2.2, respectively, are used to construct the 95% confidence intervals of the MTTF.

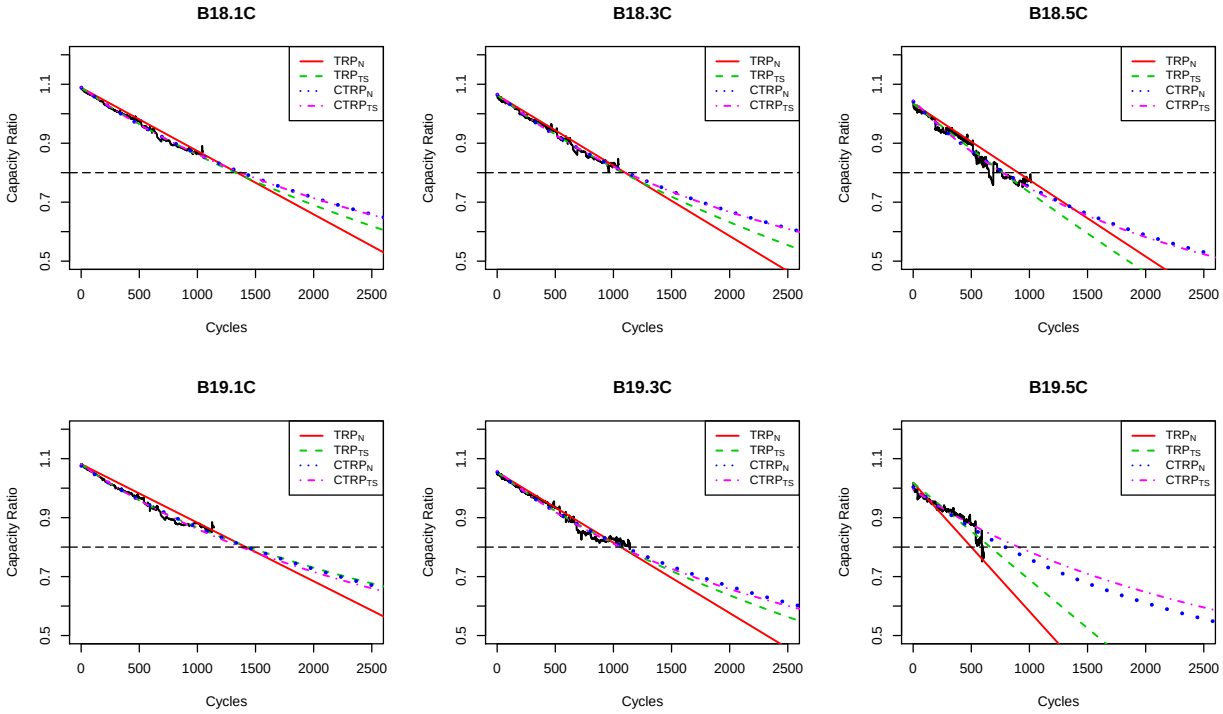

Figure 4.4: Prediction for CR degradation from TRP_N, TRP_{TS}, CTRP_N, and CTRP_{TS} models

From the results in Table 12, we can see that the MTTF estimates obtained from different methods are not substantially different from each other. Based on the proposed model selection procedure, in this case, the TRP model is selected. Therefore, from the simulation results in Section 4.4.3, we would recommend using the estimates obtained from the TRP_{TS} method (highlighted in Table 4.12).

4.6.2. NASA battery data set

The NASA battery data set presented in Saha and Goebel (2007) has been applied in many studies of degradation data analysis (see, for example, Wang et al., 2019; Mosallam et al., 2016; Liu et al., 2014; Zhou et al., 2012). In this study, we use the degradation data of batteries B0005 and B0006 to illustrate the proposed methodologies. These two bat-

Table 4.12: MTTF from the proposed methods for Lithium-ion batteries B18 and B19 for each discharging current levels

Battery	Discharge	WP	ESA	TRP_N	TRP_{TS}	TRP_{ESA}	CTRP_N	CTRP_{TS}
B18	1C	1455.5	1492.2	1410	**1395**	1577.6	1453	1445
		(736, 2175)	(773, 2211)	(1042, 2740)	**(1387, 1416)**	(754, 2401)	(1449, 1460)	(1441, 1447)
B18	3C	1239.9	1320.2	1170	**1149**	1350.3	1187	1181
		(342, 2138)	(422, 2218)	(746, 3074)	**(1148, 1172)**	(396, 2304)	(1184, 1193)	(1177, 1182)
B18	5C	956.4	1173.8	973	**838**	1174.3	853	840
		(0, 2095)	(36, 2312)	(489,4440)	**(845, 861)**	(28, 2321)	(849, 860)	(837, 843)
B19	1C	1563.3	1614.7	1485	**1510**	1784.2	1498	1447
		(685, 2441)	(736, 2493)	(1039, 3062)	**(1492, 1529)**	(669, 2899)	(1491, 1508)	(1444, 1449)
B19	3C	1227.3	1351.8	1132	**1133**	1373.4	1164	1132
		(168, 2287)	(293, 2411)	(681, 3117)	**(1130, 1150)**	(235, 2512)	(1159, 1171)	(1129, 1135)
B19	5C	633.2	820.8	571	**732**	820.8	862	977
		(0, 1501)	(0, 1689)	(295, 3995)	**(776, 817)**	(0, 1689)	(846, 881)	(970, 983)

teries have 168 CR measurements and tested under temperature 24°C with discharging rate of 2A. Furthermore, the threshold level is considered as CR drops to 80% from its initial value (i.e., $Z_c = 0.8$ or $c = 0.2$). The degradation data of these two batteries (B0005 and B0006) are plotted in Figure 4.5.

The autocorrelation plots of the differences of the degradation measurements are shown in Figure 4.6. Furthermore, the p-values of the Ljung-Box tests for the degradation differences of these two batteries are 0.94 and 0.69, respectively. These p-values indicate that modeling the degradation data with Lévy process models is appropriate. Therefore, we apply the Wiener process model and the ESA approach to estimate the FPT distributions of batteries B0005 and B0006 (see Figure 4.7). For illustration purposes, we also model the degradation data with the TRP and CTRP models discussed in this study. The point estimates and the 95% confidence intervals of the MTTF obtained from different models and methods are presented in Table 4.13. Furthermore, the associated predicted degradation paths are demonstrated in Figure 4.8. Based on the proposed model selection procedure, in this case, we would recommend using the estimates obtained from the ESA of the original degradation measurements (highlighted in Table 4.13).

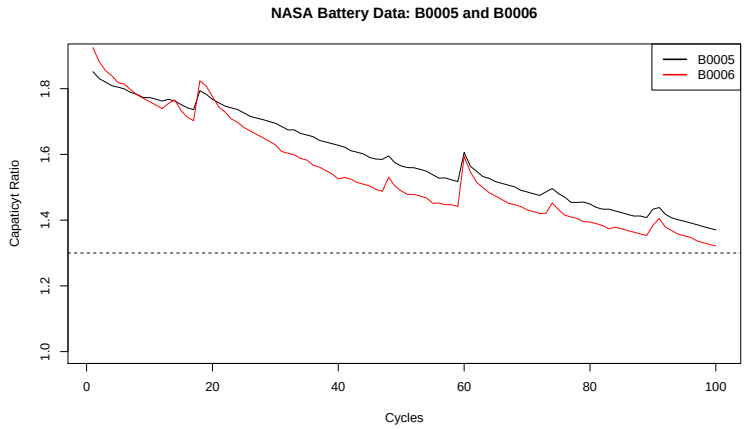

Figure 4.5: NASA battery data for batteries B0005 and B0006

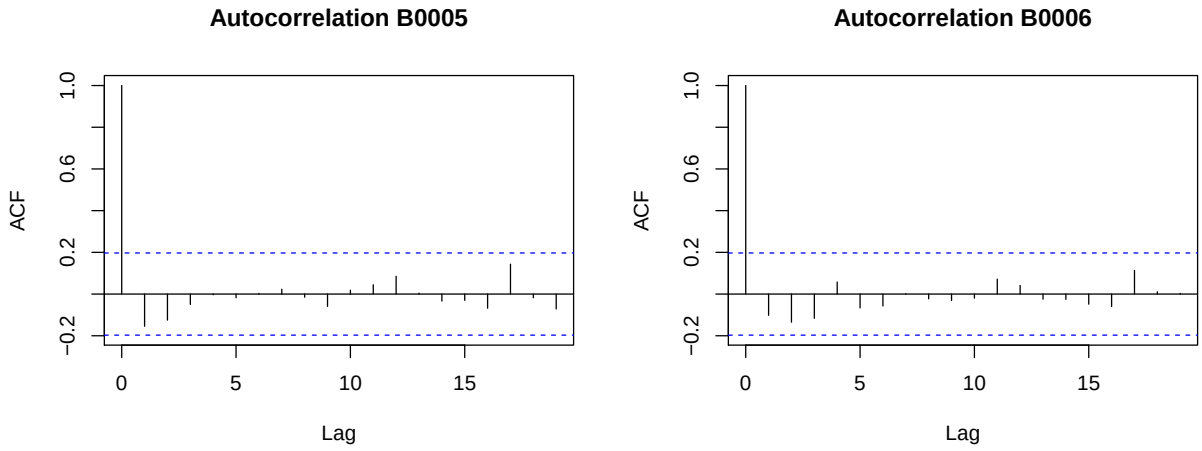

Figure 4.6: Autocorrelation plots of B0005 and B0006 for increments

4.7. Conclusion

In this chapter, we proposed different parametric and semiparametric models and approaches to estimate the MTTF based on the degradation data when this data may be non-linearly related to time. Lévy process models, trend-renewal-process (TRP) models and cumulative-sum-trend-renewal-process (CTRP) models are discussed. In addition, point and interval estimation methods for TRP and CTRP models with and without specific distributions are proposed.

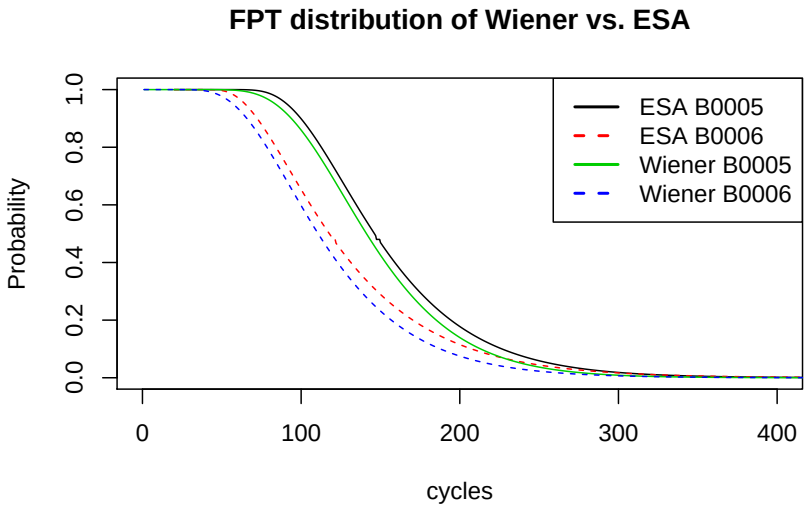

Figure 4.7: Estimated FPT distributions based on the Wiener process with MLE and the ESA for NASA B0005 and B0006 batteries with $c = 0.8$

Table 4.13: Estimates of the MTTF and 95% confidence intervals of the MTTF for NASA B0005 and B0006 batteries

Battery	**WP**	**ESA**	**TRP**$_N$	**TRP**$_{TS}$	**TRP**$_{ESA}$	**CTRP**$_N$	**CTRP**$_{TS}$
B0005	320.3	**328**	412	295	328	468	470
	(130, 511)	**(138, 518)**	(254, 1108)	(270, 286)	(138, 518)	(460, 481)	(457, 477)
B0006	238.4	**248.3**	345	298	307.4	359	360
	(76, 400)	**(86, 410)**	(207, 951)	(278, 319)	(117, 498)	(354, 366)	(358, 362)

The performance of the proposed estimation methods are evaluated using an extensive Monte Carlo simulation study in which the degradation data are generated from different models. We observed that when the model is correctly specified, the proposed estimation methods provide reasonable estimates of the MTTF in most cases. However, we found that when the model is misspecified, the estimates of the MTTF can perform poorly. Therefore, we also proposed a model selection procedure to select the appropriate model among the Lévy process, TRP, CTRP models. Based on the results from a simulation study, we observed that the proposed model selection procedure can signifi-

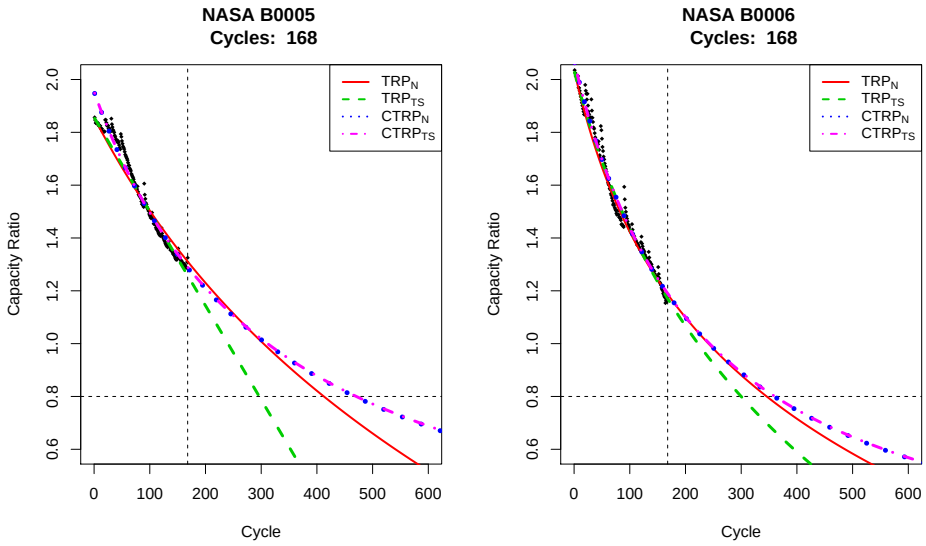

Figure 4.8: The predicted degradation paths of the batteries B18 and B19 obtained from TRP model with $\mathfrak{F} \sim Normal$ (TRP$_N$) and with non-specific $\mathfrak{F}$ (TRP$_{TS}$), and from CTRP model with $\mathfrak{F}^* \sim Normal$ (CTRP$_N$) and with non-specific $\mathfrak{F}^*$ (CTRP$_{TS}$), where log-linear trend function is used

cantly reduce the risk of model misspecification and provide a reasonably better estimate of the MTTF.

As we observed in the numerical example, the interval estimates of the MTTF based on the CTRP model are impractically narrower than the other the models, which indicates that the CTRP model may disregard a part of the variation in the data in the process of summing the degradation measurements. For future research studies, it will be interesting to evaluate the performance of the interval estimation methods for the MTTF theoretically and numerically for TRP and CTRP models.

Chapter 5
Future Research Directions and Concluding Remarks

5.1. Introduction

In this chapter, we provide some possible future research directions related to degradation data analysis discussed in this thesis. The comparison between the empirical Laplace inversion and the ESA method is discussed in Section 5.2. In Section 5.3, we discuss the comparison of the IG-based ESA method and the normal-based ESA method. In Section 5.4, importance of asymptotic properties of the proposed imputation methods for degradation data with unequal time intervals in Section 2.3.5 is discussed. In addition, to reduce the bias in the estimate of FPT distribution obtained from the ESA with unequal time intervals, a model based approach using least-squares estimation method is introduced in Section 5.5. Finally, some concluding remarks are provided in Section 5.6.

5.2. Empirical Laplace Inversion and Empirical Saddlepoint Approximation

Abate and Whitt (1992) and Abate et al. (2000) analyzed and discussed numerical inversion algorithms for both generating functions and Laplace transforms. Primarily, they inverted the transformations by applying the trapezoidal rule for complex integrals and evaluate the discretization error involved with the trapezoidal rule using a Poisson summation formula. Their proposed methods are also called the Fourier-series methods as the Poisson summation formula involves the Fourier-series.

Specifically, if f is a real valued function on the positive line, then the Laplace transform of f is defined as $\mathscr{L}(f(s)) = f(s) = \int_0^\infty \{\exp(-st) f(t) dt\}$, where $s = b + iu$ and $b > 0$. Moreover, the transform function should converge with support (a, ∞) for $b > a \geq 0$. If f is a PDF on $(0, \infty)$, then its MGF is $\mathscr{M}(s) = f(-s)$. Furthermore, the Laplace transform of the CDF is $f(s)/s$ and the survival function is $(1 - f(s))/s$.

The Fourier-series method discussed by Abate et al. (2000) starts with the Bromwich inversion integral to invert the Laplace transform. Suppose $f(s)$ is the Laplace transform of a function f, then the Bromwich inversion integral is given by,

$$f(t) = \frac{1}{2\pi i} \int_{b-i\infty}^{b+i\infty} \exp(st) \hat{f}(s) ds, t > 0, \tag{5.1}$$

where b is a real number to the right of all singularities of $\hat{f}(s)$, and the contour integral yields the value 0 for $t < 0$. Substitute $s = b + iu$ into Eq. (5.1), we have

$$f(t) = \frac{1}{2\pi} \int_{-\infty}^{\infty} \exp\{(b + iu)t\} \hat{f}(b + iu) du.$$

Since $\exp\{(b + iu)t\} = \exp(bt)\{\cos(ut) + i \sin(ut)\}$, we can obtain

$$\begin{aligned} f(t) &= \frac{2e^b t}{\pi} \int_0^\infty \mathrm{Re}\{\hat{f}(b + iu)\} \cos(ut) du \quad \text{and} \\ f(t) &= \frac{-2e^b t}{\pi} \int_0^\infty \mathrm{Im}\{\hat{f}(b + iu)\} \cos(ut) du, \end{aligned}$$

where Re and Im are real and imaginary components of a complex number. When the trapezoidal rule with step size h applies to the Bromwich inversion integral, Abate and

Whitt (1995) obtained the approximation for $f(t)$ as

$$f(t) \approx f_h(t) = \frac{h\exp(bt)}{\pi}\mathrm{Re}\{\hat{f}(b)\} + \frac{2h\exp(bt)}{\pi}\sum_{k=1}^{\infty}\mathrm{Re}\{\hat{f}(b+ikh)\}\cos(kht).$$

If we let $h = \pi/2t$, then the $\cos(kht)$ term would be either -1, 0, or 1. In addition, by letting $b = A/2t$, we can obtain

$$f_h(t) = f_A(t) = \frac{\exp(A/2)}{2t}\mathrm{Re}\{\hat{f}(A/2t)\} + \frac{\exp(A/2)}{t}\sum_{k=1}^{\infty}(-1)^k\mathrm{Re}\{f((A+2k\pi i)/2t)\}. \tag{5.2}$$

The approximation in Eq. (5.2) consists of three types of errors: discretization error, truncation error, and roundoff error. Abate et al. (2000) explained the ways to address those errors. The algorithm used to invert the Laplace transform based on Eq. (5.2) is called the Euler algorithm.

In the ESA method, we used the empirical MGF for the LR method. Similarly, we can use the empirical MGF of degradation data to obtain an estimate of the FPT distribution from the Euler algorithm. Suppose $\Delta x_1, \Delta x_2, \ldots, \Delta x_m$ are the differences of the $m+1$ degradation measurements, then, the empirical Laplace inversion is obtained by $\hat{f}_{emp}(-s) = \hat{\mathscr{M}}(s) = \sum_i^m \Delta x_i/m$. We named this method as empirical Laplace inversion.

Figures 5.1 and 5.2 show the comparison of the approximated FPT distributions obtained by the ESA method and by the empirical Laplace method for degradation data with $m = 500$ generated from gamma and IG degradation processes, respectively. From Figure 5.1, we observe that there is no noticeable difference between the two methods. On the other hand, from Figure 5.2, where the threshold levels are small, there is a substantial deviation at the left-tail of the estimated FPT distribution obtained by the empirical Laplace method, whereas the ESA method works properly.

Although the empirical Laplace method works similarly as the ESA method at large threshold values, it is better to understand the reasons of the substantial deviation at the left-tail for lower threshold levels.

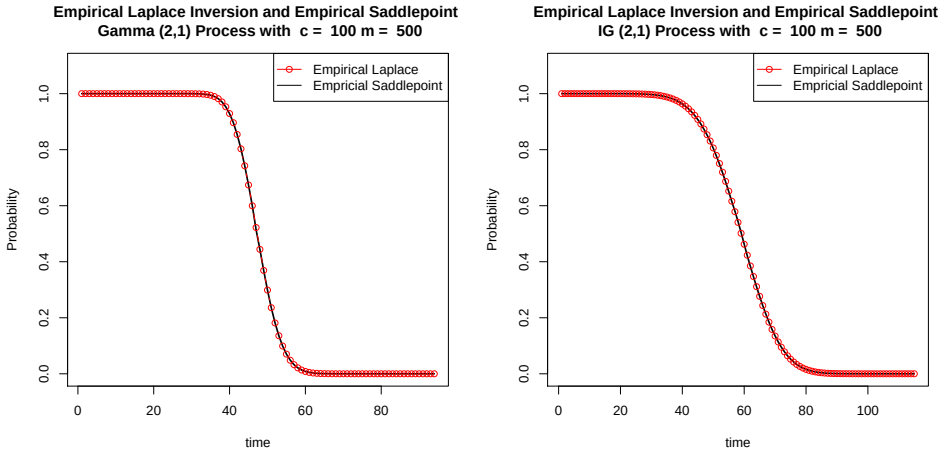

Figure 5.1: Compare empirical Laplace inversion and ESA for larger thresholds

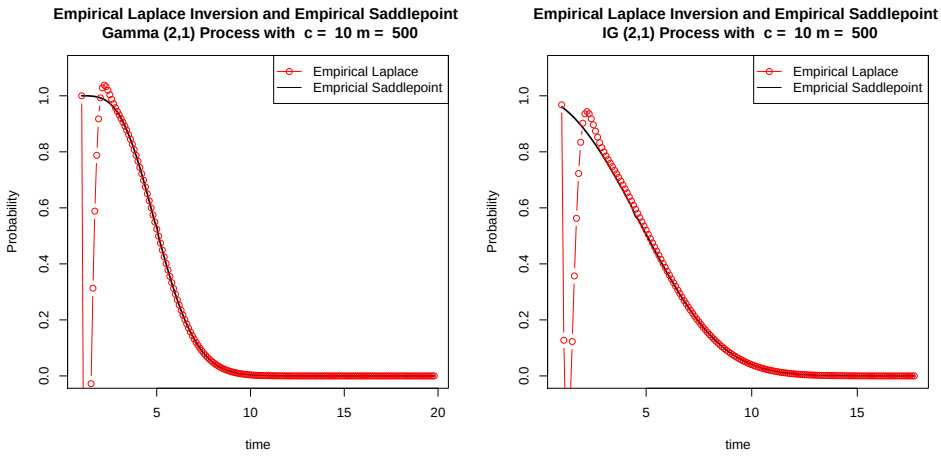

Figure 5.2: Compare empirical Laplace inversion and ESA for smaller thresholds

5.3. Inverse-Gaussian-based ESA and Normal-based Empirical Saddlepoint Approximation

In Section 2.5, we discussed the IG-based saddlepoint approximation is an option to minimize the ill behavior of the normal-based saddlepoint approximation. As analogue to the ESA approach discussed in Section 2.3.1, IG-based saddlepoint approximation can be applied with empirical MGF (IG-based ESA), which is also a fully nonparametric approach to estimate the FPT distribution. Figure 5.3 illustrates the approximated FPT distributions obtained through the normal-based ESA and the IG-based ESA approaches for the Gamma(2,1) and IG(2,1) degradation processes with 500 samples ($m = 500$) and threshold level of 100 ($c = 100$).

The IG-based saddlepoint approximation is known to be beneficial when the threshold is smaller than the mean degradation per unit time increment. However, further analyses and studies are required to evaluate the benefits and limitations of the IG-based saddlepoint approach in both parameteric and nonparametric perspectives.

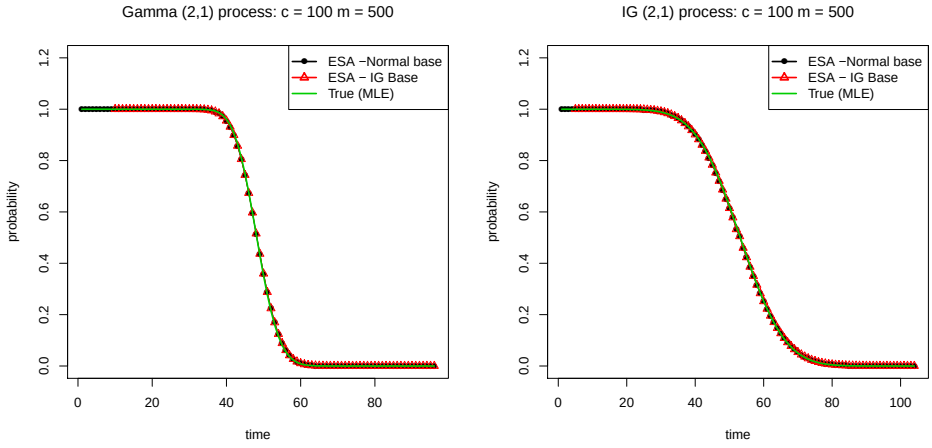

Figure 5.3: Inverse-Gaussian-based empirical saddlepoint approximation

5.4. Asymptotic Properties of Proposed Imputation Techniques

In Chapter 2, we discussed that the ESA properly works only when the degradation measurements are taken at equal time intervals, and hence, we proposed several imputation techniques in Section 2.4.2 to obtain proper approximation of the FPT distribution. It was observed that these imputation techniques provides nearly unbiased estimate for the mean of FPT distribution (i.e., MTTF). However, the variance of the estimate through these imputation methods are different from each other. Thus, it is important to study the asymptotic behaviors of these imputation techniques.

In those imputation methods, we evaluate the degradation per unit time interval for all the degradation measurements (i.e., $\Delta x_i^* = \Delta x_i/\Delta t_i$). Since ΔX_i follows a Lévy process, its mean and variance are $\mu\Delta t_i$ and $\sigma^2\Delta t_i$, then the mean and the variance of Δx_i^* can be derived as

$$\begin{aligned} \mathbb{E}(\Delta X_i^*) &= \mathbb{E}\left(\frac{\Delta X_i}{\Delta t_i}\right) = \mu \\ \text{and } \mathbb{V}(\Delta X_i^*) &= \mathbb{V}\left(\frac{\Delta X_i}{\Delta t_i}\right) = \frac{\sigma^2}{\Delta t_i}, \end{aligned}$$

respectively. Here, we show that the mean of Δx_i^* is time independent, yet the variance is time dependent. A rough estimate for the MTTF is $c/\mathbb{E}(\Delta X_i)$, and thereby, the MTTF is unbiased if we use Δx_i^* as an estimate for the imputed degradation points. On the other hand, under the normality assumption, a rough estimate of the variance of the FPT distribution is $c^2/\mathbb{V}(\Delta X_i^*) = c^2\Delta t_i/\sigma^2$. As a result, when estimating the FPT distribution based on the ESA imputation methods using Δx_i^*, the variance is time dependent. According the Section 2.3.5.2, through simulation, we have shown that the conditional random imputation technique gives a similar estimate of the FPT distribution based on the MLE.

However, it is important to evaluate the variance of the estimated FPT distribution with imputation techniques asymptotically.

5.5. Least squares estimation approach for the ESA with unequal time intervals

The imputation techniques proposed in Chapter 2 provide decent results; however, when the time intervals between two degradation measurements are large and the highest common factor (HCF) of the time intervals is relatively small, it impacts on the variability of the estimated FPT distribution. For example, if the measurements are taken at log time intervals (e.g., 1, 10, 100, ...), then the estimated FPT distributions obtained through random imputation method and conditional random imputation method will be similar to one obtained by the linear imputation method. Moreover, the imputation methods are not asymptotically efficient as when the sample size or experiment time increases the estimated FPT distribution do not converge to the MLE estimate of the FPT distribution. This is probably because of the variance of ΔX_j^* specified in Section 5.4 depends on the time.

5.5.1. Model development

In this section, we propose to estimate the FPT distribution for degradation data using the ESA method by converting the original degradation process which different time intervals to a pseudo degradation process with equal time intervals. Suppose $\{X_{t_{ij}}; t > 0, i = 1,2,\ldots,I, j = 1,2,\ldots,m\}$ follows a Lévy process which consists of I units with m measurements and the time intervals of consecutive measurements are $\{\Delta t_{ij}; i = 1,2,\ldots,I, j = 1,2,\ldots,m\}$ and differences in consecutive measurements are $\{\Delta X_{t_{ij}}; i = 1,2,\ldots,I$

, $j = 1,2,\ldots,m\}$, since $\{X_{t_{ij}}\}$ follows a Lévy process, we suggest the model

$$X_{t_{ij}} = \mu_Y t_{ij} + \varepsilon_{t_{ij}}, \qquad \varepsilon_{t_{ij}} \sim .(0, \sigma_Y^2 t_{ij}), \tag{5.3}$$

where μ_Y and σ_Y^2 are the mean and variance of the degradation per unit interval. For example, if X_t follows Gamma(α,β) process then $\mu_Y = \alpha\beta$ and $\sigma_Y^2 = \alpha\beta^2$. The variance parameter of the Lévy process is σ_Y. Because of the Lévy process is infinitely divisible, the model for $\Delta X_{t_{ij}}$ can be written as

$$\Delta X_{\Delta t_{ij}} = \mu_Y \Delta t_{ij} + \varepsilon_{\Delta t_{ij}} \qquad \varepsilon_{\Delta t_{ij}} \sim .(0, \sigma_Y^2 \Delta t_{ij}). \tag{5.4}$$

Suppose the $HCF(\Delta t_{ij}; i = 1,2,\ldots,I, j = 1,2,\ldots,m)$ of the time differences is Δt_0, the objective here is to transform the stochastic process $\Delta X_{\Delta t_{ij}}$ to $\Delta X_{\Delta t_0}$ by estimating μ_Y and σ_Y using a least-squares approach. An independent and identically distributed error estimate of the model in Eq. (5.4) is

$$\varepsilon^*_{\Delta t_{ij}} = \frac{\left(\Delta X_{\Delta t_{ij}} - \mu_Y \Delta t_{ij}\right)}{\sqrt{\Delta t_{ij}}}. \tag{5.5}$$

Then, the sum of squares of the error estimate is given by

$$\sum_{i=1}^{I}\sum_{j=1}^{m}\left\{\varepsilon^*_{\Delta t_{ij}}\right\}^2 = \sum_{i=1}^{I}\sum_{j=1}^{m}\frac{\left(\Delta X_{\Delta t_{ij}} - \mu_Y \Delta t_{ij}\right)^2}{\Delta t_{ij}}. \tag{5.6}$$

By minimizing the sum of squares of errors in Eq. (5.6), we can obtain an estimate of μ_Y as,

$$\hat{\mu}_Y = \frac{\sum_{i=1}^{I}\sum_{j=1}^{m}\Delta X_{\Delta t_{ij}}}{\sum_{i=1}^{I}\sum_{j=1}^{m}\Delta t_{ij}}. \tag{5.7}$$

If the measurements of all units are taken at the same time (i.e., $\Delta t_{ij} = \Delta t_j$), then the estimate in Eq. (5.7) can be modified to

$$\hat{\mu}_Y = \frac{\sum_{i=1}^{I}\sum_{j=1}^{m}\Delta X_{\Delta t_j}}{I\mathfrak{T}}, \tag{5.8}$$

where $\mathfrak{T} = \sum_{j=1}^{m} \Delta t_j$ is the total experiment time. The expected value of the estimate in Eq. (5.8) is μ_Y; thus it is unbiased. Furthermore, the variance of the estimate in in Eq. (5.8) is $\sigma_Y^2/(I\mathfrak{T})$; thereby, $\hat{\mu}_Y$ is consistent as its variance goes to 0 when either $I \to \infty$ (i.e., large sample) or $\mathfrak{T} \to \infty$ (i.e., long experiment time). Moreover, the estimate of the random error, $\varepsilon^*_{\Delta t_{ij}}$, can be obtained as

$$\hat{\varepsilon}^*_{\Delta t_j} = \frac{\left(\Delta X_{\Delta t_j} - \hat{\mu}_Y \Delta t_j\right)}{\sqrt{\Delta t_j}}. \tag{5.9}$$

Thus, the variance of $\hat{\varepsilon}^*_{\Delta t_j}$ is found to be $\sigma_Y^2[1 - \Delta t_j/(I\mathfrak{T})]$. Using these estimates, the transformed degradation process model for time differences with Δt_0 is estimated by

$$\Delta\tilde{X}_{\Delta t_0|\Delta t_j} = \hat{\mu}_Y \Delta t_0 + \hat{\varepsilon}_{\Delta t_0|\Delta t_j}, \tag{5.10}$$

where $\hat{\varepsilon}_{\Delta t_0|\Delta t_j} = \sqrt{\Delta t_0}\hat{\varepsilon}^*_{\Delta t_j}$ and $\Delta\tilde{X}_{\Delta t_0|\Delta t_j}$ is the estimated degradation increment for time interval Δt_0 for the j-th measurement. The expected valued of $\Delta\tilde{X}_{\Delta t_0|\Delta t_j}$ is $\mu_Y \Delta t_0$, which is thereby unbiased. In addition, the variance of $\Delta\tilde{X}_{\Delta t_0|\Delta t_j}$ is obtained as

$$\mathbb{V}(\Delta\tilde{X}_{\Delta t_0|\Delta t_j}) = \sigma_Y^2 \left[1 - \frac{(\Delta t_j - 1)}{I\mathfrak{T}}\right] \Delta t_0. \tag{5.11}$$

From Eq. (5.11), we can see that either $I \to \infty$ (i.e., large sample size) or $\mathfrak{T} \to \infty$ (i.e. long experiment time), the variance of $\Delta\tilde{X}_{\Delta t_0|\Delta t_j}$ reach $\sigma_Y^2 \Delta t_0$, which is the variance of $\Delta X_{\Delta t_0}$. Therefore, the estimate $\Delta\tilde{X}_{\Delta t_0|\Delta t_j} \to \Delta X_{\Delta t_0}$ as $I \to \infty$ or $\mathfrak{T} \to \infty$ for all $\Delta t_j,\ j = 1, 2, \ldots, m$. This shows that the estimate, $\Delta\tilde{X}_{\Delta t_0}$, is asymptotically efficient. From the estimated differences for Δt_0 (i.e., $\Delta\tilde{X}_{\Delta t_0}$), we can apply the ESA for a given threshold level.

5.5.2. Monte Carlo simulation study for the percentiles of FPT distribution

We consider generating the degradation data from gamma degradation processes with time gaps $\{1,3,5\}$ (i.e., degradation data are measured at time $t_1 = 1$, $t_2 = 4$, $t_3 = 9$, $t_4 = 10$, $t_5 = 13$, $t_6 = 18$, ...). The degradation processes Gamma(1, 2) and Gamma(0.5, 4) processes are generated with 10 and 50 items ($I = 10$ and 50) and different threshold values ($c =$ 60 and 100). Furthermore, we considered the number of measurement time points as 12 ($m = 12$ with $t_m =$ 36) and 18 ($m = 18$ with $t_m =$ 54). The performance of the approximated FPT distributions are evaluated using the MSEs of the estimated 5-th, 10-th and 90-th percentiles of the FPT distributions. The results based on 10000 simulations for each setting are presented in Tables 5.1 and 5.2 for $I = 10$ and 50, respectively. From the results in Tables 5.1 and 5.2, we observe that the conditional random imputation method (CRImp) and least-squares method proposed in this section gives MSEs closest to the MLE of the FPT distribution. However, MSEs of the estimates based on least-squares method performs better than all the other proposed imputation methods and modified CGF method except the CRImp method. As a future research direction, we can use the estimate $\Delta\tilde{X}_{\Delta t_0|\Delta t_j}$ as an imputation estimate to replace δ_i in Eq. (2.17).

In addition to evaluating the percentiles of the FPT distribution for the modified empirical CGF method, imputation techniques and LS method, we performed a Monte Carlo simulation to evaluate the variance of the FPT distribution obtained through the proposed methods for small and large sample sizes.

Table 5.1: Mean squared errors (MSEs) of the estimates of 5-th, 10-th and 90-th percentiles based on MSE, modified CGF, LImp, RImp, CRImp and LS methods when the data are generated from the Gamma(1, 2) and Gamma(0.5, 4) processes with $I = 10$.

5-th percentile			Simulated from Gamma(1, 2)						Simulated from Gamma(0.5, 4)					
I	t_m	c	MSE	MCGF	LImp	RImp	CRImp	LS	MSE	MCGF	LImp	RImp	CRImp	LS
10	36	60	2.33	11.24	15.74	3.91	2.41	3.26	3.86	20.86	27.28	5.91	4.16	6.00
10	36	100	5.90	19.47	23.81	12.65	7.09	7.74	3.86	13.53	15.64	7.34	4.23	5.30
10	54	60	1.57	9.41	14.57	3.29	1.68	2.24	7.60	23.67	35.56	28.21	8.23	9.58
10	54	100	3.94	15.11	21.17	10.96	5.19	5.21	10.79	39.76	46.39	19.95	12.20	15.06
10-th percentile			Simulated from Gamma(1, 2)						Simulated from Gamma(0.5, 4)					
I	t_m	c	MSE	MCGF	LImp	RImp	CRImp	LS	MSE	MCGF	LImp	RImp	CRImp	LS
10	36	60	2.28	7.98	10.13	3.82	2.36	2.96	11.53	34.36	36.30	17.36	12.03	15.39
10	36	100	6.11	17.72	19.65	9.49	6.28	7.95	19.26	44.93	60.79	49.72	20.36	23.66
10	54	60	1.52	6.41	9.10	3.18	1.62	1.98	2.66	17.55	25.46	4.68	2.79	4.27
10	54	100	4.06	13.58	17.12	7.61	4.31	5.31	2.56	10.70	14.07	5.99	2.86	3.55
90-th percentile			Simulated from Gamma(1, 2)						Simulated from Gamma(0.5, 4)					
I	t_m	c	MSE	MCGF	LImp	RImp	CRImp	LS	MSE	MCGF	LImp	RImp	CRImp	LS
10	36	60	3.55	9.09	13.52	13.20	4.07	4.36	4.95	20.57	33.29	23.62	5.33	6.19
10	36	100	8.83	18.41	24.29	23.49	9.85	10.92	6.95	29.86	40.04	16.74	8.33	9.70
10	54	60	2.37	7.65	12.73	11.40	2.80	2.93	7.37	25.28	30.41	13.81	7.86	9.86
10	54	100	5.92	14.91	21.86	19.55	6.67	7.36	12.65	37.50	55.76	40.05	13.13	15.39

Table 5.2: Mean squared errors (MSEs) of the estimates of 5-th, 10-th and 90-th percentiles based on MSE, modified CGF, LImp, RImp, CRImp and LS methods when the data are generated from the Gamma(1, 2) and Gamma(0.5, 4) processes with $I = 50$.

5-th percentile			Simulated from Gamma(1, 2)						Simulated from Gamma(0.5, 4)					
I	t_m	c	MSE	MCGF	LImp	RImp	CRImp	LS	MSE	MCGF	LImp	RImp	CRImp	LS
50	36	60	0.58	6.83	12.98	2.40	0.64	0.86	0.94	11.66	21.97	3.30	0.92	1.59
50	36	100	1.33	8.97	17.46	8.73	2.57	1.68	0.84	5.97	11.30	4.62	1.10	1.12
50	54	60	0.45	6.44	12.71	2.30	0.49	0.67	1.68	17.37	31.28	17.74	1.73	1.97
50	54	100	0.95	8.11	16.98	8.31	2.15	1.13	2.16	17.11	32.41	12.59	3.21	2.99
10-th percentile			Simulated from Gamma(1, 2)						Simulated from Gamma(0.5, 4)					
I	t_m	c	MSE	MCGF	LImp	RImp	CRImp	LS	MSE	MCGF	LImp	RImp	CRImp	LS
50	36	60	0.51	4.22	7.73	2.26	0.60	0.66	2.24	13.72	23.43	9.13	2.52	3.00
50	36	100	1.30	7.94	13.54	5.19	1.53	1.68	3.91	28.07	49.17	27.08	3.97	4.75
50	54	60	0.37	3.89	7.53	2.15	0.46	0.49	0.73	10.95	21.71	3.00	0.65	1.23
50	54	100	0.88	7.14	13.23	4.74	1.11	1.14	0.59	5.42	11.10	4.35	0.82	0.77
90-th percentile			Simulated from Gamma(1, 2)						Simulated from Gamma(0.5, 4)					
I	t_m	c	MSE	MCGF	LImp	RImp	CRImp	LS	MSE	MCGF	LImp	RImp	CRImp	LS
50	36	60	0.79	5.93	11.48	9.05	1.06	0.97	1.21	16.76	30.84	16.93	1.22	1.36
50	36	100	1.87	10.02	18.70	14.29	2.36	2.30	1.53	15.24	31.39	12.02	2.51	2.03
50	54	60	0.55	5.70	11.39	8.63	0.79	0.69	1.52	12.07	22.47	8.48	1.79	2.04
50	54	100	1.28	9.21	17.96	13.68	1.79	1.60	2.76	26.69	48.31	25.29	2.74	3.26

5.5.3. Monte Carlo simulation for the variance of the FPT distribution

In this simulation, the degradation data are generated from gamma and IG degradation processes with time gaps $\{1,3,5\}$ from the Gamma(1, 2), Gamma(0.5, 4), IG(2, 5), and IG(2, 10) processes with small and large number of items ($I = 5$ and 20), total time ($t_m = 36$), and different threshold values ($c = 60$ and 100). The performance of the approximated variance of the FPT distribution through the proposed methods are evaluated using the MSEs with respect to the exact variance. The MLE of the FPT distribution is obtained by estimating the parameters for a specific parametric degradation process with the maximum likelihood method.

The variance of the estimated FPT distribution can be obtained for a Lévy process model by estimating $\mathbb{E}(T_c)$ and $\mathbb{E}(T_c^2)$ in Eq. (2.12) and (2.13), respectively, by

$$\widehat{\mathbb{V}}(T_c) = \widehat{\mathbb{E}}(T_c^2) - \left\{\widehat{\mathbb{E}}(T_c)\right\}^2. \tag{5.12}$$

From Table 5.3, we observe that in all the cases considered here, both CImp and LS methods give MSEs closest to the MLE based on the correctly specified degradation process. In addition, the LS method provides the smallest MSE of the variance of estimated FPT among all the procedures. Furthermore, when the unit size increase from 5 to 20, the MSEs of variances are decreased in all methods as expected. Thereby, this simulation study demonstrates the usefulness of the ESA with the CRImp method and LS method to adjust for unequal time intervals. However, more extensive simulation study and theoretical derivations are required to understand the performance of the proposed imputation techniques and LS method.

Table 5.3: Mean squared errors (MSEs) of the variance estimates of the FPT distribution for modified CGF and different data imputation methods when the data are generated from the Gamma(1, 2), Gamma(0.5, 4), IG(2,5) and IG(2,10) processes.

			Simulated from Gamma(1, 2)						Simulated from Gamma(0.5, 4)					
n	t_m	c	MLE	MCGF	LImp	RImp	CRImp	LS	MLE	MCGF	LImp	RImp	CRImp	LS
5	36	60	0.26	3.07	5.70	3.25	0.51	0.37	0.46	6.42	11.44	3.51	0.86	0.74
5	36	100	0.44	5.17	9.57	6.00	0.88	0.63	0.89	11.12	19.54	9.91	1.71	1.55
20	36	60	0.06	2.65	5.44	2.97	0.19	0.10	0.12	5.37	10.80	3.47	0.26	0.22
20	36	100	0.11	4.40	9.08	5.29	0.34	0.17	0.23	9.19	18.34	9.42	0.51	0.44
			Simulated from IG(2, 5)						Simulated from IG(2, 10)					
n	t_m	c	MLE	MCGF	LImp	RImp	CRImp	LS	MLE	MCGF	LImp	RImp	CRImp	LS
5	36	60	0.10	1.21	2.22	1.05	0.39	0.14	0.05	0.57	1.07	0.64	0.32	0.06
5	36	100	0.17	2.05	3.76	2.13	0.69	0.24	0.08	0.97	1.84	1.08	0.53	0.10
20	36	60	0.02	1.02	2.10	1.00	0.28	0.04	0.01	0.49	1.03	0.58	0.25	0.02
20	36	100	0.04	1.73	3.57	1.91	0.48	0.06	0.02	0.84	1.76	0.95	0.41	0.03

5.6. Concluding Remarks

In this study, we introduced semiparametric and nonparametric models and methods to estimate the FPT distribution of degradation processes. Throughout the study, we considered Lévy process assumptions and related models. Nonparametric estimation procedures of the FPT distribution using the ESA method discussed in Chapter 2. Furthermore, using copula functions, semiparametric and nonparametric methods to estimate the FPT distribution for bivariate degradation data are introduced in Chapter 3. In addition, when the linearity assumption in the degradation data are violated, in Chapter 4, we proposed TRP-type models to transform the degradation data to apply Lévy process related models. For all proposed models and methods, the performance was evaluated by Monte Carlo simulation studies. Moreover, all the proposed models and methods were applied in engineering degradation data sets such as LED devices and lithium-ion batteries degradation data sets. Finally, some possible future research directions are discussed in Chapter 5 with preliminary simulation studies and theoretical proofs. In the studies in Chapters 2, 3, and 4, we obtained promising results to show that the proposed degradation models and methods perform well and they are flexible to apply in the analysis of different degradation data sets.

Appendix A

Supplementary Materials of Chapter 2

A.1. Theorem 1: Moment estimation for FPT using ESA

THEOREM 1. *If Y is the degradation per unit interval and $\mathscr{K}_Y$ is the CGF of Y, then a residue approximation for the MTTF (i.e., the first moment of T_c) and the second moment of T_c are, respectively,*

$$\mathbb{E}(T_c) \simeq \frac{c}{\mathscr{K}_Y'(0)} + \frac{\mathscr{K}_Y''(0)}{2\{\mathscr{K}_Y'(0)\}^2}$$
$$\mathbb{E}(T_c^2) \simeq \frac{1}{\{\mathscr{K}_Y'(0)\}^2}\left[c\left\{2\frac{\mathscr{K}_Y''(0)}{\mathscr{K}_Y'(0)} + c\right\} + \frac{3}{2}\left\{\frac{\mathscr{K}_Y''(0)}{\mathscr{K}_Y'(0)}\right\}^2 - \frac{2}{3}\frac{\mathscr{K}_Y'''(0)}{\mathscr{K}_Y'(0)}\right].$$

Proof.

The method proposed here can be used to obtain all the moments; however, we focus our discussion on the first and second moments. In addition, the proposed approach relies on a new asymptotic expansion for the moments as $c \to \infty$. The $\mathfrak{m}$-th moment follows from its Laplace transform in c defined as

$$\int_0^\infty \mathbb{E}(T_c^{\mathfrak{m}})e^{sc}dc = \frac{(-1)^{\mathfrak{m}+1}\mathfrak{m}!}{s\{\mathscr{K}_Y(s)\}^{\mathfrak{m}}} \qquad \mathrm{Re}(s) < 0, \tag{A.1}$$

where the right-hand side of Eq. (A.1) was given by Eliazar and Klafter (2004, Eq. (15)). For the MTTF $m = 1$ and the inversion for $\varepsilon < 0$ is

$$\mathbb{E}(T_c^{\mathfrak{m}}) = \frac{1}{2\pi i}\int_{\varepsilon-i\infty}^{\varepsilon+i\infty} \frac{(-1)^{\mathfrak{m}+1}\mathfrak{m}!}{s\{\mathscr{K}_Y(s)\}^{\mathfrak{m}}} e^{-sc} ds. \tag{A.2}$$

The inversion integral in Eq. (A.2) may be deformed to an integral over $\mathrm{Re}(s) = \varepsilon_1 > 0$ using the Cauchy's residue theorem, i.e.,

$$\mathbb{E}(T_c^{\mathfrak{m}}) = -\mathrm{Res}\left\{\frac{(-1)^{\mathfrak{m}+1}\mathfrak{m}!}{\{s\mathscr{K}_Y(s)\}^{\mathfrak{m}}} e^{-sc}; 0\right\} + \frac{1}{2\pi i}\int_{\varepsilon_1-i\infty}^{\varepsilon_1+i\infty} \frac{(-1)^{\mathfrak{m}+1}\mathfrak{m}!}{\{s\mathscr{K}_Y(s)\}^{\mathfrak{m}}} e^{-sc} ds. \tag{A.3}$$

For $\mathfrak{m} = 1$, the residue may be computed by first expanding e^{-sc} and $\mathscr{K}_Y(s)$ in Taylor series about $s = 0$. This gives

$$\begin{aligned}
\frac{e^{-sc}}{s\mathscr{K}_Y(s)} &= \frac{1 - sc + O(s^2)}{s^2\mathscr{K}_Y'\{1 + s\mathscr{K}_Y''/(\mathscr{K}_Y' 2!) + O(s^2)\}} \\
&= \frac{1}{s^2\mathscr{K}_Y'}\{1 - sc + O(s^2)\}\{1 - s\mathscr{K}_Y''/(\mathscr{K}_Y' 2!) - O(s^2)\} \\
&= \frac{1}{s^2\mathscr{K}_Y'} + \frac{1}{s\mathscr{K}_Y'}\left\{-\frac{\mathscr{K}_Y''}{2\mathscr{K}_Y'} - c\right\} + A
\end{aligned}$$

where A consists of the analytic portion of the expansion and all derivatives of $\mathscr{K}_Y$ are at $s = 0$. Thus,

$$\mathbb{E}(T_c) \simeq -\mathrm{Res}\left\{\frac{e^{-sc}}{s\mathscr{K}_Y(s)}; 0\right\} = \frac{c}{\mathscr{K}_Y'(0)} + \frac{\mathscr{K}_Y''(0)}{2\{\mathscr{K}_Y'(0)\}^2}$$

is a first-order approximation to the mean.

For the variance, we expand

$$\begin{aligned}\frac{e^{-sc}}{s\mathscr{K}_Y(s)^2} &= \frac{1-sc+s^2c^2/2!+O(s^3)}{s^3(\mathscr{K}_Y')^2\{1+s\mathscr{K}_Y''/(\mathscr{K}_Y'2!)+s^2\mathscr{K}_Y'''/(\mathscr{K}_Y'3!)+O(s^3)\}^2} \\ &= \frac{1}{s^3(\mathscr{K}_Y')^2}\left\{1-sc+\frac{s^2c^2}{2!}+O(s^3)\right\}\times \\ &\quad \left\{1-2\left(\frac{s\mathscr{K}_Y''}{2!\mathscr{K}_Y'}+\frac{s^2\mathscr{K}_Y'''}{3!\mathscr{K}_Y'}\right)+3\left(\frac{s\mathscr{K}_Y''}{2!\mathscr{K}_Y'}+\frac{s^2\mathscr{K}_Y'''}{3!\mathscr{K}_Y'}\right)^2+O(s^3)\right\}.\end{aligned}$$

The $O(1/s)$ term is

$$\begin{aligned}&\frac{1}{(\mathscr{K}_Y')^2}\left\{\frac{-2\mathscr{K}_Y'''}{3!\mathscr{K}_Y'}+\frac{3(\mathscr{K}_Y'')^2}{(2!)^2(\mathscr{K}_Y')^2}-c\frac{-2\mathscr{K}_Y''}{2!\mathscr{K}_Y'}+\frac{c^2}{2!}\right\} \\ &= \frac{1}{\{\mathscr{K}_Y'(0)\}^2}\left[c\left\{\frac{\mathscr{K}_Y''(0)}{\mathscr{K}_Y'(0)}+\frac{c}{2}\right\}+\frac{3}{4}\left\{\frac{\mathscr{K}_Y''(0)}{\mathscr{K}_Y'(0)}\right\}^2-\frac{1}{3}\frac{\mathscr{K}_Y'''(0)}{\mathscr{K}_Y'(0)}\right].\end{aligned}$$

Thus, we have

$$\begin{aligned}\mathbb{E}(T_c^2) &\simeq -\operatorname{Res}\left\{\frac{(-1)2!}{s\{\mathscr{K}_Y(s)\}^2}e^{-sc};0\right\} \\ &= \frac{1}{\{\mathscr{K}_Y'(0)\}^2}\left[c\left\{2\frac{\mathscr{K}_Y''(0)}{\mathscr{K}_Y'(0)}+c\right\}+\frac{3}{2}\left\{\frac{\mathscr{K}_Y''(0)}{\mathscr{K}_Y'(0)}\right\}^2-\frac{2}{3}\frac{\mathscr{K}_Y'''(0)}{\mathscr{K}_Y'(0)}\right].\end{aligned}$$

□

Higher-order moment expansions for $m \geq 3$ can be computed in an analogous way with increasing complexity.

A.2. Theorem 2

THEOREM 2. *Subject to condition AC below on $\mathscr{K}_Y$, an upper bound for $|E|$ is $O(e^{-(b-\varepsilon)c})$ as $c \to \infty$ for some small $\varepsilon > 0$ where b is the upper boundary for convergence of $\mathscr{K}_Y$.*

(AC) For some $\varepsilon > 0$ and $\alpha \in (0, \pi/2)$, $\mathscr{K}_Y$ can be analytically continued into the sector $S_{\varepsilon,\alpha} = \{s_{r\phi} = b - \varepsilon + r\varepsilon^{i\phi} \in \mathbb{C} : r > 0, \phi \in [\alpha, \pi/2]\}$. Furthermore, within this sector, suppose

$$\min_{\alpha \le \phi \le \pi/2} \left| \mathscr{K}_Y(b - \varepsilon + r\varepsilon^{i\phi}) \right| \to \infty \qquad r \to \infty.$$

Proof. The proof is the same for all moments so we take $m = 1$. Denote $b^- = b - \varepsilon$ so the error is

$$E = \frac{1}{2\pi i} \int_{b^- - i\infty}^{b^- + i\infty} \frac{1}{s\mathscr{K}_Y(s)} e^{-sc} ds = \mathrm{Re}\left\{ \frac{1}{\pi i} \int_{b^-}^{b^- + i\infty} \frac{1}{s\mathscr{K}_Y(s)} e^{-sc} ds \right\}. \tag{A.4}$$

Using the argument in Butler (2019, Thm. 6), the latter integral in (A.4) can be deformed to the ray $\{b^- + r\varepsilon^{i\beta} : r \ge 0\}$ where $\beta \in (\alpha, \pi/2)$. Thus,

$$\begin{aligned} E &= \mathrm{Re}\left\{ \frac{1}{\pi i} \int_{b^-}^{b^- + e^{i\beta}\infty} \frac{1}{s\mathscr{K}_Y(s)} e^{-sc} ds \right\} \\ &= \mathrm{Re}\left\{ \frac{1}{\pi i} \int_0^\infty \frac{e^{-(b^- + r\varepsilon^{i\beta})c} e^{i\beta}}{(b^- + r\varepsilon^{i\beta})\mathscr{K}_Y(b^- + r\varepsilon^{i\beta})} dr \right\}. \end{aligned}$$

By the triangle inequality,

$$\begin{aligned} |E| &\le \frac{1}{\pi} \int_0^\infty \left| \frac{e^{-(b^- + r\varepsilon^{i\beta})c} e^{i\beta}}{(b^- + r\varepsilon^{i\beta})\mathscr{K}_Y(b^- + r\varepsilon^{i\beta})} \right| dr \le \frac{1}{\pi} \int_0^\infty \frac{|e^{-(b^- + r\varepsilon^{i\beta})c}|}{r|\mathscr{K}_Y(b^- + r\varepsilon^{i\beta})|} dr \\ &\le \frac{e^{-b^- c}}{\pi} \int_0^\infty \frac{e^{-rc\cos\beta}}{r\left|\mathscr{K}_Y(b^- + r\varepsilon^{i\beta})\right|} dr \\ &\le \frac{e^{-b^- c}}{\pi} \left\{ \int_0^\infty \frac{e^{-rc\cos\beta}}{r^2} dr \right\}^{1/2} \left\{ \int_0^\infty \frac{e^{-rc\cos\beta}}{\left|\mathscr{K}_Y(b^- + r\varepsilon^{i\beta})\right|^2} dr \right\}^{1/2}, \end{aligned} \tag{A.5}$$

where the last inequality is Hölder's inequality. Both integrals in (A.5) converge so that an upper bound for $|E|$ is $O(e^{-b^- c})$. □

A.3. Additional Simulations: Advantage of the ESA under Model Uncertainty

Additional simulation results related to this section are in Tables A.1 and A.2.

Table A.1: Mean squared errors (MSEs) of the estimates of 5-th, 10-th and 90-th percentiles based on assuming different degradation models with the LR saddlepoint approximation and the ESA when the data are generated from the Gamma(1, 2) and Gamma(0.5, 4) processes.

5-th percentile			True Process: Gamma(1, 2)				True Process: Gamma(0.5, 4)			
			Assumed Process				Assumed Process			
n	t_m	c	Gamma	IG	Wiener	ESA	Gamma	IG	Wiener	ESA
10	30	60	2.3	87.7	2.5	2.5	4.1	278.1	4.7	4.6
10	30	100	7.0	211.4	7.4	7.6	13.2	893.6	13.3	14.3
10	50	60	1.5	100.5	1.7	1.6	3.0	419.3	2.5	2.4
10	50	100	4.1	243.8	4.2	4.2	6.8	989.4	7.0	7.1
20	30	60	1.1	100.2	1.2	1.2	2.1	436.9	2.1	2.0
20	30	100	3.1	247.5	3.3	3.3	6.5	1138.6	7.1	7.0
20	50	60	0.7	109.0	0.8	0.8	1.2	527.3	1.5	1.4
20	50	100	2.0	260.1	2.1	2.1	3.5	1290.5	3.8	3.7
10-th percentile			True Process: Gamma(1, 2)				True Process: Gamma(0.5, 4)			
			Assumed Process				Assumed Process			
n	t_m	c	Gamma	IG	Wiener	ESA	Gamma	IG	Wiener	ESA
10	30	60	2.5	48.6	2.5	2.5	4.5	210.3	4.7	4.8
10	30	100	7.3	118.9	7.4	7.8	14.3	656.9	13.7	15.0
10	50	60	1.6	56.6	1.7	1.7	3.4	345.7	2.5	2.5
10	50	100	4.3	137.1	4.4	4.5	7.3	791.3	7.4	7.3
20	30	60	1.2	55.7	1.2	1.2	2.3	360.9	2.1	2.0
20	30	100	3.3	140.9	3.4	3.7	6.9	946.4	7.2	7.5
20	50	60	0.7	61.4	0.7	0.8	1.3	455.0	1.5	1.4
20	50	100	2.1	145.5	2.1	2.3	3.8	1139.7	3.9	3.9
90-th percentile			True Process: Gamma(1, 2)				True Process: Gamma(0.5, 4)			
			Assumed Process				Assumed Process			
n	t_m	c	Gamma	IG	Wiener	ESA	Gamma	IG	Wiener	ESA
10	30	60	3.8	186.0	4.0	3.9	9.0	378.8	9.6	9.3
10	30	100	10.6	387.7	10.5	10.7	23.1	1229.7	22.7	22.4
10	50	60	2.6	213.3	2.8	2.7	6.4	399.2	5.6	5.1
10	50	100	6.0	424.4	6.2	6.1	12.0	1133.0	12.6	12.0
20	30	60	2.0	219.1	2.1	2.0	4.7	370.3	4.5	4.0
20	30	100	4.7	421.6	4.8	4.7	11.3	1144.6	11.8	11.6
20	50	60	1.1	236.9	1.2	1.2	2.7	364.9	3.3	2.7
20	50	100	3.0	459.4	3.1	3.1	6.4	985.9	7.2	6.7

Table A.2: Mean squared errors (MSEs) of the estimates of 5-th, 10-th and 90-th percentiles based on assuming different degradation models with the LR saddlepoint approximation and the ESA when the data are generated from the IG(2, 5) and IG(2, 10) processes.

			True Process: IG(2, 5)				True Process: IG(2, 10)			
5-th percentile			Assumed Process				Assumed Process			
n	t_m	c	IG	Gamma	Wiener	ESA	IG	Gamma	Wiener	ESA
10	30	60	1.3	1.7	1.4	1.4	0.6	0.7	0.7	0.7
10	30	100	3.7	4.5	3.9	3.9	1.8	1.9	1.9	1.9
10	50	60	0.8	1.1	0.8	0.8	0.4	0.5	0.4	0.4
10	50	100	2.1	2.6	2.2	2.2	1.1	1.1	1.1	1.1
20	30	60	0.6	1.0	0.7	0.6	0.3	0.4	0.3	0.3
20	30	100	1.8	2.4	1.9	1.9	0.9	1.0	0.9	0.9
20	50	60	0.4	0.7	0.4	0.4	0.2	0.3	0.2	0.2
20	50	100	1.0	1.7	1.1	1.1	0.5	0.6	0.5	0.5
			True Process: IG(2, 5)				True Process: IG(2, 10)			
10-th percentile			Assumed Process				Assumed Process			
n	t_m	c	IG	Gamma	Wiener	ESA	IG	Gamma	Wiener	ESA
10	30	60	1.3	1.5	1.3	1.3	0.6	0.7	0.6	0.6
10	30	100	3.7	4.2	3.8	3.8	1.8	1.9	1.8	1.8
10	50	60	0.7	0.9	0.8	0.8	0.4	0.4	0.4	0.4
10	50	100	2.1	2.3	2.1	2.1	1.1	1.1	1.1	1.1
20	30	60	0.6	0.8	0.6	0.6	0.3	0.3	0.3	0.3
20	30	100	1.8	2.2	1.8	1.8	0.9	0.9	0.9	0.9
20	50	60	0.4	0.6	0.4	0.4	0.2	0.2	0.2	0.2
20	50	100	1.0	1.4	1.0	1.0	0.5	0.6	0.5	0.5
			True Process: IG(2, 5)				True Process: IG(2, 10)			
900-th percentile			Assumed Process				Assumed Process			
n	t_m	c	IG	Gamma	Wiener	ESA	IG	Gamma	Wiener	ESA
10	30	60	1.3	1.5	1.3	1.3	0.6	0.7	0.7	0.6
10	30	100	3.6	3.9	3.7	3.7	1.8	1.8	1.8	1.8
10	50	60	0.7	1.0	0.8	0.8	0.4	0.4	0.4	0.4
10	50	100	2.1	2.5	2.1	2.1	1.1	1.1	1.1	1.1
20	30	60	0.6	0.8	0.7	0.6	0.3	0.3	0.3	0.3
20	30	100	1.8	2.2	1.8	1.8	0.9	0.9	0.9	0.9
20	50	60	0.4	0.6	0.4	0.4	0.2	0.2	0.2	0.2
20	50	100	1.0	1.3	1.1	1.0	0.5	0.6	0.5	0.5

A.4. Additional Simulations: Monte Carlo Simulation Study for Unequal Time Interval Situations

Additional simulation results related to this section are in Tables A.3 and A.4.

Table A.3: Mean squared errors (MSEs) of the estimates of 5-th, 10-th and 90-th percentiles based on the LR parametric saddlepoint approximation, the modified CGF and different data imputation methods when the data are generated from the Gamma(1, 2) and Gamma(0.5, 4) processes.

5-th percentile			Simulated from Gamma(1, 2)					Simulated from Gamma(0.5, 4)				
n	t_m	c	LR	MCGF	LImp	RImp	CRImp	LR	MCGF	LImp	RImp	CRImp
10	31	60	2.29	11.21	15.53	3.93	2.39	3.90	21.38	27.79	5.73	4.18
10	31	100	6.14	20.59	24.70	12.63	7.26	10.39	39.42	45.48	19.66	11.84
10	54	60	1.56	9.34	14.48	3.26	1.63	2.64	17.38	25.24	4.69	2.78
10	54	100	3.96	14.98	20.81	11.35	5.33	6.98	29.99	39.86	16.83	8.25
20	31	60	1.22	8.40	13.77	3.07	1.32	2.00	15.51	24.16	4.16	2.13
20	31	100	3.03	13.28	20.09	10.12	4.24	5.43	26.06	37.98	15.19	6.55
20	54	60	0.84	7.44	13.23	2.69	0.93	1.42	13.43	23.03	3.65	1.44
20	54	100	2.05	10.76	18.52	9.32	3.27	3.58	20.82	34.52	13.88	4.69
10-th percentile			Simulated from Gamma(1, 2)					Simulated from Gamma(0.5, 4)				
n	t_m	c	LR	MCGF	LImp	RImp	CRImp	LR	MCGF	LImp	RImp	CRImp
10	31	60	2.22	7.98	9.98	3.85	2.31	3.82	13.89	16.09	7.15	4.22
10	31	100	6.37	18.86	20.46	9.56	6.55	11.03	34.07	35.46	17.01	11.57
10	54	60	1.49	6.35	9.04	3.16	1.58	2.55	10.53	14.02	6.08	2.83
10	54	100	4.00	13.49	16.75	7.90	4.33	7.40	25.42	30.22	13.84	7.80
20	31	60	1.15	5.54	8.45	2.92	1.27	1.93	8.99	13.04	5.55	2.23
20	31	100	3.11	11.90	16.03	6.69	3.34	5.77	21.83	28.42	12.06	6.05
20	54	60	0.78	4.73	7.99	2.55	0.88	1.31	7.35	12.08	5.02	1.59
20	54	100	2.05	9.60	14.70	5.83	2.29	3.76	17.05	25.26	10.61	4.09
90-th percentile			Simulated from Gamma(1, 2)					Simulated from Gamma(0.5, 4)				
n	t_m	c	LR	MCGF	LImp	RImp	CRImp	LR	MCGF	LImp	RImp	CRImp
10	31	60	3.50	9.17	13.62	13.01	4.06	7.56	23.40	34.99	28.07	8.14
10	31	100	9.23	18.62	24.10	24.18	10.17	18.52	44.97	60.40	48.40	19.54
10	54	60	2.34	7.74	12.66	11.56	2.74	4.98	20.90	33.43	24.03	5.41
10	54	100	5.74	15.23	22.06	19.15	6.47	12.53	38.06	56.34	39.35	13.14
20	31	60	1.78	7.24	12.46	10.44	2.13	3.82	19.60	32.80	21.29	4.03
20	31	100	4.44	13.11	20.51	17.74	5.09	9.58	34.25	53.02	35.99	10.05
20	54	60	1.19	6.55	11.94	9.55	1.48	2.67	18.39	32.00	19.52	2.83
20	54	100	3.00	11.32	19.33	15.97	3.58	6.52	31.40	51.66	30.40	6.71

Table A.4: Mean squared errors (MSEs) of the estimates of 5-th, 10-th and 90-th percentiles based on the LR parametric saddlepoint approximation, the modified CGF and different data imputation methods when the data are generated from the IG(2, 10) and IG(2, 5) processes.

5-th percentile			Simulated from IG(2, 10)					Simulated from IG(2, 5)				
n	t_m	c	LR	MCGF	LImp	RImp	CRImp	LR	MCGF	LImp	RImp	CRImp
10	31	60	0.78	1.55	345.35	2.50	1.87	1.16	4.70	426.68	2.64	1.67
10	31	100	1.74	6.21	938.47	2.45	1.90	3.20	11.44	1072.52	4.98	3.47
10	54	60	0.61	1.23	345.07	2.33	1.69	0.83	4.01	425.45	2.27	1.32
10	54	100	1.26	5.25	936.99	1.86	1.34	2.23	9.54	1070.25	3.80	2.41
20	31	60	0.54	1.03	343.49	2.26	1.61	0.65	3.55	423.44	2.10	1.13
20	31	100	1.03	4.81	935.07	1.68	1.14	1.78	8.46	1065.61	3.45	1.99
20	54	60	0.45	0.87	343.63	2.18	1.51	0.46	3.13	422.63	1.95	0.95
20	54	100	0.76	4.31	933.66	1.40	0.86	1.24	7.42	1063.00	2.92	1.44
10-th percentile			Simulated from IG(2, 10)					Simulated from IG(2, 5)				
n	t_m	c	LR	MCGF	LImp	RImp	CRImp	LR	MCGF	LImp	RImp	CRImp
10	31	60	0.86	2.80	345.35	0.74	0.64	1.21	4.19	386.53	1.71	1.20
10	31	100	1.69	2.99	820.25	3.77	2.90	2.94	7.64	946.12	5.02	3.51
10	54	60	0.68	2.53	345.07	0.56	0.47	0.91	3.61	385.32	1.37	0.87
10	54	100	1.19	2.15	818.76	3.14	2.30	1.96	5.92	943.78	3.90	2.47
20	31	60	0.60	2.28	343.49	0.48	0.37	0.73	3.20	383.37	1.19	0.70
20	31	100	1.00	1.76	816.92	3.04	2.15	1.54	5.04	939.34	3.57	2.10
20	54	60	0.51	2.12	343.63	0.37	0.26	0.53	2.85	382.58	1.01	0.52
20	54	100	0.74	1.33	815.55	2.76	1.86	1.04	4.13	936.78	3.04	1.58
90-th percentile			Simulated from IG(2, 10)					Simulated from IG(2, 5)				
n	t_m	c	LR	MCGF	LImp	RImp	CRImp	LR	MCGF	LImp	RImp	CRImp
10	31	60	0.70	2.33	134.86	1.34	0.83	1.17	3.12	115.25	4.28	1.93
10	31	100	1.68	4.63	427.38	2.54	1.86	3.13	5.90	393.90	8.78	4.86
10	54	60	0.53	2.09	134.48	1.13	0.63	0.84	2.66	114.09	3.87	1.54
10	54	100	1.17	3.83	425.83	2.13	1.35	2.19	4.43	391.19	8.08	3.93
20	31	60	0.44	1.98	133.38	1.02	0.52	0.65	2.44	112.77	3.63	1.33
20	31	100	0.95	3.56	424.31	1.85	1.10	1.75	3.85	387.82	7.47	3.37
20	54	60	0.34	1.85	133.37	0.92	0.43	0.47	2.22	112.09	3.37	1.10
20	54	100	0.68	3.21	423.09	1.57	0.82	1.22	3.17	385.59	6.89	2.80

Table A.5: Mean squared errors (MSEs) of the estimates of 5-th, 10-th and 90-th percentiles based on the LR parametric saddlepoint approximation, the modified CGF and different data imputation methods when the data are generated from the Wiener(2, 4) and Wiener(4, 2) processes.

5-th percentile			Simulated from Wiener(2, 4)					Simulated from Wiener(4, 2)				
n	t_m	c	LR	MCGF	LImp	RImp	CRImp	LR	MCGF	LImp	RImp	CRImp
10	31	60	1.91	18.49	31.73	6.94	3.69	0.12	0.42	0.81	1.42	1.09
10	31	100	7.12	48.43	72.11	27.75	14.87	0.31	1.04	1.74	2.33	1.59
10	54	60	1.19	16.07	29.24	5.96	3.11	0.07	0.37	0.80	1.32	1.05
10	54	100	4.72	40.13	65.89	21.63	11.20	0.21	0.84	1.61	2.22	1.46
20	31	60	0.90	14.78	28.12	5.77	2.80	0.06	0.35	0.81	1.27	1.05
20	31	100	3.47	35.30	61.63	19.86	7.94	0.16	0.75	1.51	2.19	1.41
20	54	60	0.59	13.55	27.09	5.52	2.44	0.04	0.32	0.85	1.19	1.05
20	54	100	2.30	31.81	59.16	16.58	5.90	0.11	0.68	1.40	2.07	1.33
10-th percentile			Simulated from Wiener(2, 4)					Simulated from Wiener(4, 2)				
n	t_m	c	LR	MCGF	LImp	RImp	CRImp	LR	MCGF	LImp	RImp	CRImp
10	31	60	2.56	18.88	28.70	5.67	3.15	0.12	0.33	0.46	1.09	0.70
10	31	100	9.21	47.92	62.63	25.40	15.48	0.32	0.83	1.17	1.75	1.16
10	54	60	1.60	15.91	25.89	4.56	2.37	0.08	0.25	0.36	1.02	0.59
10	54	100	6.11	38.34	55.69	19.44	10.64	0.22	0.65	1.07	1.64	1.02
20	31	60	1.21	14.37	24.63	4.04	1.84	0.06	0.21	0.30	0.96	0.54
20	31	100	4.49	32.85	51.19	17.06	6.99	0.16	0.54	0.99	1.61	0.97
20	54	60	0.79	12.90	23.44	3.72	1.38	0.04	0.18	0.23	0.87	0.46
20	54	100	2.97	28.79	48.33	13.70	5.17	0.11	0.46	0.97	1.49	0.88
90-th percentile			Simulated from Wiener(2, 4)					Simulated from Wiener(4, 2)				
n	t_m	c	LR	MCGF	LImp	RImp	CRImp	LR	MCGF	LImp	RImp	CRImp
10	31	60	35.09	55.58	52.40	159.28	103.63	0.28	1.80	2.65	0.73	0.41
10	31	100	75.87	116.36	104.63	253.55	166.07	0.66	2.84	4.05	1.43	0.82
10	54	60	22.36	38.69	45.92	134.91	76.15	0.19	1.69	2.57	0.58	0.31
10	54	100	49.66	81.96	88.06	205.37	119.65	0.44	2.54	3.88	1.17	0.59
20	31	60	16.76	30.96	42.64	125.57	64.61	0.14	1.65	2.50	0.52	0.28
20	31	100	36.62	65.10	82.23	175.57	94.06	0.34	2.42	3.85	0.99	0.46
20	54	60	10.74	23.07	39.05	113.62	50.79	0.09	1.64	2.44	0.41	0.25
20	54	100	23.88	50.12	72.89	153.94	72.19	0.22	2.29	3.72	0.86	0.35

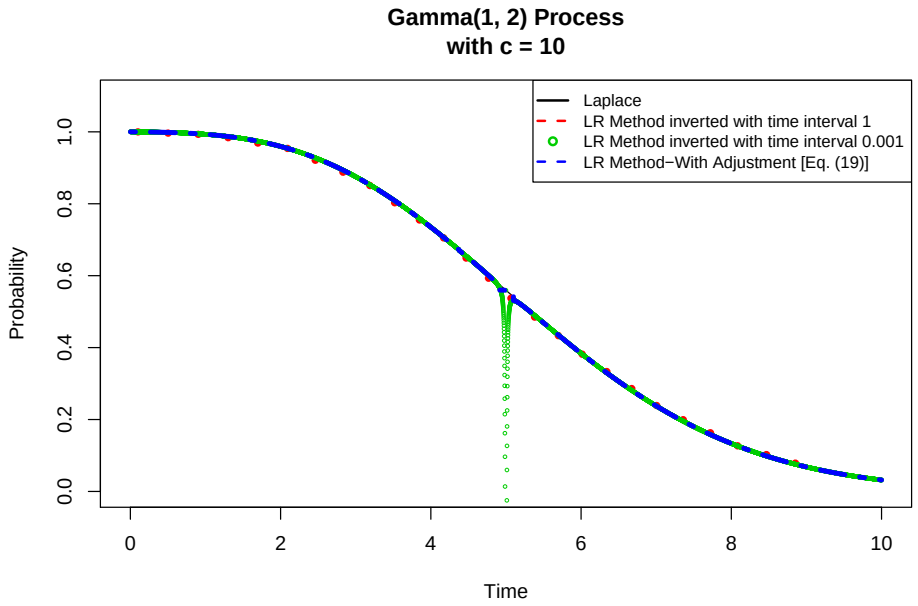

Figure A.1: FPT distribution from the Lugannani and Rice (1980) obtained with different time intervals

A.5. Laser Data: Equal Time Intervals

Additional results related to this section are in Table A.6.

A.6. Laser Data: Unequal Time Intervals

Additional results related to this section are in Table A.7.

Table A.6: Estimates and the 2.5-th and 97.5-th bootstrap percentiles of the 5-th, 10-th and 90-th percentiles of the FPT distribution for the GaAs Laser degradation data (original data with equal time intervals) with different threshold levels $c = 1(1)10$.

5-th Percentile	Bootstrap Percentile		Empirical		Parametric (Gamma)			
c	2.5%	97.5%	LR	BQ	LR	BQ	MLE	BS
1	272.6	312.8	282.5	287.5	302.5	285.0	302.5	317.5
2	673.2	713.7	682.5	652.5	705.0	655.0	705.0	720.0
3	1081.5	1139.3	1100.0	1045.0	1127.5	1052.5	1127.5	1142.5
4	1498.2	1572.1	1530.0	1452.5	1560.0	1462.5	1560.0	1577.5
5	1938.2	2011.1	1967.5	1867.5	2000.0	1882.5	2000.0	2017.5
6	2379.4	2459.6	2410.0	2292.5	2445.0	2310.0	2445.0	2462.5
7	2819.4	2907.7	2857.5	2720.0	2892.5	2740.0	2892.5	2910.0
8	3261.5	3362.0	3307.5	3152.5	3345.0	3175.0	3345.0	3362.5
9	3711.5	3818.5	3757.5	3590.0	3797.5	3615.0	3797.5	3815.0
10	4161.3	4269.4	4212.5	4027.5	4255.0	4057.5	4255.0	4272.5
10-th Percentile	Bootstrap Percentile		Empirical		Parametric (Gamma)			
c	2.5%	97.5%	LR	BQ	LR	BQ	MLE	BS
1	330.2	358.8	327.5	327.5	345.0	322.5	345.0	347.5
2	734.0	773.8	747.5	720.0	765.0	717.5	765.0	770.0
3	1167.4	1212.9	1185.0	1132.5	1202.5	1135	1202.5	1207.5
4	1609.9	1663.1	1627.5	1557.5	1647.5	1562.5	1647.5	1655.0
5	2050.7	2118.2	2077.5	1990.0	2100.0	1997.5	2100.0	2105.0
6	2496.9	2568.5	2530.0	2427.5	2555.0	2440.0	2555.0	2560.0
7	2954.6	3027.4	2987.5	2870.0	3012.5	2882.5	3012.5	3017.5
8	3410.3	3491.3	3445.0	3315.0	3472.5	3330.0	3472.5	3480.0
9	3865.7	3955.5	3905.0	3762.5	3935.0	3780.0	3935.0	3940.0
10	4329.2	4417.3	4367.5	4212.5	4397.5	4232.5	4397.5	4405.0
90-th Percentile	Bootstrap Percentile		Empirical		Parametric (Gamma)			
c	2.5%	97.5%	LR	BQ	LR	BQ	MLE	BS
1	659.9	688.3	682.5	682.5	677.5	677.5	677.5	687.5
2	1225.0	1265.6	1247.5	1247.5	1237.5	1235.0	1237.5	1247.5
3	1769.8	1816.7	1795.0	1795.0	1782.5	1780.0	1782.5	1790.0
4	2304.1	2358.1	2332.5	2332.5	2317.5	2315.0	2317.5	2325.0
5	2831.0	2895.5	2865.0	2865.0	2847.5	2845.0	2847.5	2855.0
6	3357.3	3430.9	3395.0	3392.5	3372.5	3370.0	3372.5	3382.5
7	3880.7	3957.4	3920.0	3917.5	3897.5	3895.0	3897.5	3905.0
8	4397.7	4486.1	4442.5	4440.0	4417.5	4415.0	4417.5	4427.5
9	4918.0	5007.0	4965.0	4960.0	4937.5	4935.0	4937.5	4947.5
10	5435.0	5530.4	5482.5	5480.0	5455.0	5452.5	5455.0	5465.0

Table A.7: Estimates of the 5-th, 10-th and 90-th percentiles of the FPT distribution for the GaAs Laser degradation data (altered data with unequal time intervals) with different threshold levels $c = 1(1)10$.

5-th Percentile	Parametric	Empirical			
c	MLE	MCGF	LImp	RImp	CRImp
1	287.5	310.0	317.5	225.0	237.5
2	677.5	722.5	732.5	607.5	600.0
3	1090.0	1155.0	1165.0	1012.5	982.5
4	1517.5	1595.0	1605.0	1405.0	1452.5
5	1950.0	2042.5	2052.5	1827.5	1797.5
6	2390.0	2495.0	2502.5	2242.5	2277.5
7	2832.5	2950.0	2957.5	2710.0	2710.0
8	3380.0	3407.5	3415.0	3095.0	3130.0
9	3730.0	3867.5	3872.5	3565.0	3610.0
10	4180.5	4330.0	4332.5	3937.5	4017.5
10-th Percentile	Parametric	Empirical			
c	MLE	MCGF	LImp	RImp	CRImp
1	332.5	350.0	355.0	282.5	297.5
2	745.0	782.5	787.5	690.0	685.0
3	1175.0	1227.5	1232.5	1110.0	1097.5
4	1615.0	1680.0	1685.0	1522.5	1562.5
5	2062.5	2137.5	2140.0	1955.0	1945.0
6	2512.5	2600.0	2600.0	2402.5	2425.0
7	2965.0	3062.5	3062.5	2870.0	2867.5
8	3422.5	3530.0	3527.5	3272.5	3307.5
9	3880.0	3997.5	3992.5	3745.0	3790.0
10	4340.0	4465.0	4460.0	4145.0	4215.0
90-th Percentile	Parametric	Empirical			
c	MLE	MCGF	LImp	RImp	CRImp
1	705.0	660.0	647.5	797.5	752.5
2	1275.0	1220.0	1200.0	1355.0	1337.5
3	1825.0	1765.0	1737.5	1925.0	1910.0
4	2365.0	2300.0	2267.5	2505.0	2425.0
5	2900.0	2830.0	2792.5	3072.5	3035.0
6	3432.5	3357.5	3312.5	3552.5	3527.5
7	3960.0	3882.5	3832.5	4067.5	4080.0
8	4485.0	4405.0	4350.0	4680.0	4610.0
9	5007.5	4927.5	4865.0	5192.5	5105.0
10	5527.5	5445.0	5380.0	5785.0	5670.0

A.7. Singularity at the mean

From the LR approximation of CDF presented in Eq. (2.7), there is a singularity point at $t = t_s$ and an alternate formula is used to compute the approximated value. However, as it has been well established, see Butler (2007, Section 1.2.1), that evaluating the LR approximation near the singularity point (i.e., the mean of the distribution), can sometimes be problematic numerically. In our application for approximating the FPT distribution based on degradation data, we also experienced such numerical difficulties.

To further illustrate this issue, Figure A.1 shows the LR saddlepoint approximation for the Gamma(1, 2) degradation process with a threshold value $c = 10$ where the approximate FPT distributions are obtained using the LR approximation in Eq. (2.7) with different time points $\mathbf{t} = \{1, 2, 3, \ldots\}$ and $\mathbf{t} = \{0.01, 0.02, 0.03, \ldots\}$. The plot over $\mathbf{t} = \{0.01, 0.02, 0.03, \ldots, \}$ shows the numerical instability near $t_s \approx 5$.

If one observes such numerical instability at or near t_s when plotting the approximated FPT distribution, then we recommend using the following saddlepoint approximation formula

$$\widehat{Pr}(T_c > t) = \begin{cases} \Phi(\hat{w}) + \phi(\hat{w})(\frac{1}{\hat{w}} - \frac{1}{\hat{u}}) & \text{if } t \notin (t_s - \vartheta\Delta t, t_s + \vartheta\Delta t), \\ \frac{1}{2} + \frac{\mathscr{K}'''(0)}{6\sqrt{2\pi}\mathscr{K}''(0)^{3/2}} & \text{if } t \in (t_s - \vartheta\Delta t, t_s + \vartheta\Delta t), \end{cases} \tag{A.6}$$

where ϑ is a multiplication factor and Δt is the time interval. A suitable value of the multiplication factor with a fixed value of Δt can be chosen by trial and error. For example, in Figure A.1, we used $\vartheta = 100$ and $\Delta t = 0.001$, which demonstrates that the proposed formula can correct the issue.

Bibliography

Abate, J., Choudhury, G. L., and Whitt, W. (2000). An introduction to numerical transform inversion and its application to probability models. In *Computational Probability*, pages 257–323. Springer, Boston,MA.

Abate, J. and Whitt, W. (1992). Numerical inversion of probability generating functions. *Operations Research Letters*, 12:245–251.

Abate, J. and Whitt, W. (1995). Numerical inversion of Laplace transforms of probability distributions. *ORSA Journal on Computing*, 7:36–43.

Bae, S. J. and Kvam, P. H. (2004). A nonlinear random-coefficients model for degradation testing. *Technometrics*, 46:460–469.

Balakrishnan, N. and Kundu, D. (2019). Birnbaum-Saunders distribution: A review of models, analysis, and applications. *Applied Stochastics Models in Business and Industry*, 35:4–49.

Balakrishnan, N. and Lai, C. D. (2009). *Continuous Bivariate Distributions*. Springer Science & Business Media, New York, NY.

Balakrishnan, N. and Qin, C. (2019). Nonparametric evaluation of the first passage time of degradation processes. *Applied Stochastic Models in Business and Industry*, 35:571–590.

Birnbaum, Z. W. and Saunders, S. C. (1969). A new family of life distributions. *Journal of Applied Probability*, 6:319–327.

Bleistein, N. (1966). Uniform asymptotic expansions of integrals with stationary point near algebraic singularity. *Communications on Pure and Applied Mathematics*, 19:353–370.

Bogdanoff, J. L. and Kozin, F. (1985). *Probabilistic Models of Cumulative Damage*. John Wiley & Sons, New York, NY.

Bonferroni, C. (1936). Teoria statistica delle classi e calcolo delle probabilità. *Pubblicazioni del R Istituto Superiore di Scienze Economiche e Commericiali di Firenze*, 8:3–62.

Box, G. E. and Pierce, D. A. (1970). Distribution of residual autocorrelations in autoregressive-integrated moving average time series models. *Journal of the American Statistical Association*, 65:1509–1526.

Butler, R. W. (2007). *Saddlepoint Approximations with Applications*. Cambridge University Press, Cambridge, UK.

Chaluvadi, V. (2008). Accelerated life testing of electronic revenue meters. Master's thesis, Clemson University, Clemson, SC.

Chen, D.-G., Lio, Y. L., Ng, H. K. T., and Tsai, T.-R., editors (2017). *Statistical Modeling for Degradation Data*. Springer, Singapore.

Chhikara, R. S. and Folks, J. L. (1989). *The Inverse Gaussian Distribution: Theory, Methodology, and Applications*. Marcel Dekker, Inc., New York, NY.

Clayton, D. G. (1978). A model for association in bivariate life tables and its application in epidemiological studies of familial tendency in chronic disease incidence. *Biometrika*, 65:141–151.

Cook, R. J. and Lawless, J. (2007). *The Statistical Analysis of Recurrent Events*. Springer Science & Business Media.

Copson, E. T. (1965). *Asymptotic Expansions*. Cambridge University Press, Cambridge, UK.

Cox, D. R. and Miller, H. D. (1965). *The Theory of Stochastic Processes*. Methuen and Company, London, UK.

Daniels, H. E. (1954). Saddlepoint approximations in statistics. *The Annals of Mathematical Statistics*, 25:631–650.

Daniels, H. E. (1987). Tail probability approximations. *International Statistical Review/Revue Internationale de Statistique*, 55:37–48.

Efron, B. (1979). Bootstrap methods: Another look at the Jackknife. *The Annals of Statistics*, 7:1–26.

Eliazar, I. and Klafter, J. (2004). On the first passage of one-sided Lévy motions. *Physica A: Statistical Mechanics and its Applications*, 336:219–244.

Fang, G., Pan, R., and Hong, Y. (2018). A copula-based multivariate degradation analysis for reliability prediction. In *2018 Annual Reliability and Maintainability Symposium, RAMS 2018*, volume 2018-January. Institute of Electrical and Electronics Engineers Inc.

Feng, L., Wang, H., Si, X., and Zou, H. (2013). A state-space-based prognostic model for hidden and age-dependent nonlinear degradation process. *IEEE Transactions on Automation Science and Engineering*, 10:1072–1086.

Frank, M. J. (1979). On the simultaneous associativity of $F(x,y)$ and $x+y-F(x,y)$. *Aequationes Mathematicae*, 19:194–226.

Gebraeel, N. Z., Lawley, M. A., Li, R., and Ryan, J. K. (2005). Residual-life distributions from component degradation signals: A Bayesian approach. *IIE Transactions*, 37:543–557.

Gorjian, N., Ma, L., Mittinty, M., Yarlagadda, P., and Sun, Y. (2010). A review on degradation models in reliability analysis. In *Engineering Asset Lifecycle Management*, pages 369–384. Springer.

Gumbel, E. J. (1960). Bivariate exponential distributions. *Journal of the American Statistical Association*, 55:698–707.

Hao, H. and Su, C. (2014). Bivariate nonlinear diffusion degradation process modeling via copula and MCMC. *Mathematical Problems in Engineering*, 2014:1–11.

Hao, H., Su, C., and Li, C. (2015). LED lighting system reliability modeling and inference via random effects gamma process and copula function. *International Journal of Photoenergy*, 2015:1–8.

Helstrom, C. W. and Ritcey, J. A. (1984). Evaluating radar detection probabilities by steepest descent integration. *IEEE Transactions on Aerospace and Electronic Systems*, AES–20:624–634.

Hunt, G. (1996). *USABC electric vehicle battery test procedures manual*. United States Department of Energy, Washington, DC, USA, second edition.

Joe, H. (2015). *Dependence Modeling with Copulas*. CRC Press, Boca Raton, FL.

Joe, H. and Xu, J. J. (1996). The estimation method of inference functions for margins for multivariate models. Technical report, University of British Columbia, Department of Statistics.

Kibble, W. (1941). A two-variate gamma type distribution. *Sankhyā: The Indian Journal of Statistics*, 5:137–150.

Kolassa, J. E. et al. (2003). Multivariate saddlepoint tail probability approximations. *The Annals of Statistics*, 31:274–286.

Krishnaiah, P. and Rao, M. (1961). Remarks on a multivariate gamma distribution. *The American Mathematical Monthly*, 68:342–346.

Kundu, D., Balakrishnan, N., and Jamalizadeh, A. (2010). Bivariate Birnbaum–Saunders distribution and associated inference. *Journal of Multivariate Analysis*, 101:113–125.

Leiva, V., Ferreira, M., Gomes, M. I., and Lillo, C. (2016a). Extreme value Birnbaum–Saunders regression models applied to environmental data. *Stochastic Environmental Research and Risk Assessment*, 30:1045–1058.

Leiva, V., Marchant, C., Ruggeri, F., and Saulo, H. (2015). A criterion for environmental assessment using Birnbaum–Saunders attribute control charts. *Environmetrics*, 26:463–476.

Leiva, V., Santos-Neto, M., Cysneiros, F. J. A., and Barros, M. (2016b). A methodology for stochastic inventory models based on a zero-adjusted Birnbaum-Saunders distribution. *Applied Stochastic Models in Business and Industry*, 32:74–89.

Lindqvist, B. H., Elvebakk, G., and Heggland, K. (2003). The trend-renewal process for statistical analysis of repairable systems. *Technometrics*, 45:31–44.

Lio, Y. L. and Park, C. (2008). A bootstrap control chart for Birnbaum–Saunders percentiles. *Quality and Reliability Engineering International*, 24:585–600.

Liu, D., Luo, Y., Liu, J., Peng, Y., Guo, L., and Pecht, M. (2014). Lithium-ion battery remaining useful life estimation based on fusion nonlinear degradation AR model and RPF algorithm. *Neural Computing and Applications*, 25:557–572.

Ljung, G. M. and Box, G. E. (1978). On a measure of lack of fit in time series models. *Biometrika*, 65:297–303.

Lu, C. J. and Meeker, W. Q. (1993). Using degradation measures to estimate a time-to-failure distribution. *Technometrics*, 35:161–174.

Lugannani, R. and Rice, S. (1980). Saddle point approximation for the distribution of the sum of independent random variables. *Advances in Applied Probability*, 12:475–490.

Meeker, W. Q. and Escobar, L. A. (1998). *Statistical Methods for Reliability Data*. John Wiley & Sons, New York, NY.

Meeker, W. Q., Escobar, L. A., and Lu, C. J. (1998). Accelerated degradation tests: modeling and analysis. *Technometrics*, 40:89–99.

Miao, Q., Xie, L., Cui, H., Liang, W., and Pecht, M. (2013). Remaining useful life prediction of lithium-ion battery with unscented particle filter technique. *Microelectronics Reliability*, 53:805–810.

Mosallam, A., Medjaher, K., and Zerhouni, N. (2016). Data-driven prognostic method based on bayesian approaches for direct remaining useful life prediction. *Journal of Intelligent Manufacturing*, 27:1037–1048.

Nelsen, R. B. (1999). *An Introduction to Copulas*. Springer-Verlag New York, Inc., New York, NY.

Nikulin, M., Limnios, N., Balakrishnan, N., Kahle, W., and Huber-Carol, C. (2010). Advances in Degradation Modeling: Applications to Reliability, Survival Analysis, and Finance. *Birhäuser, Boston*.

Owen, W. J. and Ng, H. K. T. (2015). Revisit of relationships and models for the Birnbaum-Saunders and inverse-Gaussian distributions. *Journal of Statistical Distributions and Applications*, 2:11.

Pan, Z. and Balakrishnan, N. (2011a). Reliability modeling of degradation of products with multiple performance characteristics based on gamma processes. *Reliability Engineering & System Safety*, 96:949–957.

Pan, Z. and Balakrishnan, N. (2011b). Reliability modeling of degradation of products with multiple performance characteristics based on gamma processes. *Reliability Engineering & System Safety*, 96:949–957.

Pan, Z., Balakrishnan, N., and Sun, Q. (2011). Bivariate constant-stress accelerated degradation model and inference. *Communications in Statistics—Simulation and Computation*, 40:247–257.

Pan, Z., Balakrishnan, N., Sun, Q., and Zhou, J. (2013). Bivariate degradation analysis of products based on Wiener processes and copulas. *Journal of Statistical Computation and Simulation*, 83:1316–1329.

Pan, Z., Sun, Q., and Feng, J. (2016). Reliability modeling of systems with two dependent degrading components based on gamma processes. *Communications in Statistics-Theory and Methods*, 45:1923–1938.

Park, C. and Padgett, W. (2005). Accelerated degradation models for failure based on geometric brownian motion and gamma processes. *Lifetime Data Analysis*, 11:511–527.

Peng, C.-Y. (2015). Inverse Gaussian processes with random effects and explanatory variables for degradation data. *Technometrics*, 57:100–111.

Peng, W., Li, Y.-F., Yang, Y.-J., Zhu, S.-P., and Huang, H.-Z. (2016). Bivariate analysis of incomplete degradation observations based on inverse Gaussian processes and copulas. *IEEE Transactions on Reliability*, 65:624–639.

Pham, H. (2006). *Springer Handbook of Engineering Statistics*. Springer Science & Business Media, London, UK.

Qin, C. (2017). *The First Passage Time of Degradation Processes*. PhD thesis, McMaster University, Hamilton, Ontario, Canada.

Saha, B. and Goebel, K. (2007). NASA Ames Prognostics Data Repository (http://ti.arc.nasa.gov/project/prognostic-data-repository). Technical report, NASA Ames Research Center.

Sari, J., Newby, M., Brombacher, A., and Tang, L. C. (2009). Bivariate constant stress degradation model: LED lighting system reliability estimation with two-stage modelling. *Quality and Reliability Engineering International*, 25:1067–1084.

Sari, J. K. (2007). *Multivariate Degradation Modeling and Its Application to Reliability Testing*. PhD thesis, National University of Singapore, Singapore.

Si, X.-S. (2015). An adaptive prognostic approach via nonlinear degradation modeling: Application to battery data. *IEEE Transactions on Industrial Electronics*, 62:5082–5096.

Si, X.-S., Wang, W., Hu, C.-H., and Zhou, D.-H. (2011). Remaining useful life estimation–a review on the statistical data driven approaches. *European Journal of Operational Research*, 213:1–14.

Si, X.-S., Wang, W., Hu, C.-H., Zhou, D.-H., and Pecht, M. G. (2012). Remaining useful life estimation based on a nonlinear diffusion degradation process. *IEEE Transactions on Reliability*, 61:50–67.

Sklar, M. (1959). Fonctions de repartition an dimensions et leurs marges. *Publ. Inst. Statist. Univ. Paris*, 8:229–231.

Tsai, C. C., Tseng, S. T., and Balakrishnan, N. (2011). Mis-specification analyses of gamma and Wiener degradation processes. *Journal of Statistical Planning and Inference*, 141:3725–3735.

Wang, S. (1990). Saddlepoint approximations for bivariate distributions. *Journal of Applied Probability*, 27:586–597.

Wang, X., Balakrishnan, N., and Guo, B. (2014). Residual life estimation based on a generalized Wiener degradation process. *Reliability Engineering & System Safety*, 124:13–23.

Wang, X. and Xu, D. (2010). An inverse Gaussian process model for degradation data. *Technometrics*, 52:188–197.

Wang, X. L., Guo, B., Cheng, Z. J., and Jiang, P. (2013). Residual life estimation based on bivariate Wiener degradation process with measurement errors. *Journal of Central South University*, 20:1844–1851.

Wang, Y.-F., Tseng, S.-T., Lindqvist, B. H., and Tsui, K.-L. (2019). End of performance prediction of lithium-ion batteries. *Journal of Quality Technology*, 51:198–213.

Wanke, P. and Leiva, V. (2015). Exploring the potential use of the Birnbaum-Saunders distribution in inventory management. *Mathematical Problems in Engineering*, 2015.

Whitmore, G. and Schenkelberg, F. (1997). Modelling accelerated degradation data using wiener diffusion with a time scale transformation. *Lifetime Data Analysis*, 3:27–45.

Widder, D. V. (1941). *Laplace Transform (PMS-6)*. Princeton University Press, Princeton, NJ.

Wiener, N. (1923). Differential space. *Journal of Mathematical Physics*, 2:131–174.

Wood, A. T., Booth, J. G., and Butler, R. W. (1993). Saddlepoint approximations to the CDF of some statistics with nonnormal limit distributions. *Journal of the American Statistical Association*, 88:680–686.

Woodward, W. A., Gray, H. L., and Elliott, A. C. (2017). *Applied Time Series Analysis with R*. Taylor & Francis Group, LLC, Boca Raton, FL.

Xu, Z., Hong, Y., and Jin, R. (2016). Nonlinear general path models for degradation data with dynamic covariates. *Applied Stochastic Models in Business and Industry*, 32:153–167.

Ye, Z. and Chen, N. (2014). The inverse Gaussian process as a degradation model. *Technometrics*, 56:302–311.

Zhou, J., Liu, D., Peng, Y., and Peng, X. (2012). Dynamic battery remaining useful life estimation: An on-line data-driven approach. In *2012 IEEE International Instrumentation and Measurement Technology Conference Proceedings*, pages 2196–2199. IEEE.

Zhou, J., Pan, Z., and Sun, Q. (2010). Bivariate degradation modeling based on gamma process. In *Proceedings of the World Congress on Engineering*, volume 3.